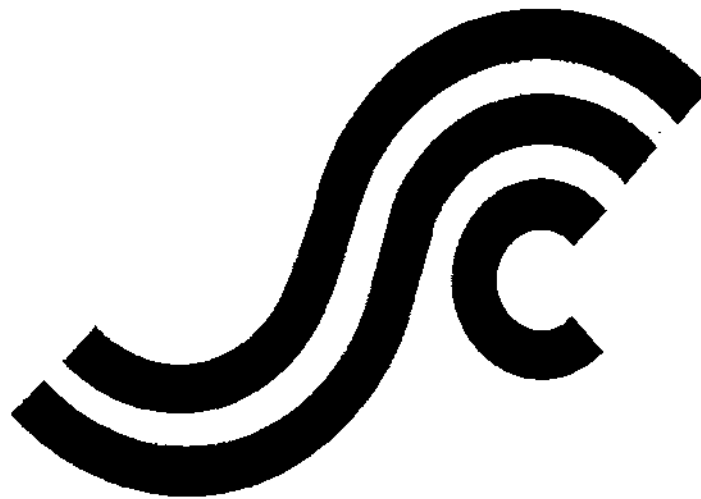


**SSC-415**

**CRACK ARREST TOUGHNESS OF  
STEEL WELDMENTS**



This document has been approved  
For public release and sale; its  
Distribution is unlimited

**SHIP STRUCTURE COMMITTEE  
2000**

---

## SHIP STRUCTURE COMMITTEE

RADM Robert C. North  
U. S. Coast Guard Assistant Commandant,  
Marine Safety and Environmental Protection  
Chairman, Ship Structure Committee

Mr. Robert McCarthy  
Director,  
Survivability and Structural Integrity Group  
Naval Sea Systems Command

Mr. Joseph Byrne  
Director, Office of Ship Construction  
Maritime Administration

Mr. Thomas Connors  
Director of Engineering  
Military Sealift Command

**CONTRACTING OFFICER TECHNICAL REP.**  
Lieutenant David J. Martyn / Ms. Dinah Mulligan  
U.S. Coast Guard R & D Center

Dr. Donald Liu  
Senior Vice President

American Bureau of Shipping

Mr. Bud Streeter  
Director General, Marine Safety,  
Safety & Security  
Transport Canada

Dr. Neil Pegg  
Group Leader - Structural Mechanics

Defence Research Establishment Atlantic

**EXECUTIVE DIRECTOR**  
Lieutenant David J. Martyn  
U. S. Coast Guard

## SHIP STRUCTURE SUB-COMMITTEE

### AMERICAN BUREAU OF SHIPPING

Mr. Glenn Ashe  
Mr. Yung Shin  
Mr. Phil Rynn  
Mr. William Hanzalek

### MARITIME ADMINISTRATION

Mr. Chao Lin

### NAVAL SEA SYSTEMS COMMAND

Mr. W. Thomas Packard  
Mr. Edward E. Kadala  
Mr. Allen H. Engle  
Mr. Charles L. Null

### UNITED STATES COAST GUARD

Captain Mark VanHaverbeke  
Mr. Rubin Sheinberg  
Mr. Walt Lincoln  
Commander Ray Petow

### DEFENCE RESEARCH ESTABLISHMENT ATLANTIC

Mr. Layton Gilroy  
Mr. John Porter  
LCDR Stephen Gibson  
Dr David Stredulinsky

### MILITARY SEALIFT COMMAND

Mr. Edward Meade  
Mr. Rick A. Anderson  
Mr. Jeffery E. Beach  
Mr. Michael W. Touma

### TRANSPORT CANADA

Mr. Nico Pau  
Mr. James Reid

### CANADIAN COAST GUARD

Mr. Justus Bunckhuysen

Member Agencies:

*American Bureau of Shipping  
Defence Research Establishment Atlantic  
Maritime Administration  
Military Sealift Command  
Naval Sea Systems Command  
Society of Naval Architects & Marine Engineers  
Transport Canada  
United States Coast Guard*



Ship  
Structure  
Committee

An Interagency Advisory Committee

Address Correspondence to:

Executive Director  
Ship Structure Committee  
U.S. Coast Guard (G-MSE/SSC)  
2100 Second Street, SW  
Washington, D.C. 20593-0001  
Ph: (202) 267-0003  
Email: dmartyn@comdt.uscg.mil

SR-1384  
SSC-415

September 2000

**CRACK ARREST TOUGHNESS OF STEEL WELDMENTS**

Both small scale compact crack arrest (CCA) tests and large scale tests were performed to evaluate crack arrest toughness in laboratory specimens and in structural situations, respectively. The objective was to evaluate the application of crack arrest toughness determined in the laboratory type specimen to a structural situation.

For a modern low carbon and low sulfur clean control rolled ship plate (ABS DH36), the full thickness (20 mm) crack arrest toughness in the L-T orientation ( $K_a$ ) exceeded 173 MPa $\sqrt{m}$  at test temperatures just above the NDTT. Since the crack bifurcated at approximately 45° angles to the L-T orientation, it suggests a lower crack arrest toughness in that plane and possibly in the T-L orientation. For a multi-pass FCAW butt weld made normal to the rolling direction,  $K_a$  was 80 to 100 MPa $\sqrt{m}$  in the temperature range 0° to 10°C, and greater than 172 MPa $\sqrt{m}$  at 10° C. A major effort was employed in selecting crack starters for this full thickness specimen geometry, and guidelines in this regard were reported at an ASTM meeting. In large scale tests, cracks initiated in the starter section either stopped before entering the main plate or deviated from the intended crack path (butt weld). Thus, the selected successful crack starting procedure in the crack starter tests in isolation, and supporting FEA, did not lead to straight running cracks in the main plate. Additional small scale testing is required, both in the base metal and weld metal, before planning a program on further large scale tests.



R. C. NORTH  
Rear Admiral, U. S. Coast Guard  
Chairman, Ship Structure Committee

### Technical Report Documentation Form

|   |  |  |
|---|--|--|
| 1. Report No.<br>SSC - 415  | 2. Government Accession No.<br>PB00-108447 | 3. Recipients Catalogue No.                                  |
| 4. Title and Subtitle<br>Crack Arrest Toughness of Steel Weldments  |  | 5. Report Date September 2000                                |
| 7. Author(s)<br>Dr. L.N. Pussegoda, Dr. L. Malik, B.A. Graville, Dr. S.J. Kennedy,<br>Yongging Han  |  | 6. Performing Organization Code<br>FTL Final Report 4496C.FR |
|   |  | 8. Performing Organization Report No.<br>SR-1384             |
| 9. Performing Agency Name and Address<br>Fleet Technology Limited Carleton University<br>311 Legget Drive Dept of Civil and<br>Kanata, ON Environmental Engineering<br>CANADA K2K 1 Z8 Ottawa, ON (CANADA) K1 S 5B6 |  | 10. Work Unit No. (TRAIS)                                    |
| 12. Sponsoring Agency Name and Address<br>Commandant (G-MSE/SSC)<br>U.S. Coast Guard Headquarters<br>2100 Second Street SW<br>Washington, DC<br>20593-0001  |  | 11. Contract or Grant No                                     |
|   |  | 13. Type of Publication and Period Covered<br>Final Report   |
|   |  | 14. Sponsoring Agency Code<br>G-M                            |
| 15. Supplementary Notes<br>Sponsored by the Ship Structure Committee and its member agencies  |  |  |

16. Abstract  
Both small scale compact crack arrest (CCA) tests and large scale tests were performed to evaluate crack arrest toughness in laboratory specimens and in structural situations, respectively. The objective was to evaluate the application of crack arrest toughness determined in the laboratory type specimen to a structural situation.

For a modern low C and low S clean control rolled ship plate (ABS DH36), the full thickness (20 mm) crack arrest toughness in the L-T orientation ( $K(a)$ ) exceeded 173 MPa/m at test temperatures just above the NDTT. Since the crack bifurcated at approximately  $45^\circ$  angles to the L-T orientation, it suggests a lower crack arrest toughness in that plane and possibly in the T-L orientation. For a multi-pass FCAW butt weld made normal to the rolling direction,  $K(a)$  was 80 to 100 MPa/m in the temperature range 0 to  $-10^\circ\text{C}$ , and greater than 172 MPa/m at 10 C. A major effort was employed in selecting crack starters for this full thickness specimen geometry, and guidelines in this regard were reported at an ASTM meeting. In large scale tests, cracks initiated in the starter section either stopped before entering the main plate or deviated from the intended crack path (butt weld). Thus, the selected successful crack starting procedure in the crack starter tests in isolation, and supporting FEA, did not lead to straight running cracks in the main plate. Additional small scale testing is required, both in the base metal and weld metal, before planning a program on further large scale tests.

|               |   |
|---------------|---|
| 17. Key Words | 18. Distribution Statement<br>Unlimited Distribution is Available<br>National Technical Information Services<br>US Department of Commerce<br>Springfield, VA 22151 (703)605-60000 |
|---------------|---|

|  |                                      |                  |           |
|--|--------------------------------------|------------------|-----------|
| 19. Security Classif. (of this report) | 20. SECURITY CLASSIF. (of this page) | 21. No. of Pages | 22. Price |
|--|--------------------------------------|------------------|-----------|

**CONVERSION FACTORS**  
(Approximate conversions to metric measures)

| To convert from   | to  | Function    | Value    |
|---|---|-------------|----------|
| <b>LENGTH</b>   |   |             |          |
| inches  | meters  | divide      | 39.3701  |
| inches  | millimeters                                       | multiply by | 25.4000  |
| feet  | meters  | divide by   | 3.2808   |
| <b>VOLUME</b>   |   |             |          |
| cubic feet  | cubic meters                                      | divide by   | 35.3149  |
| cubic inches  | cubic meters                                      | divide by   | 61.024   |
| <b>SECTION MODULUS</b>                                    |   |             |          |
| inches <sup>2</sup> feet <sup>2</sup>                     | centimeters <sup>2</sup> meters <sup>2</sup>      | multiply by | 1.9665   |
| inches <sup>2</sup> feet <sup>2</sup>                     | centimeters <sup>3</sup>                          | multiply by | 196.6448 |
| inches <sup>4</sup>                                       | centimeters <sup>3</sup>                          | multiply by | 16.3871  |
| <b>MOMENT OF INERTIA</b>                                  |   |             |          |
| inches <sup>2</sup> feet <sup>2</sup>                     | centimeters <sup>2</sup> meters                   | divide by   | 1.6684   |
| inches <sup>2</sup> feet <sup>2</sup>                     | centimeters <sup>4</sup>                          | multiply by | 5993.73  |
| inches <sup>4</sup>                                       | centimeters <sup>4</sup>                          | multiply by | 41.623   |
| <b>FORCE OR MASS</b>                                      |   |             |          |
| long tons   | tonne   | multiply by | 1.0160   |
| long tons   | kilograms   | multiply by | 1016.047 |
| pounds  | tonnes  | divide by   | 2204.62  |
| pounds  | kilograms   | divide by   | 2.2046   |
| pounds  | Newtons   | multiply by | 4.4482   |
| <b>PRESSURE OR STRESS</b>                                 |   |             |          |
| pounds/inch <sup>2</sup>                                  | Newtons/meter <sup>2</sup> (Pascals)              | multiply by | 6894.757 |
| kilo pounds/inch <sup>2</sup>                             | mega Newtons/meter <sup>2</sup><br>(mega Pascals) | multiply by | 6.8947   |
| <b>BENDING OR TORQUE</b>                                  |   |             |          |
| foot tons   | meter tons  | divide by   | 3.2291   |
| foot pounds   | kilogram meters                                   | divide by   | 7.23285  |
| foot pounds   | Newton meters                                     | multiply by | 1.35582  |
| <b>ENERGY</b>   |   |             |          |
| foot pounds   | Joules  | multiply by | 1.355826 |
| <b>STRESS INTENSITY</b>                                   |   |             |          |
| kilo pound/inch <sup>2</sup> inch <sup>3/2</sup> (ksi√in) | mega Newton MNm <sup>3/2</sup>                    | multiply by | 1.0998   |
| <b>J-INTEGRAL</b>   |   |             |          |
| kilo pound/inch   | Joules/mm <sup>2</sup>                            | multiply by | 0.1753   |
| kilo pound/inch   | kilo Joules/m <sup>2</sup>                        | multiply by | 175.3    |

## PREAMBLE

The body of the report is presented in two parts: Part I – Compact Crack Arrest Tests (Small Scale Tests) comprises the work done at Fleet Technology Limited and Part II – Large Scale Tests contains the findings of large scale tests done at Carleton University. Outlined below is what was done, why and what happened as a result.

### **Measuring Crack Arrest Toughness**

Tests that have been developed to measure crack arrest toughness can be divided into two categories, small scale tests and large scale tests. In this program, the following selections were made for the two types of tests.

#### ➤ *Compact Crack Arrest (CCA) Tests - Small Scale Tests*

Given the relative high toughness of modern marine construction steels, it was anticipated that valid crack arrest toughness data would not be obtainable using the ASTM E1221-96 procedure, which requires plane strain conditions. Therefore, the procedure for non-plane strain crack arrest testing proposed by Crosley and Ripling, that has some of the features of the E1221 method, was selected.

It is important to note that historically, the success rate in obtaining valid crack arrest toughness in these small scale tests has been low. The main difficulty is the scatter in the crack initiation stress intensity factor and its control in relation to the crack arrest toughness being measured. Thus, a significant proportion of the total project effort was employed in this task. The test materials were a DH 36 grade steel manufactured by controlled rolling practice and a weld metal deposited using E71T-1 flux cored arc welding wire.

#### ➤ *Large Scale Tests*

The specimen design was to simulate a short crack arrest event in a structural situation with minimum effect of the stress wave reflections. Specimen selection was made following a review of the literature and previous experience from an FTL/WIC effort. An outline of the various types of tests is presented in Part II of the report. The double tension tests, under isothermal conditions, provide the best way of obtaining crack arrest toughness measurement in a structural situation. A short crack in an embrittled zone will encounter tougher test material in this design. The crack is initiated in a separately loaded starter plate with little influence on the main plate load.

It is a risky test, from the point of view of obtaining crack arrest toughness. This is because it is usually a ‘go’ – ‘no go’ test as the crack runs into an increasing stress intensity factor (K) region. By comparison in the CCA test, the crack runs into a decreasing K field and thus the possibility of arrest is enhanced. The determination of crack arrest toughness in CCA tests is based on the arrested crack length, whereas for example, in the large scale tests with temperature gradient, the change in temperature becomes a variable as well and there is less control of K at crack arrest.

The latter approach of gradient test, leads to difficulty in designing a test matrix, where the objective was to demonstrate that the crack arrest toughness determined by the CCA test can be used to predict arrest/propagation in a structural situation.

## Findings

### ➤ *CCA Results*

- 1) It was not possible to produce a mode I brittle crack run and arrest event in the CCA specimens at test temperatures of interest, i.e., above the NDTT, for the base material in the L-T orientation. When sufficient driving force is applied, the initiated crack stops soon after entering the base metal, or bifurcates, at approximately 45° angles to the L-T orientation. Inference is that the mode I crack arrest toughness of the DH 36 plate in the L-T orientation exceeds 173 MPa√m, the design capacity/limit of the small scale specimen.
- 2) The weld metal crack arrest toughness was 80 to 100 MPa√m in the temperature range 0 to -10°C, and greater than 172 MPa√m at 10°C. This was an unexpectedly large increase in arrest toughness at 10°C that could not be inferred from standard Charpy or dynamic tear (DT) tests conducted on the weld metal (Part I). This behaviour indicates that crack arrest in the weld metal could be dominated by the tougher regions of this heterogeneous material, whereas it is known that the initiation toughness is controlled by the lowest toughness region sampled by the crack front.
- 3) Results from instrumentation of the specimens gave average crack speeds in the range 700 to 900 m s<sup>-1</sup>.
- 4) Assessment of the various crack starters. A major effort was expended on this task, as it was a critical factor in increasing the success rate. The results indicated the importance of matching the starter initiation toughness to the crack arrest toughness of the test material. As the crack extends into a decreasing K field the starter initiation toughness needs to be greater than the crack arrest toughness. For a successful test, tougher materials require larger specimens and higher stored energy before crack initiation, and the crack starter should be able to delay triggering the crack run. Similarly, less tough materials need smaller specimens and lower stored energy. A number of alternatives were evaluated.
- 5) The findings from the CCA test program were reported to the ASTM committee E08.07.05 in a presentation at the fall meeting, November 1998. The implications of establishing a standardized procedure for a full thickness specimen were highlighted. These were:
  - (a) Specimen size dependence on arrest toughness to be measured.
  - (b) Matching the selection of the starter toughness with arrest toughness.
  - (c) The need to experiment with these options before determining the specimen size to measure specific crack arrest toughness with a reasonable success rate.

## Large Scale Test Results

### ➤ *Crack Arrest Starter Design and Tests*

- 1) Several options were considered based on the information from the FEA of the starter plate design, and initiation toughness values determined from the crack starters evaluated in the CCA tests. As proposed, the first option evaluated was the use of a brittle weld metal. UTPDUR 400 hardfacing electrode, which is the replacement for Foxdur 500, was used to fill the double V-groove that spanned the starter and part of the test section. Most of the latter was to contain the FCAW weld. Welding procedure trials led to cold cracking even with 300°C pre-heat, in combination with a warm blanket.
- 2) The second option, employing 10% lateral pre-compression of the FCAW test weld metal in the starter section, using 25 mm diameter circular indenter, was proposed as the initiation toughness of the flux cored arc weld metal was lower than that of E7024 weld metal.
- 3) After trials, 15% lateral pre-compression, using rollers, was employed to initiate and propagate brittle cracks. The 15% thickness reduction was measured at the apex of the compressed impression left by the 50 mm diameter roller. Testing resulted in brittle propagation along an extreme edge just outside the compressed region, shown to be a result of the residual stress distribution in the compressed zone.
- 4) As an alternative, side grooving was employed to help retain the crack path along the weld centerline. As 3D-FEA indicated that the stress intensity did not drop sufficiently to cause arrest of the crack, as it extended beyond the groove, an alternative was to have the test plate at a higher temperature with respect to the starter of the double tension configuration in order to achieve arrest in the test section, when performing the large scale test.

The above crack starter modifications required the starter to be maintained at a lower temperature. The transition temperature zone between the starter and main plate results due to heat transfer, but was kept narrow by separate cooling of the two sections.

### ➤ *Large Scale Test Results*

- 1) There was difficulty in reproducing the performance of the starter tests in conjunction with the main (test) plate. After the initial extension of a few millimeters along the side grooves, the crack deviated and did not enter the main plate.
- 2) Modification of the starter loading apparatus was carried out to bring it close to the loading arrangement of the starter test apparatus albeit with the main plate. In these tests, the crack entered the main plate, however, again it deviated consistently to the bottom plate of the welded joint in contrast to the opposite direction in the previous tests.

- 3) In the final test performed, with a further modification to the starter loading arrangement, the crack stopped in the starter plate and stayed in the groove. Further loading was curtailed when indications of yielding took place as in the test in (1) above.
- 4) Crack arrest toughness values could not be calculated from any of the larger scale tests.

## CONCLUSIONS

### ➤ *CCA Tests*

- 1) Crack arrest toughness of the controlled rolled ship plate used was in excess of  $173 \text{ MPa}\sqrt{\text{m}}$  when following the Crosley and Ripling full thickness testing approach. This was for mode I propagation in the L-T orientation. Bifurcation of the crack took place in one specimen indicating lower arrest toughness in planes at  $45^\circ$  to the main rolling direction.
- 2) Crack arrest toughness of the weld metal was 80 to  $100 \text{ MPa}\sqrt{\text{m}}$  in the temperature range  $-10$  to  $0^\circ\text{C}$ . It was inferred to be greater than  $172 \text{ MPa}\sqrt{\text{m}}$  at  $10^\circ\text{C}$ .
- 3) Crack propagation events in instrumented specimens gave average crack speeds in the range 700 to  $900 \text{ m s}^{-1}$ .
- 4) A selection criterion for crack starter options was developed and was related to the anticipated crack arrest toughness, and consequently, the CCA specimens size. A number of brittle weld metals and strain age embrittlement strategy were evaluated for initiating a crack run.

### ➤ *Large Scale Tests*

- 1) Lateral compression employed for the crack starter plates resulted in crack deviation from the weld centerline due to residual stress distributions resulting from compression. The alternative side grooving approach was effective in initiating and directing the crack propagation along the intended path.
- 2) FEA of the double tension specimen indicated that the final crack length at arrest could be estimated from the normal strain distribution measured across the weld under static conditions.
- 3) The double tension tests, performed with the starter at a lower temperature than the main plate, provided two contrasting failure mechanisms. With a center-crack starter, as those used for the starter tests, the crack propagated in two stages. In the first event, crack arrest took place after a few (5 to 10) millimeters of extension along the side grooves. In the second event, at a higher load, the crack deviated from the groove and propagated along the top side of the ligament connecting the starter to the main plate. Evaluation of the tests suggested that symmetrical loading of the starter was not taking place resulting in the above behaviour.

In the second series of tests, the crack starter was modified to an edge crack configuration to account for the lower loads that could be applied with the modified starter section loading arrangement. This resulted in crack deviation in the second run-arrest event, but the propagation took place into the bottom side of the main plate.

- 4) The difficulty in reproducing the crack starter performance in the double tension tests led to the unsuccessful outcome of the large scale test program. Thus, crack arrest toughness in the context of short propagating cracks in a structural situation could not be determined.

## **RECOMMENDATIONS FOR FUTURE WORK**

In the current program, the limitations of the full thickness CCA specimen were highlighted. For a reasonable specimen size that can be categorized as a CCA test ( $W \leq 300$  mm), the maximum arrest toughness that can be measured for modern ship plate (400 MPa yield) is about 172 MPa $\sqrt{m}$ . In case of the low C, low S, TMCP materials the crack arrest toughness in the L-T orientation at the temperatures of interest is expected to exceed this value. However, there is a possibility of lower toughness in an orientation that is different from L-T; i.e., T-L or 45° to L-T, as demonstrated by bifurcation of the crack. It would be worthwhile to perform CCA testing of the same base material in an orientation coincident with the bifurcated crack path and the T-L orientation. This evaluation becomes important as new ships are built with these modern steels, and in the regions of details, the principal stresses may not coincide with the ship long axis, and the crack could take the least resistant path.

The weld metal indicated a large increase in crack arrest toughness when the test temperature was raised from 0 to 10°C. A program that will investigate this, with the objective of determining an upper limit of this toughness, is recommended. This could be a statistical analysis of initiation toughness data with the objective of obtaining fracture toughness distributions using a probabilistic approach.

Once the above investigations are complete, a large scale test program needs to be initiated with the same objective of the present program. The following factors from the lessons learned are of worthy consideration for this phase of work.

- When the weld metal was used as a crack starter, either as an embrittled chevron notch (in CCA specimens) or under plane strain conditions in the double tension test, crack initiation was followed by arrest after relatively small extensions. This could be associated with regions of high toughness adjacent to local brittle zones in a multi-pass weld, consequently, progressively higher loads/strains needed at the new crack tip for further extension. This led to crack deviation in the double tension tests. It would be worthwhile to consider a homogeneous material instead of the test weld. In this case, a challenge would be to obtain good fusion between the test weld and the starter material.

- The apparatus of the large scale test set up used in this program needs to be re-assessed. A major issue was crack deviation in the second stage of propagation in the starter plate section, whereas, the starter by itself, when independently loaded in isolation, gave crack runs along the potential crack path beyond the starter section. This could be associated with change of the 2D stress state especially at the ‘throat’ as the crack progresses beyond the starter in these two configurations. A contribution may also come from the current test set up where some degree of load transfer could exist between the starter and the main plate.
- It has become clear that conducting structural tests is risky from the point of cost effectiveness and this factor needs to be kept in mind as well. To date, most large scale tests have been conducted on steel base metals, and testing of the weld metal might have introduced added complications. A rising load test with a temperature gradient may fall into a lower risk category compared to a double tension test.

## Crack Arrest in Ship Structures

The Charpy V-notch toughness examination of numerous steel plates from Liberty class vessels, of which several suffered catastrophic failure by brittle crack propagation<sup>(1)</sup> strongly suggested that fast propagating, and relatively long brittle fractures could be arrested if they encountered steel plates possessing higher toughness (greater than 20 J (15 ft.lbs.) at the temperature of interest) in their path. This led to the practice of including welded crack arrestor plates in the U.S. naval surface ship design. Essentially, the sheer and stringer strakes, and the lower turn of the bilge areas are specified to be fabricated from HY80 steel while the rest of the ship structure is fabricated from standard ABS grades of ship structural steels or their equivalent. HY 80 steel is an extremely tough steel required to display at least 47 J (35 ft.lbs.) Charpy absorbed energy at – 85°C (–120°F). At the design temperature, typically 0°C (32°F), this steel always displays an upper-shelf toughness behaviour.

The use of HY80 steel for crack arrestor strakes can be considered as a success in that there is no reported incidence of a ship with HY80 crack arrestor strakes breaking into two in the manner of some Liberty class vessels. However, it is not clear if the absence of such catastrophic failures is due to the HY80 steel strakes serving their intended purpose, or because there have been no long brittle fractures that needed to be arrested due to the general improvement in the toughness of the conventional ship structural steels, either by specification or by improved steel making practices.

In recent years, with the advances in the field of fracture mechanics, attempts have been made to provide a fundamental basis for the design of crack arrestor plates in ships. Unfortunately, a direct and simple application of these principles would indicate that crack arrestor plates should not be effective in arresting long, propagating brittle cracks [Czyryca and Porr<sup>(2)</sup>]. For example, these authors considered the case of a 30 m (100 feet) wide deck comprised of 26 m (84 feet) of mild steel in the center, and bounded by 2.5 m (8 feet) wide HY 80 steel strakes at each end. A brittle fracture is assumed to initiate and propagate in the mild steel section until it encounters the HY 80 steel strakes at each end. Ignoring the possible role of stiffeners in crack arrest, and using an experimentally obtained value of  $J_{1c}$  for HY 80 steel, the authors estimated that the far field stress must be below 15 MPa (2.1 ksi) to ensure stable, ductile crack extension in the HY 80 strakes. The design stress is of course much higher, thus implying that the HY 80 strakes in this example would not be able to arrest the crack, contrary to experience and to the design practice for US naval ships. One can consider the use of more frequent crack arrestor strakes, however, once again ignoring a possible role of stiffeners in crack arrest and assuming the far field stress to be 100 MPa (14 ksi), they estimate that 0.63 m (25”) wide HY 80 crack arrestor plates would need to be included after every 2.54 m (100 inches) of the mild steel. This is clearly an uneconomic and unrealistic fabrication scenario.

While the estimates made above could be improved by more rigorous fracture mechanics and geometrical modeling<sup>(3)</sup>, it is doubtful that the main conclusions above would change. It has therefore been suggested that principles of fracture mechanics are not applicable to long crack arrest. An intuitive reason for this could be that after the propagating crack has achieved certain length, the crack tips no longer know the length of crack behind them.

In other words, the crack tip stress and strain states no longer depend on the crack length and therefore the standard fracture mechanics expression for stress intensity factor loses its significance. The fact that the crack arrest temperature (CAT) in Robertson's tests is essentially independent of applied stress until it is reduced to very low levels supports this contention and points to the use of CAT as the design basis for long crack arrest<sup>(4)</sup>.

It is noteworthy that fracture mechanics concept based on experimentally measured plain strain compact crack arrest toughness has been successfully applied in the nuclear industry. Here one is dealing with "short crack arrest" as a semi-elliptical surface crack is envisaged to propagate in the through thickness direction, and then get arrested due to thermal gradient and increasing toughness, before becoming a through thickness crack. Perhaps the longest crack arrest situation that has been rationalized on fracture mechanics basis is that of storage tanks. In this case, a crack is assumed to propagate along the full length of a vertical weld seam ( $2a = 2$  to  $3$  m) and then get arrested as it emerges into the base metal<sup>(5)</sup>. It is worth noting however that the base material selection is still based on the concept of crack arrest temperature as inferred from the Pellini's nil-ductility transition (NDT) temperature.

Another issue in the application of fracture mechanics concept to short crack arrest pertains to the need of dynamic versus static analysis. Sumpter<sup>(6)</sup> has considered this issue and concluded that  $K_D$  (dynamic  $K$  for a propagating crack) will lie below  $K_A$  (static  $K$  at the arrest crack length). This is in the absence of reflected stress waves and is reasonable assumption in a structural situation. Therefore a static stress analysis would give a conservative  $K$ . This suggests that it would usually be conservative to predict crack arrest in a structure based on  $K_A$  observed in small scale tests. There is, however, a complication when reflected stress waves are to be considered for the possibility of re-initiation immediately following arrest<sup>(6)</sup>.

Based on this background, the objective of the current project was to determine the full thickness crack arrest toughness of a marine structural steel and an appropriate weld metal for the same, and then demonstrate its use /applicability/validity in short crack arrest situation. Such situations arise due to brittle fractures in welds in the secondary structure that are required to get arrested due to decrease in the stress/driving force (structural redundancy/stress redistribution) or due to encountering a tougher base material.

## References

1. The design and methods of construction of welded steel merchant vessels, Report of an investigation, Final report, Government Printing Office, Washington, DC, (1947)
2. E.J. Czyryca and W.C. Porr: "Technical assessments of crack arrest requirements in the LDP 17 design, CARD/NSWC-TR-61-94/46, Aug. 1995, NSWC (Carderock Division), Bethesda, MD, 20084-5000
3. A.V. Clarke and D.T. Read: "Ductile tearing stability analysis of ship containing a crack arrester strake", National Bureau of Standards Report NBSIR 85-3038 (January 1986)
4. T.S. Robertson: "Propagation of brittle fracture in steel", J. Iron Steel Inst., v. 175, (1953), pp. 361-74
5. A.A. Willoughby and Y. Kawaguchi: "Arrest of long cracks in storage tanks", Proc.Conf. Fracture safe design for large storage tanks, TWI, Abington, Cambridge, U.K., (1986), pp.137-150.
6. J.D.G. Sumpter and R.M. Curr: "Crack arrest concepts for failure prevention" TWI, Abington, Cambridge, U.K., (1995).

## TABLE OF CONTENTS

### PART I – SMALL SCALE TESTING

|       |   |    |
|-------|---|----|
| 1.    | INTRODUCTION  | 1  |
| 2.    | STEEL CHARACTERIZATION                                      | 2  |
| 3.    | SMALL SCALE CRACK ARREST TESTS OF THE BASE METAL            | 5  |
| 3.1   | Compact Crack Arrest (CCA) Specimen Design                  | 5  |
| 3.1.1 | Specimen Size Determination                                 | 5  |
| 3.1.2 | CCA Test Procedure  | 7  |
| 3.1.3 | Selection of Crack Starter                                  | 8  |
| 3.2   | Findings of CCA Test Results from the First Phase           | 9  |
| 3.2.1 | Laterally Compressed and Aged Crack Starter                 | 9  |
| 3.2.2 | Brittle Weld Bead Crack Starter                             | 9  |
| 3.2.3 | Modified Long Chevron Notch (Bonenberg) Specimen            | 10 |
| 3.2.4 | Summary   | 11 |
| 3.3   | CCA Test Results from the Second Phase                      | 12 |
| 4.    | WELD METAL CHARACTERIZATION                                 | 16 |
| 4.1   | Procedure Development                                       | 16 |
| 4.2   | Characterization of the Weld Metal                          | 17 |
| 4.3   | CTOD Testing and Crack Arrest Toughness Estimates           | 17 |
| 5.    | SMALL SCALE CRACK ARREST TESTS OF THE WELD METAL            | 20 |
| 5.1   | CCA Specimen Design and Crack Starter                       | 20 |
| 5.2   | Findings of Starter Options for CCA Test                    | 20 |
| 5.2.1 | Starter Options for the Small Specimen (W = 100 mm)         | 20 |
| 5.2.2 | Starter Options for the Larger Specimen (W = 200 mm)        | 22 |
| 5.3   | CA Testing Using Multiple Load Cycles                       | 25 |
| 5.3.1 | Testing Specimens with W = 100 mm                           | 25 |
| 5.3.2 | Testing Specimens with W = 200 mm                           | 28 |
| 5.3.3 | Testing Specimens with W = 300 mm                           | 28 |
| 5.4   | Discussion of the Weld Metal Crack Arrest Toughness Results | 29 |
| 6.    | REFERENCES  | 36 |

### APPENDIX A – CCA TESTS

## PART II – LARGE SCALE CRACK ARREST TESTS

|        |   |     |
|--------|---|-----|
| 7.     | CRACK ARREST TESTS AND EVALUATIONS OF TOUGHNESS         | 37  |
| 7.1    | Small Scale Crack Arrest Tests                          | 37  |
| 7.2    | Large Scale Crack Arrest Tests                          | 38  |
| 7.3    | Determination of $K_I$ by Finite Element Analysis (FEA) | 47  |
| 8.     | SMALL SCALE TEST PROGRAM                                | 52  |
| 8.1    | General   | 52  |
| 8.2    | Finite Element Analysis of Compact Crack Arrest Tests   | 53  |
| 8.3    | Finite Element Analysis of Starter Plate Tests          | 55  |
| 8.3.1  | General   | 55  |
| 8.3.2  | Lateral Compression of the Weld                         | 56  |
| 8.3.3  | Double-Side Face Grooves                                | 63  |
| 9.     | LARGE SCALE DOUBLE TENSION TEST PROGRAM                 | 67  |
| 9.1    | Objective and Scope                                     | 67  |
| 9.2    | Stress Intensity Factor Curves and Data Interpretation  | 67  |
| 9.3    | Large Scale Double Tension Tests                        | 75  |
| 9.3.1  | Test Specimen Description                               | 75  |
| 9.3.2  | Test Set-Up   | 75  |
| 9.3.3  | Instrumentation   | 78  |
| 9.3.4  | Measurement of Temperature Gradients                    | 83  |
| 9.3.5  | Large Scale Double Tension Test Summary                 | 84  |
| 9.3.6  | Test LSP1 Discussion                                    | 87  |
| 9.3.7  | Modified Load Sequence                                  | 909 |
| 9.3.8  | Test LSP2 Discussion                                    | 95  |
| 9.3.9  | Test LSP3 Discussion                                    | 96  |
| 9.3.10 | Test LSP4 Discussion                                    | 97  |
| 9.3.11 | Test LSP5 Discussion                                    | 100 |
| 9.3.12 | Test LSP6 Discussion                                    | 104 |
| 9.3.13 | Test LSP7 Discussion                                    | 104 |
| 10.    | SUMMARY, CONCLUSIONS AND FUTURE WORK                    | 109 |
| 10.1   | Summary   | 109 |
| 10.2   | Conclusions   | 111 |
| 11.    | REFERENCES  | 114 |

## LIST OF FIGURES

|            |   |    |
|------------|---|----|
| Figure 2.1 | Microstructure in the L-T Orientation   | 2  |
| Figure 2.2 | Mid-plane Split in Tensile Specimen   | 3  |
| Figure 2.3 | Charpy Transition Curves of the Base Material   | 4  |
| Figure 3.1 | Full Thickness CCA Test Specimen with Proportionate Dimensions  | 6  |
| Figure 3.2 | CCA Test Set Up for Specimen Size $W = 300$ mm  | 7  |
| Figure 3.3 | Surface Specimen T16 Displaying the Crack Bifurcation   | 14 |
| Figure 4.1 | Cross-Section of the Weld, Identified as W2, Selected for Testing from Procedure Development  | 16 |
| Figure 4.2 | Charpy Transition Curve for Weld at (T/4) Location  | 18 |
| Figure 4.3 | ASTM E604 DT Transition Curve for Weld Centreline   | 18 |
| Figure 4.4 | Schematic Representation of the Load-CMOD Curve to Display the Crack Initiation and Arrest in a (b x B) Specimen  | 19 |
| Figure 5.1 | Fracture Surface Displaying a Crack Run in a Specimen with Foxdur 500 Weld Bead Starter (a). In (b) a Cross-Section at the Location of Crack Arrest is Shown              | 21 |
| Figure 5.2 | Fracture Surface of the Second Specimen with $W = 200$ mm (a) In (b) a Cross-Section at the Location of Crack Arrest is Shown   | 24 |
| Figure 5.3 | Strain-CMOD Plot for Specimen CCA W2(2)2 Tested at $-10^{\circ}\text{C}$  | 26 |
| Figure 5.4 | Strain-Time Plot for the above Test During and after the Crack Run-Arrest Event   | 26 |
| Figure 5.5 | Fracture Surface Displaying (a) Crack Run in the Specimen with Results Given in Figure 5.3 and Table 5.2. In (b) a Cross-Section at the Location of Crack Arrest is Shown | 27 |
| Figure 5.6 | Fracture Surface Displaying a Crack Run in Specimen with $W = 300$ mm In (b) a Cross-Section at the Location of Crack Arrest is Shown                                     | 29 |
| Figure 5.7 | Crack Arrest Toughness vs Temperature for the Weld Metal  | 33 |
| Figure 5.8 | Relation Between Crack Arrest Toughness and Initiating Toughness  | 34 |
| Figure 5.9 | Stress Intensity Factor at Initiation vs Test Temperature for Various Brittle Weld Starters   | 35 |
| Figure 7.1 | Small Scale Test Types  | 40 |
| Figure 7.2 | Large Scale Test Types  | 44 |
| Figure 7.3 | Coordinate System and Stress Components Ahead of a Crack Tip  | 47 |
| Figure 7.4 | Displacement Extrapolation Method   | 49 |
| Figure 7.5 | FEA Modeling for Standard Crack Geometry and Loading  | 50 |
| Figure 7.6 | Comparison of Stress Intensity Factors for a Single-Edge Crack in a Finite Width Plate Subjected to Uniform Tension ( $\sim 400$ MPa)                                     | 51 |
| Figure 7.7 | Comparison of Stress Intensity Factor for a Centre Crack in a Finite Width Plate Subjected to Uniform Tension ( $\sim 400$ MPa)   | 51 |
| Figure 8.1 | Compact Crack Arrest Test Specimen and Analytical Model   | 54 |
| Figure 8.2 | Comparison of Crack Arrest Toughness Values Evaluated by Crosby & Ripling (1990) and the Displacement Method  | 55 |
| Figure 8.3 | Test Set Up of Lateral Compression of Weld and the Lateral Deformation after the 15% Compression  | 58 |

LIST OF FIGURES (continued)

|             |  |     |
|-------------|--|-----|
| Figure 8.4  | 3-Dimensional FEA Model for Lateral Compression Indented by a Rigid Steel Roller                         | 59  |
| Figure 8.5  | X-Direction Stress across the Potential Crack Face, 15% Lateral Compression                              | 60  |
| Figure 8.6  | Von Mises Strain, 15% Lateral Compression  | 60  |
| Figure 8.7  | Starter Plate Test Setup   | 61  |
| Figure 8.8  | Ductile Branching Crack – Starter Plate Test, STP1   | 62  |
| Figure 8.9  | Crack Location – Starter Plate Test, STP2  | 62  |
| Figure 8.10 | Double-Side Face Groove Finite Element Model   | 63  |
| Figure 8.11 | Stress Intensity Factor versus Depth of Grooves  | 64  |
| Figure 8.12 | Side View of Double-Side Face Grooves  | 65  |
| Figure 8.13 | Crack Surfaces for Starter Plate   | 66  |
| Figure 9.1  | Large-Scale Double Tension Test Specimen with Double-Side Grooves  | 68  |
| Figure 9.2  | FEA Model for Large-Scale Test Specimen with Face Grooves  | 70  |
| Figure 9.3  | Details of FEA Model for Large-Scale Test Specimen   | 71  |
| Figure 9.4  | Stress Intensity Factor versus Crack Propagation as Predicted by FEA                                     | 72  |
| Figure 9.5  | Data Interpretation and Design   | 74  |
| Figure 9.6  | Schematic Diagram of the Double Tension Test in Load Frame   | 76  |
| Figure 9.7  | Assemble View of Large-Scale Test  | 77  |
| Figure 9.8  | Section View of the Temperature Control Chamber  | 78  |
| Figure 9.9  | Thermocouples, Strain Gauges and Cooling Pipes   | 79  |
| Figure 9.10 | Location and Identification of Strain Gauges and Thermocouples on the Two Sides of the Specimen (S1, S2) | 80  |
| Figure 9.11 | Strain Distributions for Varying Crack Lengths   | 81  |
| Figure 9.12 | Temperature Gradient Curves  | 83  |
| Figure 9.13 | Brittle Crack Propagation  | 88  |
| Figure 9.14 | Deformation and Shear Stress Contours, LSP1  | 89  |
| Figure 9.15 | Deformation in the y-direction, Modified Load Sequence   | 91  |
| Figure 9.16 | Shear Stresses across the Gap Plate, Modified Load Sequence  | 93  |
| Figure 9.17 | Results of Fracture for LSP2   | 95  |
| Figure 9.18 | Schematic Diagram of Articulating Starter Loading System   | 98  |
| Figure 9.19 | Articulating Starter Load System   | 99  |
| Figure 9.20 | Stress Intensity Factor Distributions for Varying Starter Load and Crack Condition                       | 100 |
| Figure 9.21 | Crack Initiation of LSP4   | 101 |
| Figure 9.22 | Brittle Shear Failure for LSP4   | 102 |
| Figure 9.23 | Brittle Shear Failure for LSP5   | 103 |
| Figure 9.24 | Modification of Cooling System for Main and Starter Plate of LSP6  | 105 |
| Figure 9.25 | Brittle Shear Failure of LSP6  | 106 |
| Figure 9.26 | Temperature Gradient Curves for Large-Scale Test 6   | 107 |
| Figure 9.27 | Temperature Gradient Curves for Large-Scale Test 7   | 107 |
| Figure 9.28 | Loading Apparatus for LSP7   | 108 |
| Figure 10.1 | Starter Plate Load System  | 113 |

## LIST OF TABLES

|           |   |    |
|-----------|---|----|
| Table 3.1 | CCA Test Results of Brittle Weld Bead Specimens   | 13 |
| Table 4.1 | CTOD Results and Crack Arrest Estimates   | 19 |
| Table 5.1 | CCA Test Results of the Weld Metal Specimens  | 23 |
| Table 5.2 | CCA Test Results of the Weld Metal (W2) Specimens (Multiple Load Cycles)                                | 30 |
| Table 5.3 | CCA Test Results from Specimens Extracted from the W = 300 mm Size Made from Weld Panel 3               | 32 |
| Table 5.4 | Vickers Hardness Results on Weld Cross-Sections Extracted from CCA Specimens                            | 32 |
| Table 5.5 | Proportion of the Categories of Microstructure Close to the Weld Centreline of the Above Cross-Sections | 33 |
| Table 7.1 | Summary of Small Scale Tests  | 39 |
| Table 7.2 | Summary of Large Scale Tests  | 43 |
| Table 8.1 | CCA Test Results and FEA Results  | 53 |
| Table 9.1 | SOLID45 Element Description   | 69 |
| Table 9.2 | Large-Scale Double Tension Test Summary   | 84 |
| Table 9.3 | Modified Load Sequence  | 90 |
| Table 9.4 | Modifications to Promote Crack Propagation and Corresponding Effects                                    | 96 |

## NOMENCLATURE

|      |  |
|------|--|
| ABS  | American Bureau of Shipping                |
| ASTM | American Society for Testing and Materials |
| CCA  | Compact crack arrest                       |
| CSA  | Canadian Standards Association             |
| CVN  | Charpy Vee Notch                           |
| CMOD | Crack mouth opening displacement           |
| CTOD | Crack tip opening displacement             |
| DA   | Data acquisition                           |
| DCB  | Double cantilever beam                     |
| DND  | Department of National Defense (Canada)    |
| DT   | Dynamic tear                               |
| EDM  | Electric discharge machined                |
| FCAW | Flux cored arc welding                     |
| FTL  | Fleet Technology Limited                   |
| HAZ  | Heat affected zone                         |
| L-T  | Longitudinal orientation                   |
| NDTT | Nil-ductility transition temperature       |
| NSWC | Naval Surface Warfare Centre               |
| PTC  | Project Technical Committee                |
| TDCB | Tapered double cantilever beam             |
| T-L  | Transverse orientation                     |
| T.S. | Tensile strength                           |
| YS   | Yield strength                             |

## LIST OF SYMBOLS

|              |   |
|--------------|---|
| A            | Projected area of the crack   |
| a            | Crack length  |
| $a_a$        | Crack arrest length   |
| $a_{eff}$    | Effective crack arrest length   |
| $a_f$        | Final crack length  |
| $a_o$        | Initial crack length  |
| $a_a^{stat}$ | Static crack arrest length  |
| $a_a^{dyn}$  | Dynamic crack arrest length   |
| B            | Thickness of plate  |
| $B_N$        | Thickness between the bottom of the grooves on each side of surface   |
| c            | Material property constant  |
| E            | Young's Modulus   |
| G            | Energy release rate   |
| $G_a$        | Crack arrest energy release rate                                      |
| $G_{cr}$     | Critical energy release rate  |
| K            | Stress intensity factor   |
| $K_{eff}$    | Effective stress intensity factor                                     |
| $K_I$        | Stress intensity factor of Mode I                                     |
| $K_{Ia}$     | Crack arrest toughness  |
| $K_{Ia}^*$   | Plasticity corrected crack arrest toughness                           |
| R            | Crack resistant force   |
| r            | Distance from the crack tip to any arbitrary point ahead of crack tip |
| T            | Kinetic energy  |
| t            | Specimen length   |
| $U_a$        | Decrease in elastic energy for initiating the crack in the plate      |
| $U_o$        | Elastic energy of an uncracked plate                                  |
| $u_x$        | Displacement of any arbitrary point in x direction                    |
| $u_y$        | Displacement of any arbitrary point in y direction                    |
| $u_z$        | Displacement of any arbitrary point in z direction                    |
| $v_p$        | Measured plastic crack tip opening displacement                       |

|                  |   |
|------------------|---|
| $W$              | Width of plate  |
| $W_s$            | Work required to create new crack surface                           |
| $\beta$          | Dimensionless constant  |
| $\phi$           | Dimension correction factor   |
| $\delta_o$       | Crack Mouth Opening Displacement (CMOD) at crack initiation         |
| $\delta_a$       | CMOD at the arrested point measured by clip gauge                   |
| $\delta_f$       | CMOD at crack arrest  |
| $\delta_{max}$   | Upper CMOD limit  |
| $\delta_{min}$   | Lower CMOD limit  |
| $\kappa$         | Property constant   |
| $K_a$            | Crack arrest toughness  |
| $K_o$            | Crack initiation stress intensity factor                            |
| $K_v$            | Anticipated crack arrest toughness                                  |
| $\mu$            | Shear modulus   |
| $\mu\varepsilon$ | Micro-strain  |
| $\nu$            | Poisson's ratio   |
| $\theta$         | Projection angle  |
| $\sigma$         | Applied normal stress   |
| $\sigma_x$       | x-direction normal stress at any arbitrary point ahead of crack tip |
| $\sigma_y$       | y-direction normal stress at any arbitrary point ahead of crack tip |
| $\sigma_{ys}$    | Yield stress  |
| $\sigma_z$       | z-direction normal stress at any arbitrary point ahead of crack tip |
| $\tau_{xy}$      | Shear stress on xy plane  |
| $\tau_{yz}$      | Shear stress on yz plane  |
| $\tau_{zx}$      | Shear stress on zx plane  |
| $\Pi$            | Total potential energy of the system                                |
| $W$              | Specimen width  |

## **PART I – SMALL SCALE TESTING**

### **1. INTRODUCTION**

This report describes the findings from the small scale tests conducted on the base metal and the weld metal in this program. Considerable effort was spent in performing the full thickness non-plane strain compact crack arrest (CCA) tests on the base metal and weld metal. The main objectives for this phase of the program were:

- (a) To evaluate the specimen design in the ASTM draft standard<sup>(1)</sup> for testing full thickness steel plate and weldments. Given the relatively high toughness of modern steel plates used in ship construction, it was anticipated that valid crack arrest data would not be obtainable using the ASTM Standard E1221, which requires plane strain conditions. ASTM E1221 was developed for applications in the power generation industry where plate thicknesses are large and therefore most of the through thickness crack front is under plane strain. Here, considerable effort was employed to select the optimum crack starter by evaluating various options.
- (b) Using the selected test procedure, determine the full thickness crack arrest toughness of a modern controlled steel plate and its weldment.

The crack arrest values determined from these small scale (CCA) specimens were used to plan the test matrix for the large scale tests. These large scale tests represent a simple structural loading situation.

---

<sup>1</sup> Reference

## 2. STEEL CHARACTERIZATION

ABS Grade DH 36 plate (20 mm thickness) was received from Bethlehem Steel Corporation. The chemical composition (in wt%) from the mill test certificate is: 0.08 C, 1.27 Mn, 0.023 P, 0.007 S, 0.325 Si, 0.015 Cu, 0.01 Ni, 0.04 Cr, 0.005 Mo, 0.034 V, 0.044 Al and 0.033 Cb. Microstructure examination indicated a ferrite-fine pearlite structure with the ferrite grains being slightly elongated in the rolling direction. The average ferritic grain size was estimated to be ASTM 7 to 9.

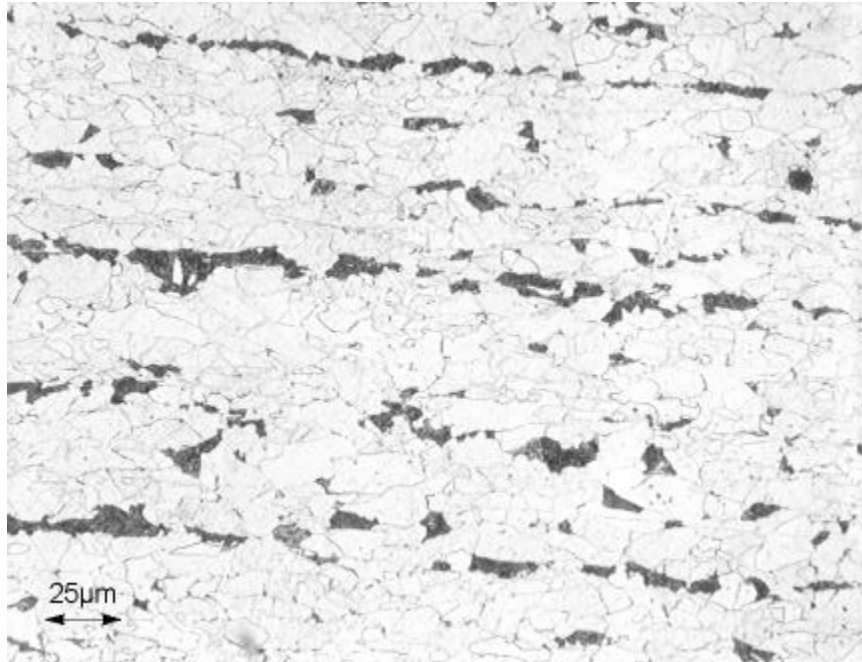


Figure 2.1: Microstructure in the L-T Orientation

As part of the preliminary assessment of the plate, the following tests were performed.

- i) Full thickness tensile testing in the L-T orientation. The 0.2% off-set yield strength and tensile strength were determined to be 483 MPa (70 ksi) and 567 MPa (82.3 ksi), respectively. Prior to the final fracture, the plate developed a pronounced split at the mid-thickness plane (Figure 2.2).
- ii) Full thickness Charpy V-notch testing, in accordance with ASTM E 23<sup>2</sup>. Transition curves were obtained in L-T and T-L orientations. In the L-T orientation the transition temperature is about -80°C and therefore the steel meets the toughness requirements of ABS Grade DH 36. A second series was tested where the V-notch was pressed following the same procedure as for dynamic tear specimens in ASTM E 604<sup>2</sup>. This modification increased the transition temperature to about -40°C.

<sup>2</sup> ASTM E 23 and E 604: Standard test methods for (i) notched bar impact testing of metallic materials, and (ii) dynamic tear testing of metallic materials.

Figure 2.3 shows the Charpy results and indicates a large scatter in the transition temperature range and is typical of clean steels. The transition temperatures are estimated at the 40J energy level.

- iii) The nil-ductility transition temperature (NDTT) of the steel as per ASTM E 208<sup>3</sup> was found to be -35°C (two no-breaks at -30° and a break at -35°C).

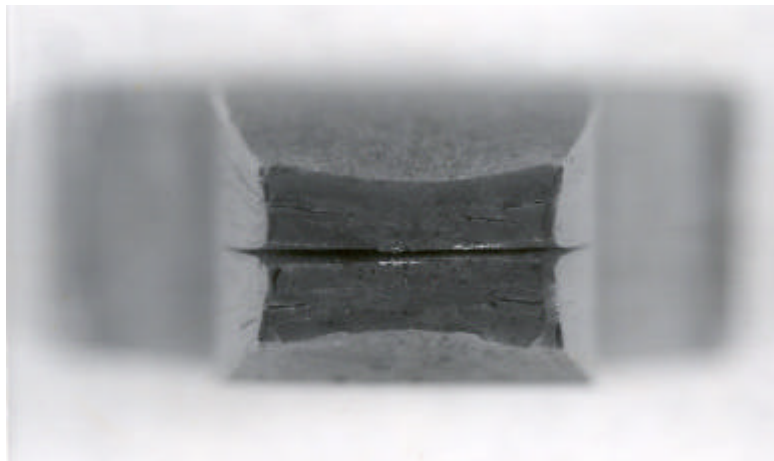
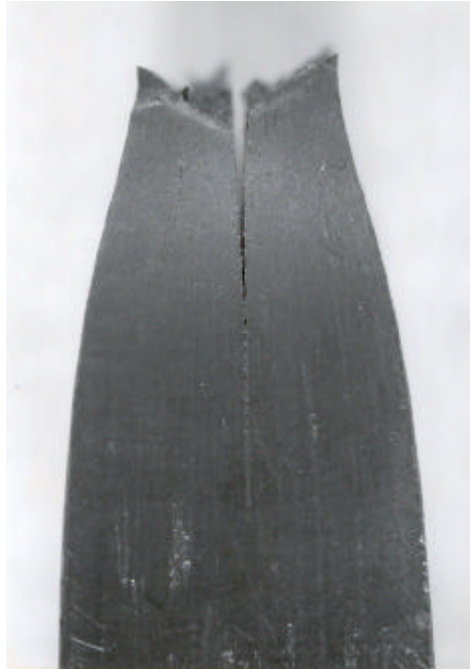


Figure 2.2: Mid-Plane Split in Tensile Specimen.

---

<sup>3</sup> E 208: Standard test methods for conducting drop weight test to determine nil-ductility transition temperature of ferritic steels.

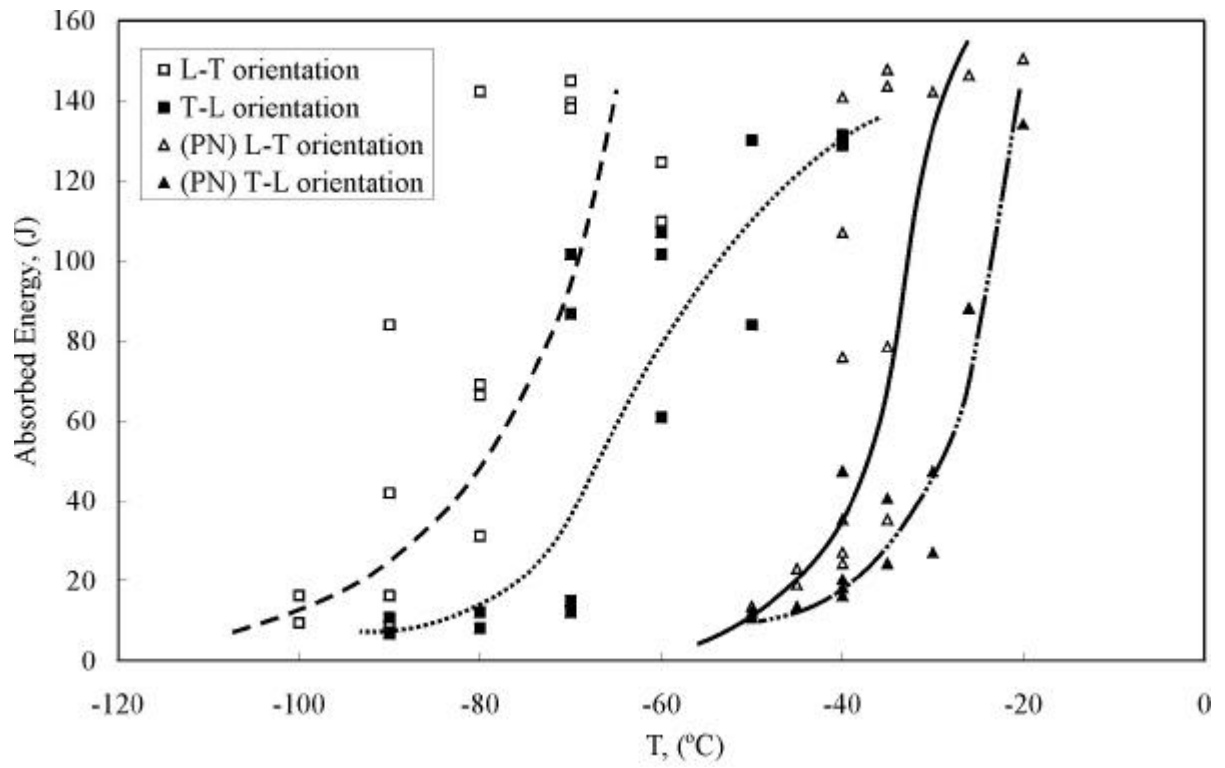


Figure 2.3: Charpy Transition Curves of the Base Material

### 3. SMALL SCALE CRACK ARREST TESTS OF THE BASE METAL

#### 3.1 Compact Crack Arrest (CCA) Specimen Design

Since the steel NDTT is  $-35^{\circ}\text{C}$ , the highest temperature at which the small scale tests could be successful was judged to be  $-10^{\circ}\text{C}$  ( $25^{\circ}\text{C}$  above the NDTT). This was gained through from previous experience in testing full thickness controlled rolled plate used by the Canadian Navy<sup>(2)</sup>. At this temperature above the NDTT, the estimated crack arrest toughness was  $160 \text{ MPa}\sqrt{\text{m}}$  for controlled rolled ship steel plate<sup>(2)</sup>. However, due to splitting reported above, the transition temperature could be reduced.

##### 3.1.1 Specimen Size Determination

The full thickness CCA specimen size was determined using the approach of Crosley and Ripling<sup>(3)</sup> where specimen design was based on an anticipated value of the full thickness crack arrest toughness ( $K_v$ ) of  $165 \text{ MPa}\sqrt{\text{m}}$ . The specimen dimensions, displayed in Figure 3.1, are expressed in terms of  $W$ , which in turn is based on the expression:

$$W \geq 2.83 \left( \frac{K_v}{s_y} \right)^2 \quad (3.1)$$

As the test temperature is decreased,  $K_v$  is expected to drop, and the yield strength ( $\sigma_y$ ) increases, and therefore the required specimen size has to decrease. To obtain valid values of the actual crack arrest toughness,  $K_a$ , the crack mouth opening displacements (CMOD) at the beginning of the run-arrest event ( $\delta_o$ ) and at the arrest point ( $\delta_f$ ) must both fall between specified limits. The lower CMOD limit ( $\delta_{\min}$ ) is intended to be sufficient to provide a minimum crack run to the 0.5W point before the crack is arrested. Similarly, the upper limit ( $\delta_{\max}$ ) takes into consideration that the arrested crack length should be less than 0.8W if there is to be sufficient remaining ligament to contain the plastic zone, and thus allow a linear-elastic or small-scale plasticity analysis to be employed. These crack length limits are different from the validity requirements in ASTM E 1221. The CMOD range is smaller than the range stipulated for unload-reloading locations in the ASTM E1221 procedure<sup>(4)</sup>. When the above conditions are met, the standard expression from ASTM E 1221 is used to determine  $K_a$ .

$$K_a = \frac{d_f E f(a/W)}{W^{1/2}} \quad (3.2)$$

where  $E$  is the Young's Modulus.

In determining the CMOD limits, refinements have been made to some of the original equations used in Reference 3. In that article, errors were found in equations 2a and 5, after publication,<sup>(1)</sup> and  $f(a/W)$  in equation 3 have been revised in the current edition of ASTM E 1221<sup>(4)</sup>. The revised equations are given below:

$$\delta_{\min} = \frac{K_V W^{1/2}}{E f(x = 0.525)} \quad (\text{equation 2a [Ref. 3]} \quad (3.3)$$

$$f(x) = (1-x)^{0.5}(0.748 - 2.176x + 3.56x^2 - 2.55x^3 + 0.6x^4)$$

where  $x = a/W$

$$K_a^* = K_a [1 - 0.01\phi^2(1-a/W)^2] \quad (\text{equation 5 [Ref. 3]} \quad (3.4)$$

where  $K_a^*$  is the plasticity corrected crack arrest toughness,  
and  $\phi = E\delta_f/\sigma_y W$ .

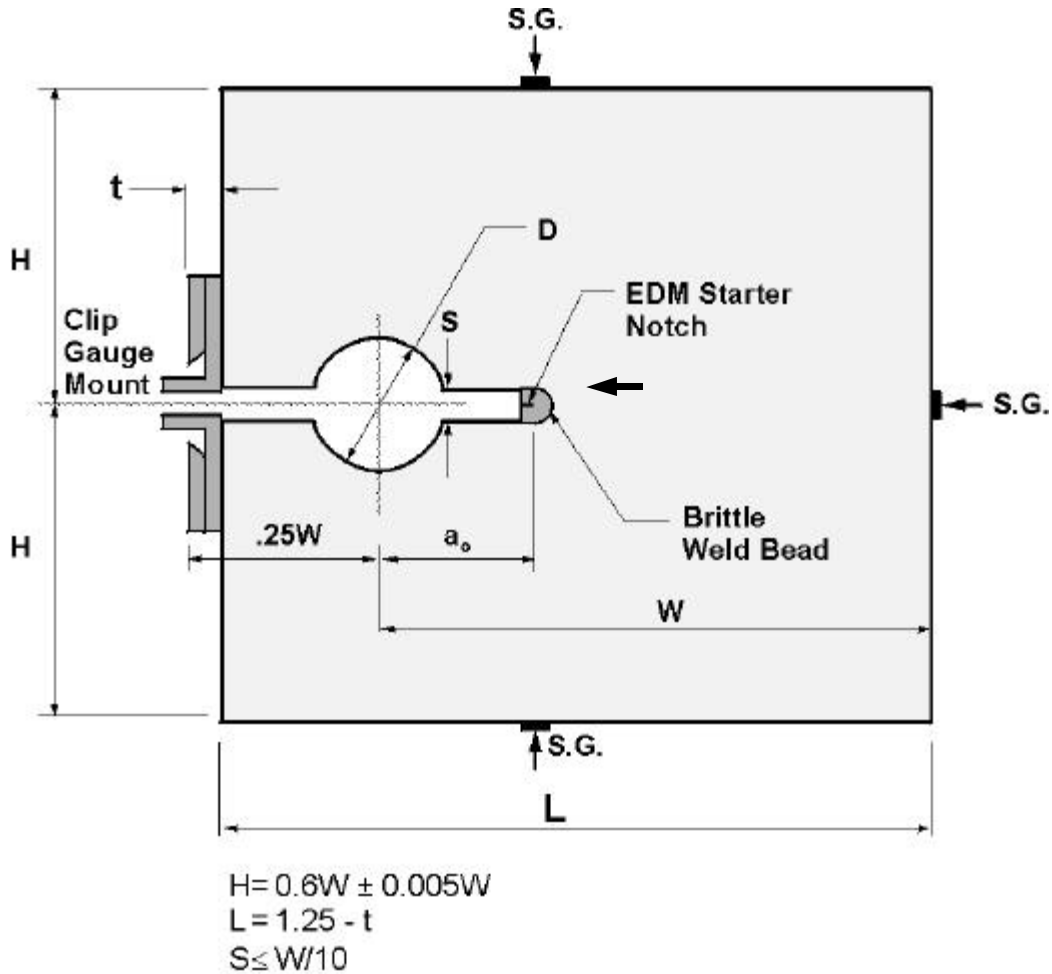


Figure 3.1: Full thickness CCA test specimen with proportionate dimensions. The brittle weld bead starter is shown here. A typical EDM notch root radius was 0.254 mm. Locations where strain gauges were attached are also indicated by arrows.

The  $W$  dimension for  $(K_{Ic})$  of 165  $\text{MPa}\sqrt{\text{m}}$  was 300 mm.

### 3.1.2 CCA Test Procedure

Monotonic loading was applied using an arrangement similar to the one described in ASTM E 1221 (Figure 3.2). A Teflon sheet was used both on the split pin and also on support blocks and hold down plates. These reduce friction during load and unload cycles and also insulate the specimen for temperature control purposes. The test specimen was cooled by a liquid nitrogen spray using a temperature control solenoid. The specimen temperature was measured using a thermocouple spot welded to the specimen, about 25 mm from the root of the starter notch; a second thermocouple was located 25 mm from the back edge. The test temperature was controlled by the thermocouple located 25 mm from the root of the starter notch. The temperature was maintained for a minimum of 20 minutes before commencing the loading. For smaller specimens,  $W = 100$  mm, only one thermocouple located 25 mm from the root of the starter notch was used. Once stabilisation occurred, typically the temperature remained with  $\pm 2^{\circ}\text{C}$  during the test.



Figure 3.2: CCA test set up for specimen size  $W = 300$  mm.

The CMOD was measured using a calibrated clip gauge mounted on the specimen in accordance with ASTM E 1221. The CMOD limits, as determined above, within which the run-arrest event should occur in order that  $K_a$  can be determined, were marked before the test was started. In the case of specimens that were subjected to multiple load cycles with successively higher mouth opening displacements in accordance with ASTM E 1221, these CMOD locations were marked as well. The load was applied using a cross-head rate of 7.5 mm/min and load vs. CMOD was recorded during the test using an X-Y plotter. The load was applied until the run-arrest event was detected, both audibly and by observing an abrupt load drop. If this did not occur by the time the CMOD reached or just exceeded the upper limit, the specimen was unloaded.

The crack extension was marked by heat tinting at about 300 °C for 1 hour. The specimens were then placed in the same loading arrangement as for testing, cooled down to below -80 °C and broken in two by the wedging action of the split pin.

### 3.1.3 Selection of Crack Starter

The first phase of the work was to determine the best option for the crack starter of the CCA specimen. The ideal crack starter would initiate a brittle crack, from a notch, **after** the specimen has accumulated a threshold of stored energy. In quantitative terms, this can be expressed as the initiating stress intensity factor ( $K_o$ ) which needs to be greater than the crack arrest toughness ( $K_a$ ) of the material. (It is well known that the arrest toughness is smaller than the initiation toughness. The test specimen design and test procedure ensures that the crack run takes place in a decreasing K field that enhances crack arrest.) The following methods were explored:

- A standard chevron notch (90° included angle) in the strain age embrittled base material. This has been used in the past with reasonable success in full thickness CCA tests on ship steel plate<sup>(2)</sup>
- Brittle weld bead with an electric discharge machined (EDM) notch (Figure 3.1). This is the recommended procedure in ASTM E1221.
- A long chevron notch (20° included angle). The chevron was EDM notched with 0.010" (0.25 mm) wire and the notch was deepened by 3 mm by a 0.15 mm saw cut. The total depth was approximately 19 mm so that  $a_o/W = 0.18$  which is less than 0.3 employed in the previous two configurations. The original objective was to get a run-arrest event within the chevron and a second event in the full thickness region of the specimen during re-loading<sup>(5)</sup>.

## 3.2 Findings of CCA Test Results from the First Phase

### 3.2.1 Laterally Compressed and Aged Crack Starter

The objective here was to perform tests on instrumented specimens with in-plane dimensions based on the Crosely and Ripling approach described previously, and with an embrittled chevron notch as a crack starter. The chevron notch was machined so that its tip coincided with the center location of the pre-compressed region. A 10% thickness reduction was employed using two 25 mm diameter circular indentors. Subsequently, aging was performed at 250°C for one hour. At Fleet Technology Limited (FTL), this crack starter has been most successful in initiating running cracks in CCA specimens for ship plate<sup>(2)</sup> and HAZ's of offshore structural welds<sup>(6)</sup>.

The instrumentation consisted of strain gauges to measure dynamic response of the specimen during the crack run-arrest event and a crack gauge to measure the crack velocity. A method for triggering the high speed DA system was evaluated and two possibilities were identified. However, these could not be evaluated as brittle cracks did not initiate in any of the three specimens tested (T1 through T3). The strain gauge readings were monitored and gauges performed as expected. The details are presented in the Appendix A.

Splitting was observed approximately at the mid-thickness location, similar to what took place in the tensile tests in these CCA specimens.

Due to the failure of the laterally pre-compressed and strain age embrittled chevron notch crack starter in getting a brittle crack initiated, it is concluded this method was not successful for the base material selected for this program. (Lateral compression produces **residual** tensile stresses in the through thickness direction which will aid splitting.)

### 3.2.2 Brittle Weld Bead Crack Starter

The brittle weld bead was deposited following the procedure outlined in ASTM E 1221 Appendix X1 (Guidelines on starter notch preparation techniques) using Foxdur 500 electrodes. As the previous crack starter approach was unsuccessful, it was decided to strain gauge the first specimen (T10) in this series. In two of the three specimens tested (T11 and T12), a brittle crack initiated when the crack mouth opening displacement (CMOD) was still below the first (CMOD) limit of the load cycling adopted in the ASTM method. In these two specimens, the initiation was detected by an abrupt load drop that was audible. The stress intensity factors at initiation ( $K_0$ ) were low, the larger value was 117 MPa $\sqrt{m}$ , thus it was concluded that there was insufficient driving force for a sufficient crack run to occur.

Two of the specimens, one that produced a detectable crack run (T11) and the other that did not display a load drop (T10) during the first loading cycle, were re-loaded in a subsequent cycle up to the upper CMOD limit. (Loading beyond this limit, in order to force a run-arrest event, usually does not result in a meaningful crack arrest toughness determination<sup>(3,4)</sup>.) However, T11 was loaded in a third cycle beyond this upper CMOD limit until a maximum load plateau was realized when clearly ductile tearing would have commenced.

In-plane observations on the surface indicated crack extension into the base metal in T11 and T12, as would be expected from the drop in load in the first cycle, while in T10 only the brittle bead appeared to be cracked. However, metallography performed on T10 showed that the crack from the EDM notch in the brittle bead starter arrested immediately upon entering the base metal. This could be associated with the absence of a detectable load drop. Further, at the location of arrest for this specimen loaded up to the upper CMOD limit, there was no splitting in the mid-plane. See Appendix A3 for detailed results.

Due to the difficulty of opening up the crack after heat tinting, to expose the crack extension by the usual method of driving the wedge at a very low temperature ( $\approx -80^\circ\text{C}$ ), a rectangular specimen was cut out from the CCA specimens to include the notch and the unbroken ligament. This specimen was subjected to a three-point bend after immersion in liquid nitrogen to expose the crack extension. The heat-tinted region showed that the crack extension had occurred without any splitting in the mid-plane.

### 3.2.3 Modified Long Chevron Notch (Bonenberger) Specimen

With the difficulty in getting a crack to initiate in the base material without any embrittlement, even at  $-80^\circ\text{C}$ , plastic straining of the chevron notch tip was carried out with the objective of embrittling it further by aging. The method was different compared to lateral compression employed for the first series. Lateral compression produces **residual** tensile stresses in the through thickness direction which will aid splitting. In contrast, compressive **residual** stresses are produced in the through thickness direction after unloading the specimen as in the procedure adopted for the CCA test. Therefore, the latter method was employed by loading at room temperature for embrittling the notch tip.

The first loading of the specimens was carried out using the CMOD limits<sup>(4)</sup> calculated from the notch location ( $a_0/W = 0.18$ ) and the  $(B/B_N)$  of the chevron at this location. This is because it is not a full thickness test for the first expected run-arrest event. In one of the tests (T9) carried out at the lower temperature ( $-45^\circ\text{C}$ ), a minute load drop took place within the CMOD limits, and this was audible while the other specimen (T8) did not indicate any form of brittle crack extension when loaded to the upper limit. See Appendix A3 for detailed results.

After heat tinting to mark any crack extensions, load cycles were employed using the CMOD limits based on the full thickness specimens. It should be noted that these limits were upper bound values as any crack extension was not expected to progress beyond the full length of the chevron. These load cycles were applied with the objective of evaluating if a desired crack run could result from this extensive straining. T8 produced a small abrupt load drop within the CMOD limits while T9 had no event when loaded up to the upper limit.

The attempt at opening up the cracks by driving the wedge at very low temperature ( $\approx 80^{\circ}\text{C}$ ) in the case of T9, produced a peculiar fracture where the brittle fracture propagated on two symmetrical planes approximately at  $60^{\circ}$  to the notch plane starting from the chevron notch region. Because of this, T8 was opened up following the procedure adopted for T11.

The opened up fractures indicated splitting had occurred in the mid-plane. This was similar to the mid-plane splitting of the laterally compressed crack starter. The heat tinted region displayed an inverted parabolic shape that is similar to the fatigue crack growth that was produced in the specimens tested by Bonenberger<sup>(5)</sup>. In the current specimens, it is postulated that this crack growth occurred by a ductile mode. If this is so, the load drops that occurred during testing can be attributed to the splits. More importantly, the splitting indicates that this type of crack starter was not worthwhile pursuing further.

#### 3.2.4 Summary

Testing of two of the proposed types of specimens identified a major problem with getting a crack started in this steel. The two chevron notch starters that impose a tensile stress in the through thickness direction, due to plane strain constraints, assist in splitting at the mid-plane.

The predominant lateral tensile stress in the strain aged embrittled chevron notch is due to residual stresses arising from lateral compression. On the other hand, in the long chevron notch crack starter, the tensile stress in the through thickness direction would arise from the lateral constraint in the chevron region during loading.

The crack starter in the third type of specimen tested, i.e., the brittle bead with the EDM notch, does not impose a tensile residual stress in the through thickness orientation of the base material. During loading, in the vicinity of the EDM notch, a lateral tensile component due to plane strain constraint at the notch tip will be imposed. However, since the base material is about 4 mm below the notch tip, the influence of this tensile stress will be reduced. These arguments are supported as the crack run occurred without splitting in these specimens. The problem was that the driving force was insufficient as the initiation occurred prematurely at a low  $K_0$  (117  $\text{MPa}\sqrt{\text{m}}$ ) and therefore the crack arrested as soon as it entered the base material.

The fourth type of specimen proposed was to have a starter with a 6 mm deep EDM notch with an option for strain age embrittlement of the region containing the notch. Lateral compression was avoided due to the reason described in the previous paragraph. A second method of embrittling the notch tip is by loading the specimen with the split pin arrangement at room temperature and subsequent aging as described for the long chevron. During loading, the local notch tip region will be subject to lateral tensile stress and after unloading, a residual compressive stress will be imposed in this region. The critical issue will be the extent of strain to be applied before unloading to get the maximum effect of embrittlement and at the same time to avoid splitting during load application. This option will need different degrees of embrittlement that need to be tested and would be a major development effort.

### 3.3 CCA Test Results from the Second Phase

The objective of the next phase was to develop a starter that delays initiation to a later stage of crack mouth opening displacement (CMOD) and therefore result in a higher  $K_{IC}$ . This would also result in a higher stored energy in the specimen and therefore drive the crack a reasonable distance into the base material in order to give an arrest toughness value that is representative.

Three brittle bead welds made with Foxdur 500, Foxdur 350, and E7024 electrodes were investigated. The latter two were expected to have higher toughness compared to Foxdur 500 that was used in the first phase. As the objective was to determine the relative toughness of the weld metals in the test temperature range of the CCA tests, the specimens containing the welds were three-point bend type with an EDM notch and load vs deflection was monitored during quasi-static testing. This was a cost-effective method of making these comparisons as the CCA tests are much more expensive. The results confirmed the predictions, i.e., higher toughness starters displayed higher  $K_{IC}$ , and also indicated that Foxdur 350 and E 7024 weld metal deposits have similar toughness<sup>(7)</sup>.

Based on the above results, CCA tests were performed using starter weld beads with Foxdur 350, and E7024. For each of the weld metals, CCA specimens ( $W=300$  mm) were prepared and EDM notched with a 0.010" wire (Figure 3.1). The test results are presented in the Table 3.1.

The crack initiation behaviour of the brittle weld beads of the CCA specimens corresponded well with the observations made with the three-point bend specimens. For example, the ductile behaviour of the E7024 three-point bend specimen was reproduced in the CCA specimen tested at  $-20^{\circ}\text{C}$ . When the temperature was decreased to  $-40^{\circ}\text{C}$  brittle extension occurred. The CCA results also showed that the more ductile starter materials delayed the initiation to a latter stage in the test, further, in three of them the initiation and arrest occurred within the CMOD limits that is expected to give valid results in accordance with Crosely & Rippling<sup>(3)</sup>.

In summary, the use of higher toughness starter weld beads was successful in delaying the initiation to a later stage and resulting a much high  $K_o$  value compared to the low  $K_o$  for specimens containing the Foxdur 500 weld bead.

Table 3.1: CCA Test Results of Brittle Weld Bead Specimens.

| I.D. | Brittle weld type       | T (°C) | CMOD range <sup>(3)</sup> | $a_o/W$ | $a_a/W$ | $K_v$ , (MPa√m) | $K_o$ , (MPa√m) | $K_{Qa}$ , (MPa√m) | ASTM validity* |
|------|-------------------------|--------|---------------------------|---------|---------|-----------------|-----------------|--------------------|----------------|
| T4   | Foxdur 350              | -20    | below                     | 0.3     | 0.33    | 167             | 195             | 180                | no (D, E)      |
| T5   | Foxdur 350              | -20    | within                    | 0.3     | 0.34    | 167             | 270             | 246                | no (D, E)      |
| T6   | E7024                   | -20    | exceeded                  | 0.3     |         | 167             |                 |                    |                |
| T6   | E7024                   | -35    | exceeded                  | 0.3     |         | 172             |                 |                    |                |
| T13  | E7024                   | -40    | within                    | 0.31    | 0.35    | 173             | 251             | 226                | no (D, E)      |
| T16  | Foxdur 350              | -40    | within                    | 0.32    |         | 173             | 280             | #                  |                |
| T14  | Foxdur 350 <sup>+</sup> | -40    | below                     | 0.31    |         | 173             | 125             |                    |                |

$K_o$  initiating stress intensity factor

$K_{Qa}$  crack arrest toughness calculated linear elastic expression

<sup>+</sup> two weld passes

# cannot determine as the branched to two parts at approximately 45° to the notch after about 10 mm run from the EDM notch. The branched lengths are approximately 75 mm long.

\* Validity requirements in ASTM E1221

(A)  $W - a_a \geq 0.15W$

(B)  $W - a_a \geq 1.25(K_{Qa}/\sigma_{yd})^2$

(C)  $B \geq (K_{Qa}/\sigma_{yd})^2$

(D)  $a_a - a_o \geq 2N$

(E)  $a_a - a_o \geq (K_o/\sigma_{ys})^2/2\pi$

The condition (C) is not applied here as the specimens are full thickness non-plane strain type, while this requirement is for plane strain validity

In two of the above specimens, T5 and T13, the load drop, as a result of crack extension, was less than 15%, whereas, in the third (T16) it was substantial with a drop in excess of 50%. However, in the latter one, the crack bifurcated after about 10 mm of propagation in the mode I plane (Figure 3.3), thus an arrest toughness cannot be determined for the mode I propagation.



Figure 3.3: Surface of Specimen T16 Displaying the Crack Bifurcation, Marked by Arrow.

From load-CMOD data and crack lengths of three specimens that produced mode I brittle crack runs  $K_{Ic}$  and  $K_{Ic,ar}$  were calculated and presented in Table 3.1.  $K_{Ic,ar}$  is an arrest toughness that has to be qualified as a valid or meaningful value to be identified as a crack arrest toughness  $K_{Ic}$ .

In the Crosely & Ripling approach, the arrested crack length has to be within  $0.5W$  and  $0.8W$ . Therefore, the crack run lengths of the specimens are insufficient in the current tests as all of them are within  $0.33W$  and  $0.35W$ . However, when the crack run occurs within the specified CMOD limits, the driving force at initiation is considered sufficient and the  $K_{Ic}$  values represent a lower bound. Using this approach, therefore, for the two specimens, T5 (tested at  $-20^{\circ}\text{C}$ ) and T13 (tested at  $-40^{\circ}\text{C}$ ) the crack arrest toughness in the L-T orientation should be greater than 167 and 173  $\text{MPa}\sqrt{\text{m}}$ , respectively. This approach, therefore, suggested a specimen design with larger  $W$ , i.e., greater than 300 mm is required to determine the crack arrest value in this temperature range.

The  $K_{Ic,ar}$  value was also checked for validity in accordance with ASTM E 1221 and the crack run was also found to be insufficient. Another observation in this analysis was that  $K_{Ic}$  at 195  $\text{MPa}\sqrt{\text{m}}$  was at its limit for this specimen size, thus at higher  $K_{Ic}$ ,  $W$  at 300 mm would be insufficient. This assessment is based conditions (B) and (E) in Table 3.1.

The above analysis indicates that the specimen size at  $W = 300$  mm is too small to measure the crack arrest toughness of this plate in the L-T orientation at  $-40^{\circ}\text{C}$ . It is important to note that the small scale test performed on this steel plate indicated an NDTT of  $-35^{\circ}\text{C}$ . Published experimental data indicate that at the NDTT the crack arrest toughness is less than  $100 \text{ MPa}\sqrt{\text{m}}$  in steel. For this steel, the results indicate much higher toughness at  $-40^{\circ}\text{C}$ .

In conclusion, the CCA testing showed that the crack arrest toughness was in excess of  $173 \text{ MPa}\sqrt{\text{m}}$  for mode I extension at a test temperature of  $-40^{\circ}\text{C}$ . Analysis of this specimen design ( $W = 300$  mm) also showed that the maximum  $K_0$  that can be applied is about  $195 \text{ MPa}\sqrt{\text{m}}$  if a linear elastic crack arrest toughness is to be determined. To determine a higher crack arrest toughness, one needs to increase the specimen size.

A progress review meeting was held on the 10th of September, 1997 at the National Academy of Sciences in Washington D.C. The above findings were presented. At this meeting, the PTC decided to terminate any further CCA testing of the base material, and proceed with the weld metal with the objective of determining crack arrest toughness using reasonable size CCA specimens.

## 4. WELD METAL CHARACTERIZATION

### 4.1 Procedure Development

A flux cored arc welding (FCAW) procedure employing a double V-groove was developed with the following requirements:

- i) Minimum distortion, as compact crack arrest (CCA) and large scale (double tension) tests on distorted plate are undesirable.
- ii) Sufficient width (4 mm) at the root of the weld. This region is at the mid-thickness of the plate.

The weld had eight passes with the average heat input/pass being about 1.18 kJ/mm (30 kJ/in). The filler metal classification is E71T-1 and the specific wire had been used in naval ship construction. The heat input was similar to those adopted in shipyard practice and obtained from information provided by NSW. The filler metal Brand Name is Verti-Cor 70 (COREX). A ceramic backing bar was used to reduce removal of the root pass. The weld was made perpendicular to the rolling direction of the plate used for the base metal tests and the welded panel was 400 mm wide. A macro-photograph of the weld is presented in Figure 4.1. A weld procedure data sheet is included (Appendix A) for more details.

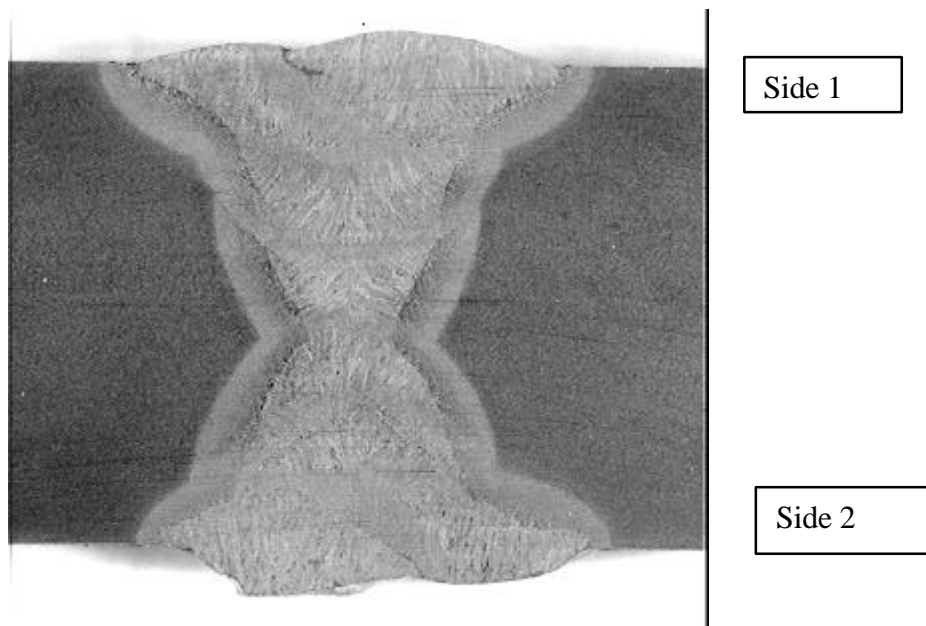


Figure 4.1: Cross-Section of the Weld, Identified as W2, Selected for Testing from Procedure Development.

## 4.2 Characterization of the Weld Metal

The following tests were performed to characterize the weld.

- i) Charpy V-notch specimens were extracted from quarter thickness locations of the weld. Tests were conducted in the temperature range  $-29^{\circ}\text{C}$  ( $-20^{\circ}\text{F}$ ) to room temperature. The specimens from Side 2 of the weld (T/4-S2) contain some of the weld root, while those from Side 1 of the weld (T/4-S1) do not include the weld root. The notch was placed in the through thickness plane at the weld centreline. Thus the slightly higher absorbed energy of the Side 1 specimens in the transition temperature range can be associated with the absence of root region weld metal (Figure 4.2).
- ii) Dynamic tear (DT) tests were performed in accordance with ASTM E604. Standard 16 mm thick specimens were machined by removing 2 mm from each surface of the 20 mm plate. This effectively removed the capping passes of the weld. The absorbed energy was determined from the load measured at the instrumented tip. The shear lip was also measured. The transition curve is presented in Figure 4.3.
- iii) Quasi-static tension tests were performed on specimens machined transverse to the weld. A reduced gage length (6 mm) was machined at the weld to ensure yielding and fracture occurs in the weld. The measured yield strength (Y.S.) is expected to be slightly elevated because of the constraining effect on the short parallel gage length of the specimen design<sup>(8)</sup>. Therefore, correction factor (1.15) was employed to determine the weld metal uni-axial Y.S. The average (from two tests) weld metal Y.S. was 523 MPa and tensile strength (T.S.) was 653 MPa. The average modulus of elasticity was 214 GPa. The T.S./Y.S ratio is 0.81. The weld metal is overmatched in terms of the yield strength with respect to the base metal by a factor of 1.08.

## 4.3 CTOD Testing and Crack Arrest Toughness Estimates

Six (BxB) CTOD specimens were tested in accordance with BS 5762. The through thickness notch was placed to sample the weld centerline. Fatigue pre-cracking was performed after lateral compression, to ensure a straight fatigue crack front<sup>(9)</sup>. (One specimen, W2-1-6, was not laterally compressed with the objective of observing the fatigue crack front shape in the presence of through thickness residual stress that is typical of this weld. In this case, the crack profile indicated a residual compressive stress in the root region indicated by less growth at the mid-thickness. This is expected in welds made under lateral restraint, as was employed in the current procedure<sup>(10)</sup>. The fatigue crack was grown for approximately 2 mm as observed on both surfaces of the specimen to give an  $a_0/W$  ratio of close to 0.3. This specimen geometry and crack depth has been adopted by Sumpter<sup>(11)</sup> for estimating crack arrest toughness from pop-in events that occur in weld metal CTOD testing.

The tests were carried out at a quasi-static rate (cross-head speed of  $0.01 \text{ mm s}^{-1}$ ) in accordance with BS 5762, at the temperatures currently selected for performing the CCA testing. These test temperatures were selected from the Charpy V-notch and dynamic tear (DT) transition curves shown in Figure 4.2 and 4.3, respectively. The CTOD results are presented in Table 4.1.

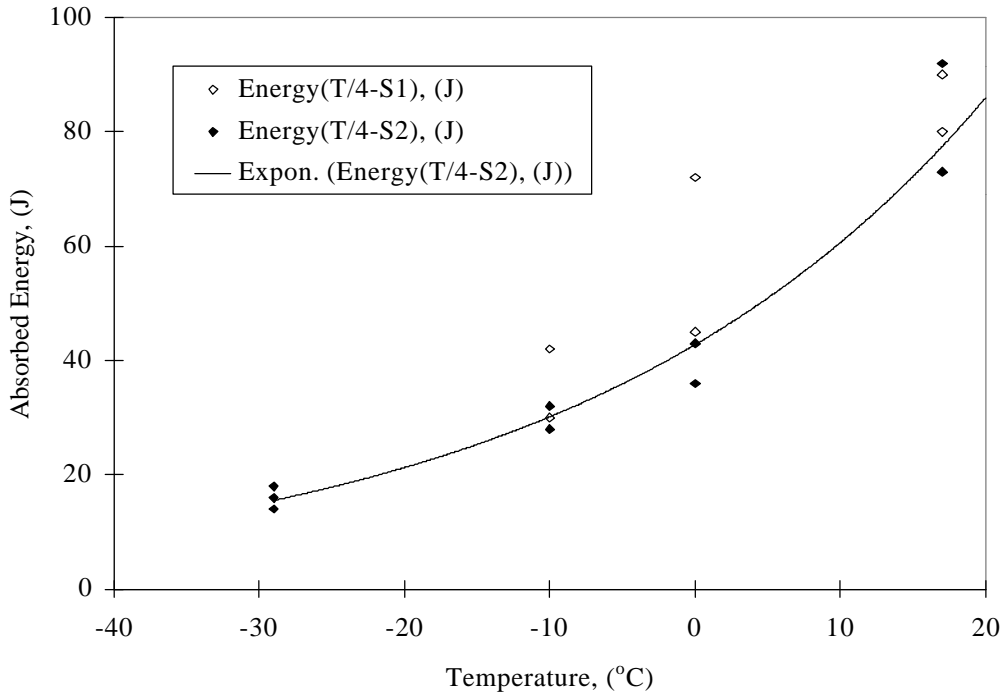


Figure 4.2: Charpy Transition Curve for Weld at (T/4) Location.

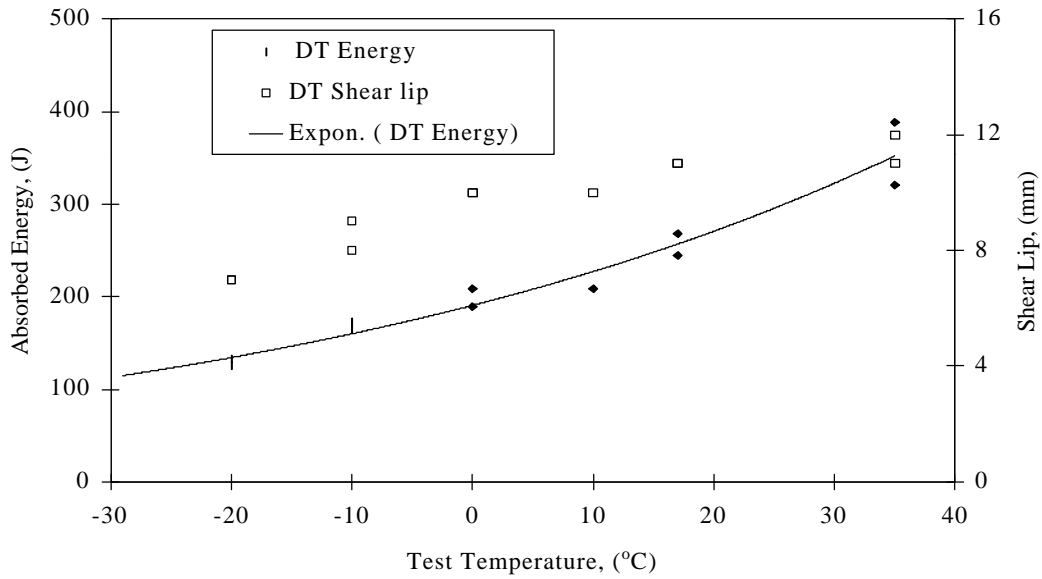


Figure 4.3: ASTM E604 DT Transition Curve for Weld Centerline.

Table 4.1: CTOD Results and Crack Arrest Estimates

| Specimen I.D. | Temp., (°C) | a/W   | Elastic CTOD (mm) | Plastic CTOD (mm) | Total CTOD (mm) | Type of Failure | K <sub>Ja</sub> (initiating load), (MPa√m) | K <sub>Ja</sub> (arrest load), (MPa√m) |
|---------------|-------------|-------|-------------------|-------------------|-----------------|-----------------|--|--|
| W2-1-2        | 0           | 0.339 | 0.027             | 0.050             | 0.077           | δ <sub>c</sub>  | 151  | 100                                    |
| W2-1-3        | 0           | 0.318 | 0.029             | 0.097             | 0.126           | δ <sub>u</sub>  | 177  | 86                                     |
| W2-1-4        | 19          | 0.326 | 0.030             | 0.109             | 0.139           | δ <sub>m</sub>  |  |  |
| W2-1-5        | 19          | 0.332 | 0.031             | 0.135             | 0.166           | δ <sub>m</sub>  |  |  |
| W2-1-6*       | 0           | 0.323 | 0.026             | 0.100             | 0.126           | δ <sub>u</sub>  | 162  | 84                                     |

\* The fatigue crack curvature limit allowed in BS 5762 was exceeded.

The initiation toughness results indicate that 0°C is in the transition range while 19°C is in the upper shelf range for this weld. The Charpy V-notch results shown in Figure 4.2 are in agreement with this assessment.

Following Sumpter’s approach the arrest toughness values were calculated for the specimens tested at 0°C. Two estimates of K<sub>Ja</sub> were made; (a) it was assumed that the crack will not experience the drop in load at arrest, in other words the crack arrest occurs under the initiating load; (b) when the crack extends the drop in load sensed by the machine is also experienced by the crack, thus here the crack arrests under the arrest load. Results from both cases are presented in Table 4.1. Considering the load drop that occurs in these tests and the associated crack extensions, the more appropriate estimate is obtained from the arrest load. Thus using this method, the crack arrest toughness at 0°C is in the range 84 to 100 MPa√m. The arrest toughness

$$J_a = \frac{3P(V_e + \Delta V)}{BW}$$

(J<sub>a</sub>) is estimated from:

where V<sub>e</sub> is the elastic CMOD, B and W are the specimen thickness and width, respectively. P was either P<sub>i</sub> or P<sub>a</sub>, (see Figure 4.4) for the two cases (a) and (b), respectively. J<sub>a</sub> was converted to K<sub>a</sub> using the standard plane strain conversion.

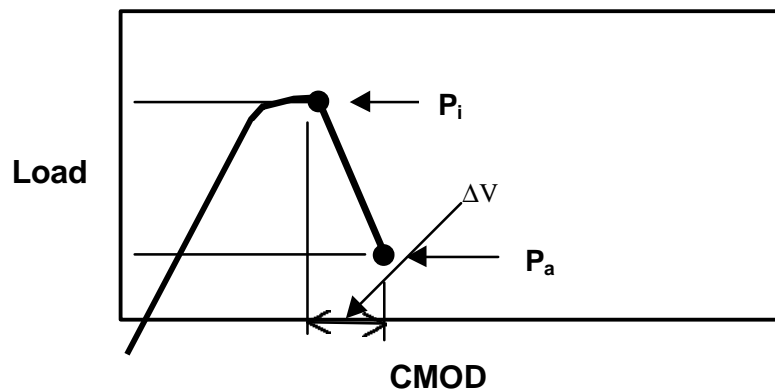


Figure 4.4: Schematic Representation of the Load-CMOD Curve to Display the Crack Initiation and Arrest in a (B x B) Specimen.

## 5. SMALL SCALE CRACK ARREST TESTS OF THE WELD METAL

### 5.1 CCA Specimen Design and Crack Starter

The anticipated crack arrest toughness ( $K_{Ic}$ ) of 100 MPa $\sqrt{m}$  at 0°C was based on results in Table 4.1. For test at this temperature, specimen size was  $W = 100$  mm following the method described in Section 3.1.1. Specimen size was proportioned as given in Figure 3.1. The weld centerline was aligned with the starter notch so that the mode I crack extension would occur as intended along the weld. The first series of tests were performed to assess the following starter options:

- Strain age embrittled chevron notch. Lateral compression was limited to 5% thickness reduction to eliminate any possibility of splitting of the base metal and because the weld metal did not have good toughness in the as welded condition. After deformation, strain aging was employed at 250°C for 1 hour. Higher compression could also lead to excessive embrittlement and give rise to premature crack initiation as described in Section 3.1.2.
- Brittle weld bead following the ASTM E1221-96 recommendations with an EDM starter notch with a root radius of 0.254 mm. Both Foxdur 350 and 500 electrodes were used.

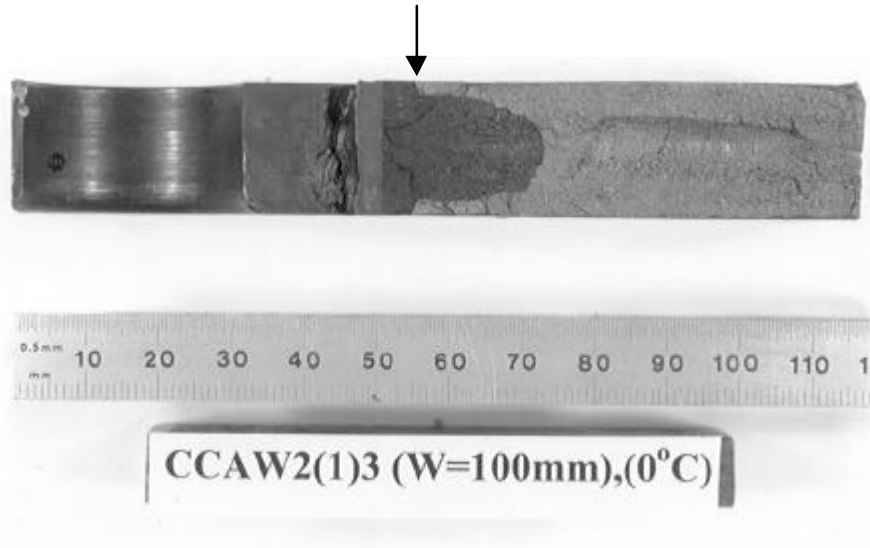
### 5.2 Findings of Starter Options for CCA Test

Specimens with two sizes ( $W = 100$  and 200 mm) were made and tested. The smaller specimens were tested at the lower temperature (about 0°C) and the larger ones at a higher temperature, closer to room temperature. The specimen sizes were designed for anticipated arrest toughness ( $K_{Ic}$ ) levels of 100 and 140 MPa $\sqrt{m}$ , respectively, at the above temperatures. The results from the CCA tests are presented in Table 5.1.

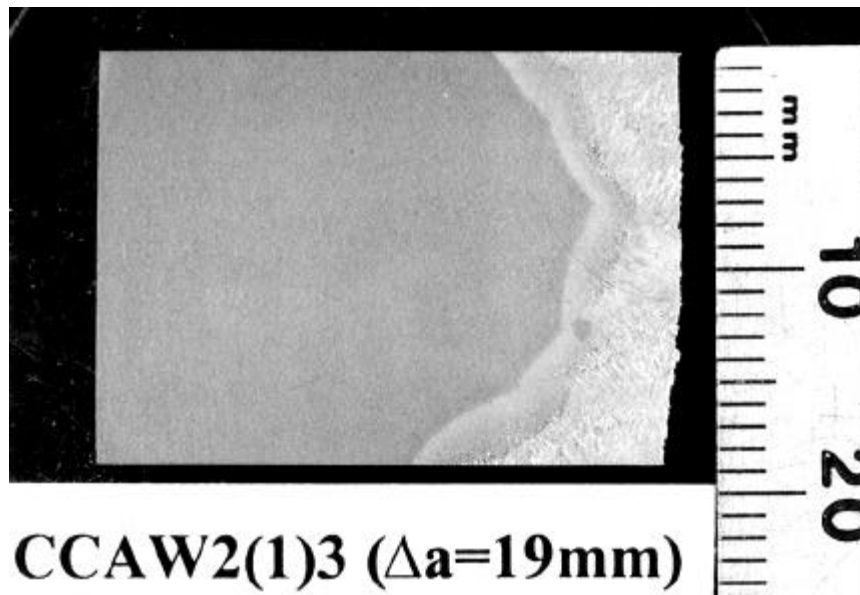
The tests were performed in a two cycle loading sequence. In the first cycle, the specimen was unloaded after reaching the CMOD level in ASTM E1221<sup>(4)</sup>, to allow for settling of the loading arrangement.

#### 5.2.1 Starter Options for the Small Specimen ( $W = 100$ mm)

The most successful crack starter for  $W = 100$  was the Foxdur 500 brittle weld bead deposited in accordance with ASTM E 1221-96, Appendix X1 (CCAW2(1)-3 and CCAW2(1)-4 in Table 5.1). This starter withstood the first loading cycle and initiated a crack run with about a 30% load drop in the second cycle at the lower CMOD limit<sup>(3)</sup>. The initiating stress intensity factor ( $K_{I0}$ ) was relatively low and the crack run was sufficient to meet the applicable validity criterion of ASTM E 1221. A marked crack run starting from the root of the EDM notch is presented in Figure 5.1(a). It shows the crack, marked by heat tinting, starts to tunnel after emerging out of the Foxdur 500 brittle weld bead. A characteristic feature of arrested cracks, frequently, is a tendency to tunnel along the specimen centreline, leaving unbroken or sheared material on the outer surfaces where there is lower constraint, especially in full thickness specimens<sup>(2)</sup>. However, no unbroken ligaments were observed in the weld metal samples tested. Figure 5.1(b) displays the cross-section at the termination of the crack and shows that it occurred at the weld centerline.



(a)



(b)

Figure 5.1: Fracture Surface Displaying a Crack Run in a Specimen with Foxdur 500 Weld Bead Starter (a). Arrow marks the bottom of the weld bead. In (b) a Cross-Section at the Location of Crack Arrest is Shown.

Using the Foxdur 350 weld bead starter (CCAW2(1)-5), crack initiation occurred after reaching the upper CMOD limit and consequently results in much higher  $K_o$ . Thus, it is inferred that this starter bead is too tough for this size of specimen and arrest toughness. In other words, the applied  $K_o$  at the upper CMOD limit is insufficient to cause initiation. By contrast, the strain age embrittled chevron displayed initiation events during the first loading cycle, indicating the lowest initiation toughness among the three starter options (CCAW2(1)-1 and CCAW2(1)-2). The low driving force of these events appears to have arrested the crack as it propagated in the chevron.

Loading was continued in a second loading cycle until a sufficient load drop took place, following the Crosley & Ripling approach<sup>(3)</sup> (with the crack running beyond the chevron before arresting). These later  $K_o$  values and the corresponding  $K_a$  values are reported in Table 5.1, (CCAW2(1)-1 and CCAW2(1)-2) and hence indicate higher  $K_o$  for the strain age embrittled starter compared to the Foxdur 500 starter. As in this two cycle loading sequence, there is no clear method of correcting for the plastic component of the CMOD, the arrest toughness values are higher than that would be obtained from the multiple load cycle sequence of the ASTM procedure.

### 5.2.2 Starter Options for the Larger Specimen (W = 200 mm)

In the two specimens that had Foxdur 500 weld as a starter bead (CCAW2(1)-6 and CCAW2(1)-7), initiation events occurred in the first cycle with negligible load drops, indicating a low toughness of the weld bead for this size of specimen and arrest toughness. One of the specimens (CCAW2(1)-6) was taken to the upper CMOD limit in the second cycle without a further run-arrest event. Therefore, in the second specimen (CCAW2(1)-7), the test was terminated after the first cycle. These findings are similar to those reported when testing the base metal with this starter option. In that case, the specimen was much larger (W = 300 mm) and tested at significantly lower temperature of -40°C.

The first specimen with the Foxdur 350 starter weld (CCAW2(2)-4) was tested at room temperature and loaded up to the upper CMOD limit with no run-arrest event. After examining the starter weld for any cracks, a repeat test was done at 10°C. A run-arrest event occurred within the CMOD range in this repeat test. The second specimen (CCAW2(1)-5) was also tested at 10°C and that too produced a run-arrest event within the CMOD range. In both cases, the load drops were small (about 10%). The crack runs were insufficient to calculate an arrest toughness value. Figure 5.2 shows the fracture surface and a cross-section to display that the crack propagated beyond the starter bead, shown by the arrow, and stopped in the weld. Therefore, the anticipated value,  $K_v = 140 \text{ MPa}\sqrt{\text{m}}$  can be considered a lower bound, i.e., the arrest toughness at 10°C is greater than  $140 \text{ MPa}\sqrt{\text{m}}$ . With these results, the CCA specimen size had to be further increased with the objective of having the capability of measuring higher arrest toughness.

Table 5.1: CCA Test Results of the Weld Metal Specimens.

| I.D.       | Crack starter           | T<br>(°C) | CMOD<br>range <sup>(3)</sup> | W,<br>(mm) | a <sub>o</sub> /W | a <sub>a</sub> /W | K <sub>v</sub> ,<br>(MPa√m) | K <sub>o</sub> ,<br>(MPa√m) | K <sub>a</sub> ,<br>(MPa√m) | K* <sub>a</sub> ,<br>(MPa√m) | ASTM<br>validity <sup>#</sup> |
|------------|-------------------------|-----------|------------------------------|------------|-------------------|-------------------|-----------------------------|-----------------------------|-----------------------------|------------------------------|-------------------------------|
| CCAW2(1)-1 | strain aged             | 0         | within                       | 100        | 0.35              | 0.542             | 100                         | 185                         | 129                         | 121                          |                               |
| CCAW2(1)-2 | strain aged             | 0         | within                       | 100        | 0.35              | 0.487             | 100                         | 157                         | 120                         |                              |                               |
| CCAW2(1)-3 | Foxdur 500              | 0         | within                       | 100        | 0.35              | 0.558             | 100                         | 137                         | 93                          | 90                           |                               |
| CCAW2(1)-4 | Foxdur 500              | -10       | below                        | 100        | 0.35              | 0.537             | 102                         | 112                         | 81                          | 79                           |                               |
| CCAW2(1)-5 | Foxdur 350              | 0         | reached                      | 100        | 0.35              |                   | 100                         |                             |                             |                              |                               |
| CCAW2(1)-5 | Foxdur 350 <sup>+</sup> | -15       | exceed                       | 100        | 0.35              | 0.675             | 103                         | 252                         | 142                         |                              | no (B, E)                     |
| CCAW2(2)-4 | Foxdur 350              | 21        | reached                      | 200        | 0.35              |                   | 138                         |                             |                             |                              |                               |
| CCAW2(2)-4 | Foxdur 350 <sup>+</sup> | 10        | within                       | 200        | 0.35              |                   | 140                         |                             |                             |                              |                               |
| CCAW2(2)-5 | Foxdur 350              | 10        | within                       | 200        | 0.35              | 0.395             | 140                         |                             |                             |                              |                               |
| CCAW2(2)-6 | Foxdur 500              | 20        | reached                      | 200        | 0.35              |                   |                             |                             |                             |                              |                               |
| CCAW2(2)-7 | Foxdur 500              | 0         | below                        | 200        | 0.35              |                   |                             |                             |                             |                              |                               |

K<sub>v</sub> anticipated crack arrest toughness

K<sub>o</sub> initiating stress intensity factor

K<sub>a</sub> full thickness crack arrest toughness calculated from linear elastic expression

K\*<sub>a</sub> crack arrest toughness after plasticity correction employed by Crosely & Ripling (Section 3.1.1)

<sup>+</sup> repeat test at lower temperature

# Validation requirements in ASTM E1221

(A)  $W - a_a \geq 0.15W$

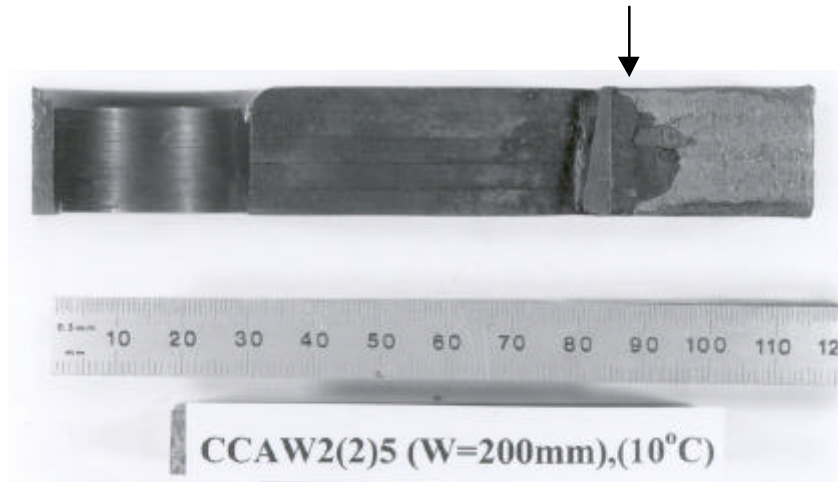
(B)  $W - a_a \geq 1.25(K_{Qa}/\sigma_{yd})^2$

(C)  $B \geq (K_{Qa}/\sigma_{yd})^2$

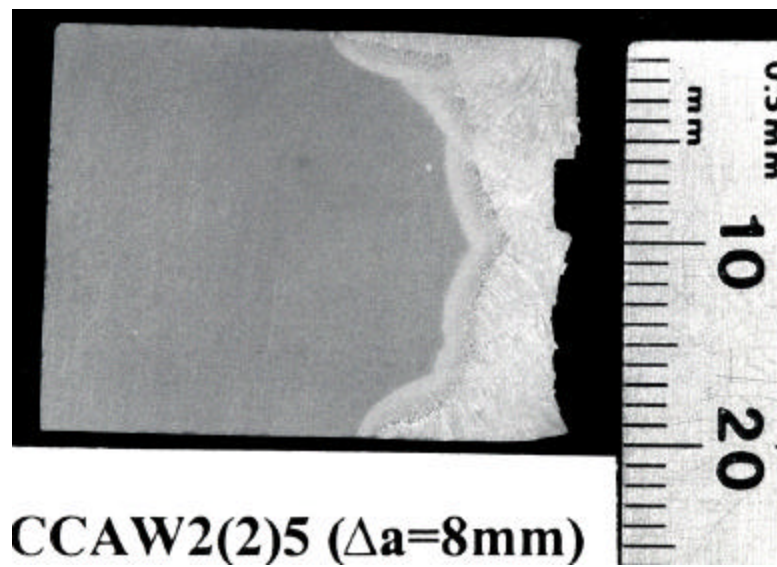
(D)  $a_a - a_o \geq 2N$

(E)  $a_a - a_o \geq (K_o/\sigma_{ys})^2/2\pi$

The condition (C) is not applied here as the specimens are full thickness non-plane strain type, while this requirement is for plane strain validity



(a)



(b)

Figure 5.2: Fracture Surface of the Second Specimen with  $W = 200$  mm (a).  
In (b) a Cross-Section at the Location of Crack Arrest is Shown.

### 5.3 CCA Testing Using Multiple Load Cycles

Multiple load cycles recommended in ASTM E1221 ensure that the plasticity component of the CMOD is reduced in determining the initiation ( $K_{I0}$ ) and arrest toughness ( $K_{Ia}$ ). As the fracture mechanics analysis is a linear elastic determination, this test method gives more accurate toughness values compared with a single load cycle procedure. The differences in the values are negligible when crack initiation takes place in the second or third cycle.

Three specimen sizes were tested;  $W = 100, 200$  and  $300$  mm. The small specimens were tested at the lower temperature while the larger ones were tested at the higher temperature since the crack arrest toughness increases with temperature. The crack starters were accordingly matched from the experiences described above.

The final series of CCA tests were performed using multiple load cycling. The specimens were instrumented with strain gauges with the objective of determining the dynamics of crack arrest. A high speed digital oscilloscope with the capability of capturing and later analyzing data that can be collected at a frequency of 2MHz was employed for these tests. The load and the strain gauge output was captured for a period of 10 ms before and after the set trigger level. At the same time, digital data from load, CMOD and the strain gauge, was acquired at a frequency of 100 Hz using a Labview system for each load cycle. The data file was over-written in each cycle until a run-arrest occurred. To have a complete record of the history of load cycles, the load-CMOD plots were recorded using a X-Y plotter. The gauges used for this purpose, both for triggering and acquiring data, were those that were placed on the two sides of the specimen as shown in Figure 3.1. For these specimens the one at the back end was not attached.

#### 5.3.1 Testing Specimens with $W = 100$ mm

Three specimens were tested and all specimens produced run-arrest events. However, in the first one (CCAW(2)-1), the load drop occurring in the 3rd cycle was insignificant, and therefore, it was cycled up to the 6th cycle without any further crack extensions. The other two produced load drops of about 30%. In CCAW(2)-1, the crack stopped at the end of the brittle bead, and appears to have deviated from a straight path. The results are presented in Table 5.2.

Figure 5.3 displays the strain measured at one side wall of a specimen in line with the root of the EDM notch (see Figure 3.1). This location is under compressive strain during loading, and when the run-arrest event takes place, a strain decrease is displayed. Figure 5.4 shows a part of the captured data in the high speed DA system during this event where the strain drops from about 1400 to about 1000  $\mu\epsilon$ . The data was captured at a frequency of 500 kHz, i.e., a period of 2  $\mu\text{s}$  between data points. Similar observations have been presented by Bonenberger<sup>(5)</sup>.

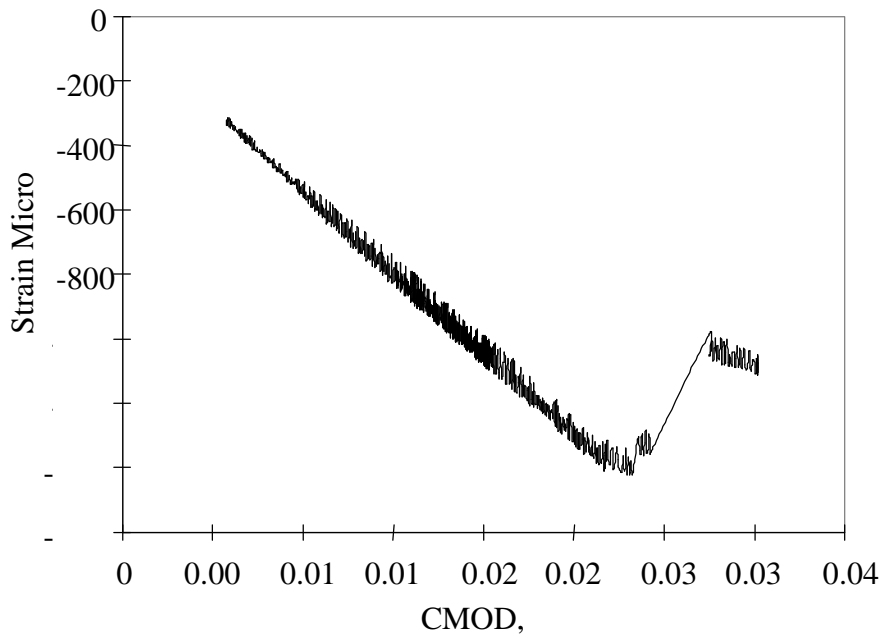


Figure 5.3: Strain-CMOD Plot for Specimen CCAW2(2)2 Tested at  $-10^{\circ}\text{C}$ .

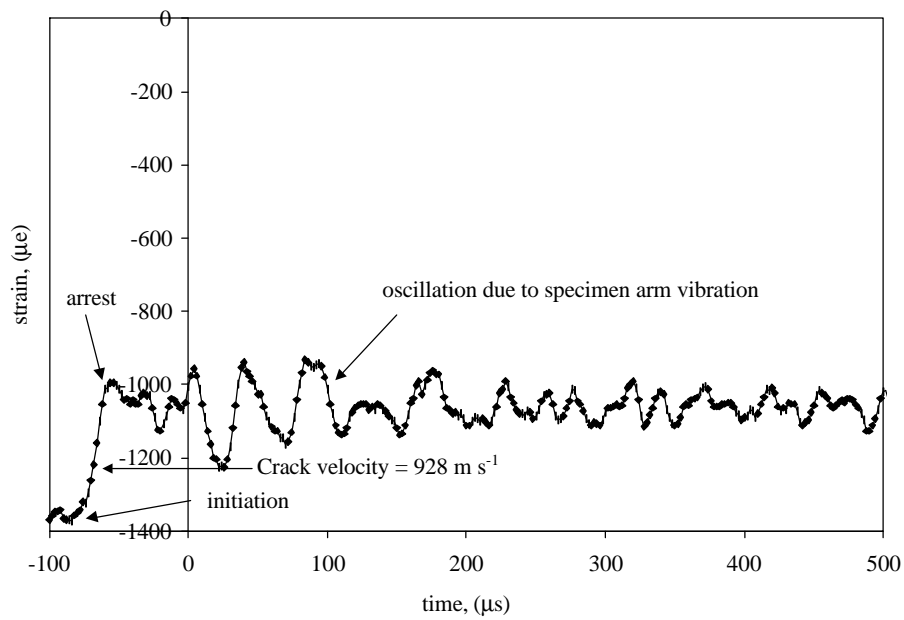
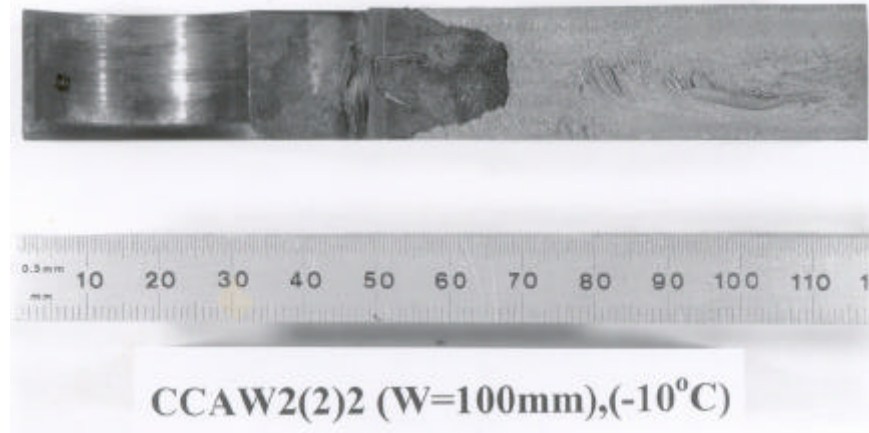
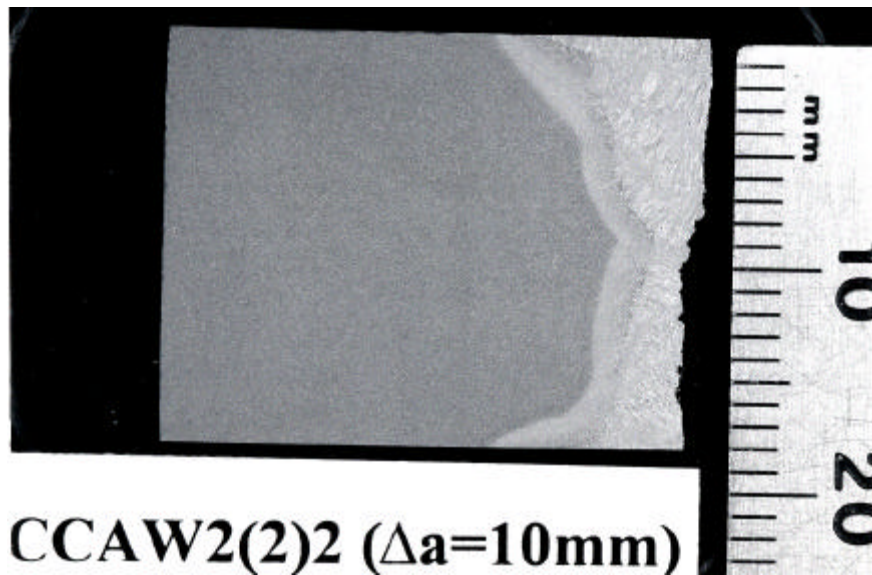


Figure 5.4: Strain-Time Plot for the above Test during and after the Crack Run-Arrest Event.

The information in Figure 5.4 is used to estimate the crack speed based on the time elapsed during the load drop at the first event and the measured crack extension. Figure 5.5(a) displays the crack, marked by heat tinting, and Figure 5.5(b) shows a cross-section at the termination. The fracture and the cross-section confirm that the crack run occurred in the weld. In Figure 5.4 the subsequent load fluctuations are a result of specimen arm vibration after crack arrest.



(a)



(b)

Figure 5.5: Fracture Surface Displaying a Crack Run in the Specimen with Results Given in Figure 5.3 and Table 5.2. In (b) a Cross-Section at the Location of Crack Arrest is Shown.

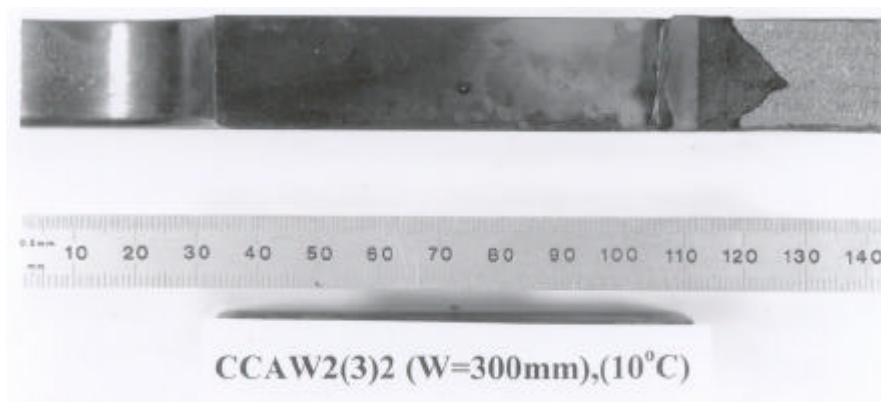
### 5.3.2 Testing Specimens with $W = 200$ mm

These specimens are repeats of the tests performed with Foxdur 500 in Table 5.1. Following the method given in ASTM E 1221, these specimens were reused by removing the starter weld and some associated material. Foxdur 350 weld was deposited and an EDM notch (root radius 0.254 mm) was placed for the re-test. Both specimens were tested at 10°C. One was continued to the last cycle as no run-arrest event took place. The second specimen produced a run-arrest event in the 4<sup>th</sup> cycle within the CMOD range resulting in a small load drop. In this way, the behaviour was similar to the two cycle tests and the crack run was insufficient to calculate an arrest toughness value. A useful  $K_0$  value was calculated for crack initiation as the plastic component of the CMOD for the corresponding load cycle is small (Table 5.2).

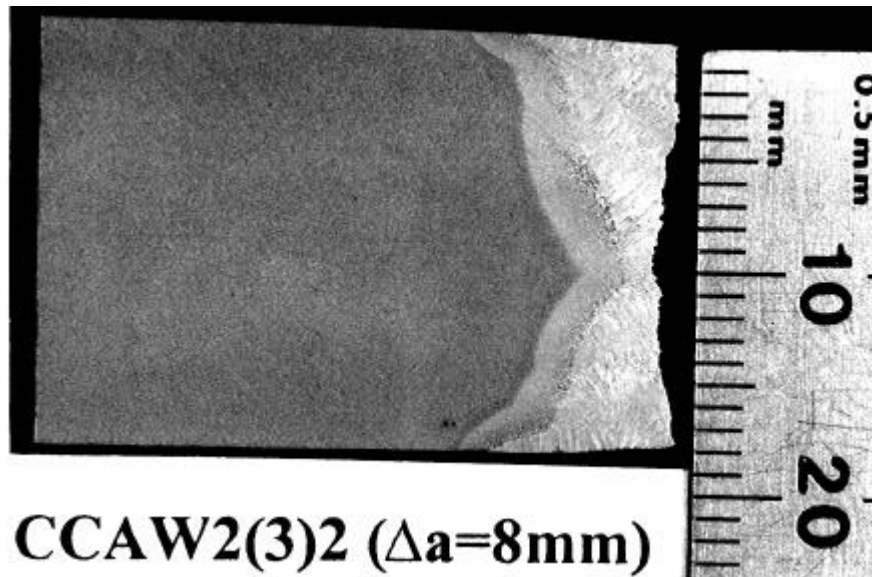
### 5.3.3 Testing Specimens with $W = 300$ mm

Four tests were performed at 10°C. In two of them, CCAW2(3)-2 and CCAW2(3)-4, a small detectable load drop (less than 10%) took place in the 2<sup>nd</sup> cycle when the CMOD was below the lower limit required to get a sufficient crack extension. In the first of these, therefore, the loading was continued up to the last (6<sup>th</sup>) cycle without any further sudden load drop and in this cycle loading was continued beyond the upper limit with no success. The second test was stopped after the 4<sup>th</sup> cycle as further crack extension did not take place. In the other two specimens, no crack extensions were detected during testing and hence the tests were continued to the 6<sup>th</sup> cycle and terminated when the upper CMOD limit was reached.

Surface observation of these specimens showed that in all of them the Foxdur 350 starter weld was cracked. The cracks, in the two specimens that did not produce any detectable load decrease, did not run straight and stopped at the end of the starter weld. One of the specimens that did result in a load drop was opened up after heat tinting and the fracture surface is presented in Figure 5.6(a). The crack stopped soon after entering the test weld.



(a)



(b)

Figure 5.6: Fracture Surface Displaying a Crack Run in Specimen with  $W = 300$  mm.  
In (b) a Cross-Section at the Location of Crack Arrest is Shown.

The  $K_v$  for this specimen size ( $W = 300$  mm) is  $172 \text{ MPa}\sqrt{\text{m}}$  and is taken as a lower bound crack arrest toughness value for the weld metal.

#### 5.4 Discussion of the Weld Metal Crack Arrest Toughness Results

The crack arrest toughness was successfully measured at  $-10^\circ\text{C}$  and  $0^\circ\text{C}$  using the CCA specimens and the values ranged from 80 to  $100 \text{ MPa}\sqrt{\text{m}}$  (Tables 5.1 and 5.2). These values were in the crack arrest toughness range estimated from the 3-point bend specimens following Sumpter's approach. At  $10^\circ\text{C}$ , the arrest toughness is inferred to be greater than  $172 \text{ MPa}\sqrt{\text{m}}$  which is the  $K_v$  estimate from the Crosley and Rippling approach of the quality assurance test procedure<sup>(3)</sup>. Although toughness is expected to increase with temperature, this rate of increase within  $10^\circ\text{C}$  envelope is rather large. The impact test results presented in Figures 4.2 and 4.3 do not indicate such an increase. On the other hand, crack arrest toughness is necessarily influenced by all the microstructural regions, tough and not so tough, sampled by the crack front<sup>(6)</sup> whereas initiation toughness is governed by the least toughness regions, even if present in small amounts.

Table 5.2: CCA Test Results of the Weld Metal (W2) Specimens (Multiple load cycles).

| I.D.                    | Crack starter | T (°C) | CMOD range <sup>(3)</sup> | W, (mm) | a <sub>o</sub> /W | a <sub>a</sub> /W | K <sub>v</sub> , (MPa√m) | K <sub>o</sub> , (MPa√m) | K <sub>a</sub> , (MPa√m) | K <sub>a</sub> <sup>*</sup> , (MPa√m) | ASTM validity <sup>#</sup> |
|-------------------------|---------------|--------|---------------------------|---------|-------------------|-------------------|--------------------------|--------------------------|--------------------------|---------------------------------------|----------------------------|
| CCAW2(2)-1 <sup>+</sup> | Foxdur 350    | 0      | within                    | 100     | 0.35              |                   | 100                      | 135                      |                          |                                       |                            |
| CCAW2(2)-2              | Foxdur 350    | -10    | within                    | 100     | 0.35              | 0.517             | 102                      | 132                      | 107                      | 103                                   | no (D)                     |
| CCAW2(2)-3              | Foxdur 350    | -10    | within                    | 100     | 0.35              | 0.483             | 102                      | 122                      | 99                       | 96                                    | no (D)                     |
| CCAW2(2)-6R             | Foxdur 350    | 10     | exceed                    | 200     | 0.36              |                   | 140                      |                          |                          |                                       |                            |
| CCAW2(2)-7R             | Foxdur 350    | 10     | within                    | 200     | 0.36              |                   | 140                      | 218                      |                          |                                       |                            |
| CCAW2(3)-1 <sup>+</sup> | Foxdur 350    | 10     | reached                   | 300     | 0.35              |                   | 172                      |                          |                          |                                       |                            |
| CCAW2(3)-2              | Foxdur 350    | 10     | below                     | 300     | 0.35              | 0.385             | 172                      | 204                      |                          |                                       |                            |
| CCAW2(3)-3 <sup>+</sup> | Foxdur 350    | 10     | reached                   | 300     | 0.35              |                   | 172                      |                          |                          |                                       |                            |
| CCAW2(3)-4              | Foxdur 350    | 10     | below                     | 300     | 0.35              |                   | 172                      |                          |                          |                                       |                            |

K<sub>v</sub> anticipated crack arrest toughness

K<sub>o</sub> initiating stress intensity factor

K<sub>a</sub> full thickness crack arrest toughness calculated from linear elastic expression

K<sub>a</sub><sup>\*</sup> crack arrest toughness after plasticity correction employed by Crosely & Ripling (3.1.1)

<sup>+</sup> crack stopped at the end of the starter weld as it did not run straight

R repeat tests from (2)-6 and (2)-7 with Foxdur 350

# Validation requirements in ASTM E1221

(A)  $W - a_a \geq 0.15W$

(B)  $W - a_a \geq 1.25(K_{Qa}/\sigma_{yd})^2$

(C)  $B \geq (K_{Qa}/\sigma_{yd})^2$

(D)  $a_a - a_o \geq 2N$

(E)  $a_a - a_o \geq (K_o/\sigma_{ys})^2/2\pi$

The condition (C) is not applied here as the specimens are full thickness non-plane strain type, while this requirement is for plane strain validity

In order to rule out any effects of variations in toughness of the weld panel made for machining the largest specimens (panel 3) the following tasks were performed.

- Small specimens ( $W = 100$  mm) were cut out from the two large specimens CCAW2(3)-1 and CCAW2(3)-3 where the crack stopped at the end of the starter weld and test were done at  $-10^{\circ}\text{C}$ .
- Hardness traverses were carried out on weld cross-sections presented in Figures 5.1(b), 5.2(b), 5.5(b) and 5.6(b).
- Microstructural evaluation was also done on the above cross-sections.

In one CCA specimen (CCA2(3)-5<sup>+</sup>), the crack initiation occurred in the first cycle with insufficient driving force, while in the other (CCA2(3)-6), a successful crack propagation and arrest took place. These two results are presented in Table 5.3 and show the crack arrest toughness at  $-10^{\circ}\text{C}$  is in the scatter band of the values from previous weld panels. As these specimens were instrumented, it was possible to capture the propagation-arrest event with the high speed DA system and from a strain-time plot similar to the one presented in Figure 5.4, the estimated crack speed was  $750\text{ m s}^{-1}$ .

Individual Vickers hardness readings ( $S_{\text{kg}}$ ) obtained from traverses made at three locations, with respect to specimen thickness, on above weld cross-sections are presented in Table 5.4. The “mean” value thus represents an average for the cross-section and indicates some differences. In one specimen, CCA2(2)-5, the crack run occurred close to the upper CMOD limit and the other, CCA2(3)-2, was taken beyond the upper limit after the crack run occurred in the 2<sup>nd</sup> cycle. It is likely that the higher hardness may be due to strain hardening as these cross-sections would be within the plastic zone associated with the crack tip.

The results from the microstructural evaluation are presented in Table 5.5. The proportion of the various regions across the thickness at the weld centerline does not indicate any significant differences in the three weld panels made for extracting CCA specimens.

Figure 5.7 shows all of the results, for both single cycle and multiple cycle CCA tests. The two values from single cycle tests at  $0^{\circ}\text{C}$  that display slightly higher arrest toughness is from the strain age embrittled starter (Table 5.1) where valid crack extensions took place after loading well past the lower CMOD limit. By contrast, the Foxdur 500 starter, produced initiation early and  $K_a$  from these specimens have no difference with respect to the results from multiple load tests. The  $K_a$  data points at  $10^{\circ}\text{C}$  have upward arrows to indicate that they are lower bound estimates.

Table 5.3: CCA Test Results from Specimens Extracted from the W = 300 mm size made from weld panel 3.

| I.D.                    | Crack starter | T (°C) | CMOD range <sup>(1)</sup> | W, (mm) | a <sub>o</sub> /W | a <sub>a</sub> /W | K <sub>v</sub> , (MPa√m) | K <sub>o</sub> , (MPa√m) | K <sub>Qa</sub> , (MPa√m) | K <sub>a</sub> <sup>*</sup> , (MPa√m) | ASTM validity <sup>#</sup> |
|-------------------------|---------------|--------|---------------------------|---------|-------------------|-------------------|--------------------------|--------------------------|---------------------------|---------------------------------------|----------------------------|
| CCAW2(3)-5 <sup>+</sup> | Foxdur 500    | -10    | below                     | 100     | 0.35              |                   | 102                      |                          |                           |                                       |                            |
| CCAW2(3)-6              | Foxdur 500    | -10    | within                    | 100     | 0.35              | 0.53              | 102                      | 124                      | 94                        | 92                                    |                            |

K<sub>v</sub> anticipated crack arrest toughness

K<sub>o</sub> initiating stress intensity factor

K<sub>a</sub> full thickness crack arrest toughness calculated from linear elastic expression

K<sub>a</sub><sup>\*</sup> crack arrest toughness after plasticity correction employed by Croseley & Ripling (Section 3.1.1)

# Validation requirements in ASTM E1221

(A)  $W - a_a \geq 0.15W$

(B)  $W - a_a \geq 1.25(K_{Qa}/\sigma_{yd})^2$

(C)  $B \geq (K_{Qa}/\sigma_{yd})^2$

(D)  $a_a - a_o \geq 2N$

(E)  $a_a - a_o \geq (K_o/\sigma_{ys})^2/2\pi$

The condition (C) is not applied here as the specimens are full thickness non-plane strain type, while this requirement is for plane strain validity.

Table 5.4: Vickers Hardness Results on Weld Cross Sections Extracted from CCA specimens

| I.D.       | W, (mm) | VHN <sub>5KG</sub> |         |             |        |
|------------|---------|--------------------|---------|-------------|--------|
|            |         | Side 1             | Center  | Side 2      | Mean   |
| CCAW2(1)-3 | 100     | 192,188            | 212     | 183,183,188 | 191±11 |
| CCAW2(2)-5 | 200     | 229,236,210        | 221,223 | 212,216,223 | 221±9  |
| CCAW2(2)-2 | 100     | 206,203            | 204     | 201,199,192 | 201±5  |
| CCAW2(3)-2 | 300     | 219,216,225        | 203     | 210,214     | 215±8  |

Table 5.5: Proportion of the Categories of Microstructure Close to the Weld Centerline of the Above Cross-sections

| I.D.       | Non-recrystallized | Recrystallized |            |
|------------|--------------------|----------------|------------|
|            | Columnar, (%)      | Coarse*, (%)   | Fine+, (%) |
| CCAW2(1)-3 | 55                 | 15             | 30         |
| CCAW2(2)-5 | 62                 | 12             | 26         |
| CCAW2(2)-2 | 62                 | 13             | 25         |
| CCAW2(3)-2 | 49                 | 10             | 41         |

\* greater than 50 $\mu$ m

+ less than 50 $\mu$ m

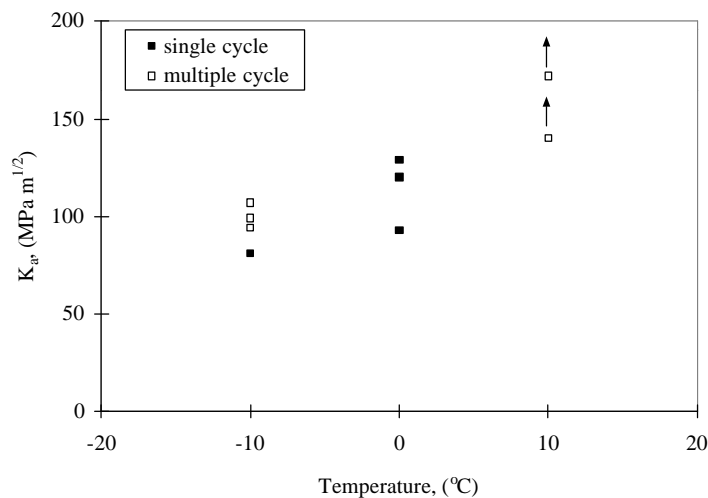


Figure 5.7: Crack Arrest Toughness vs Temperature for the Weld Metal.

Full thickness CCA tests showed that both types of crack starters were successful; strain age embrittled Chevron notch and the use of a brittle bead weld deposited using Foxdur 500 and 350 types. The brittle bead weld method follows ASTM E1221 guidance. In this case, the findings showed the importance of tailoring the starter weld toughness ( $K_o$ ) to the arrest toughness ( $K_a$ ) to be measured. As the arrest toughness increased, the stored energy in the CCA specimen need to be increased for a single run-arrest event to occur leading to a successful test. The Foxdur 500 is good for lower levels of arrest toughness and the 350 is required when the arrest toughness gets higher.

Figure 5.8 displays the relation between the crack arrest toughness and initiating toughness to demonstrate the above. Results from work done in a parallel project contracted by the Canadian DND for a Canadian Standards Association (CSA) specification 350 WT base material are also included in this figure to provide a broad picture. The data points for this figure only include results from multiple loading cycle test as it is important to remove any plastic component of the CMOD at crack initiation. It is also important to keep in mind that following the Crosely and Ripling approach the specimen size has to be increased as well to successfully measure higher arrest toughness. This fits with the requirement of a larger stored energy inferred in Figure 5.8.

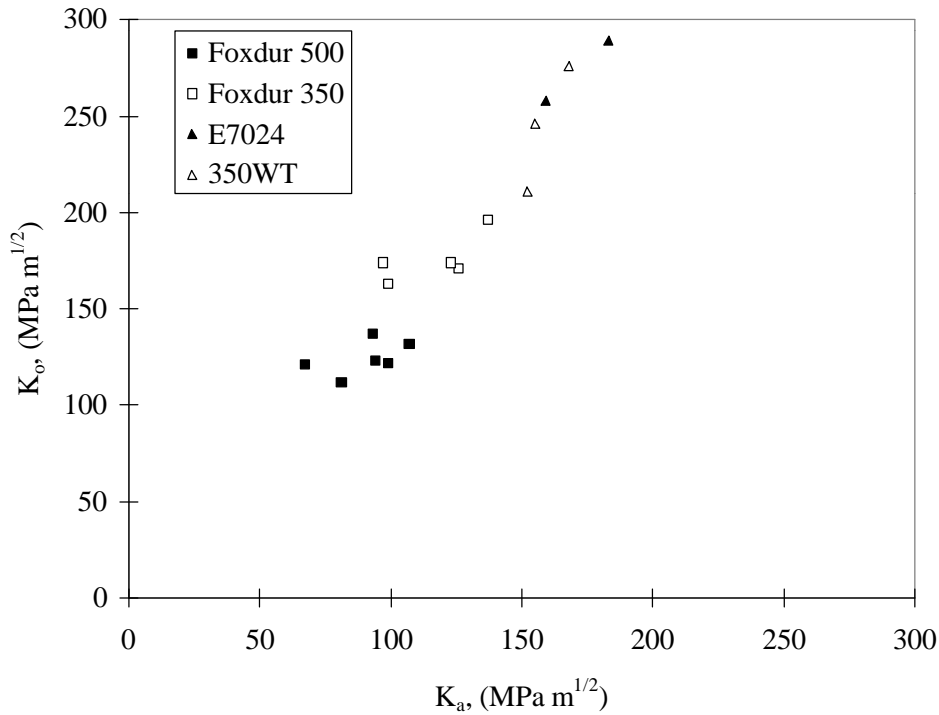


Figure 5.8: Relation Between Crack Arrest Toughness and Initiating Toughness.

Figure 5.9 shows some useful results in selecting starter weld beads for CCA testing. The weld beads cover a large range of stored energies as inferred from the range of initiation toughness values. The figure also adds information on the toughness variability with temperature. Foxdur 500 displays negligible effect on toughness for the temperature range evaluated.

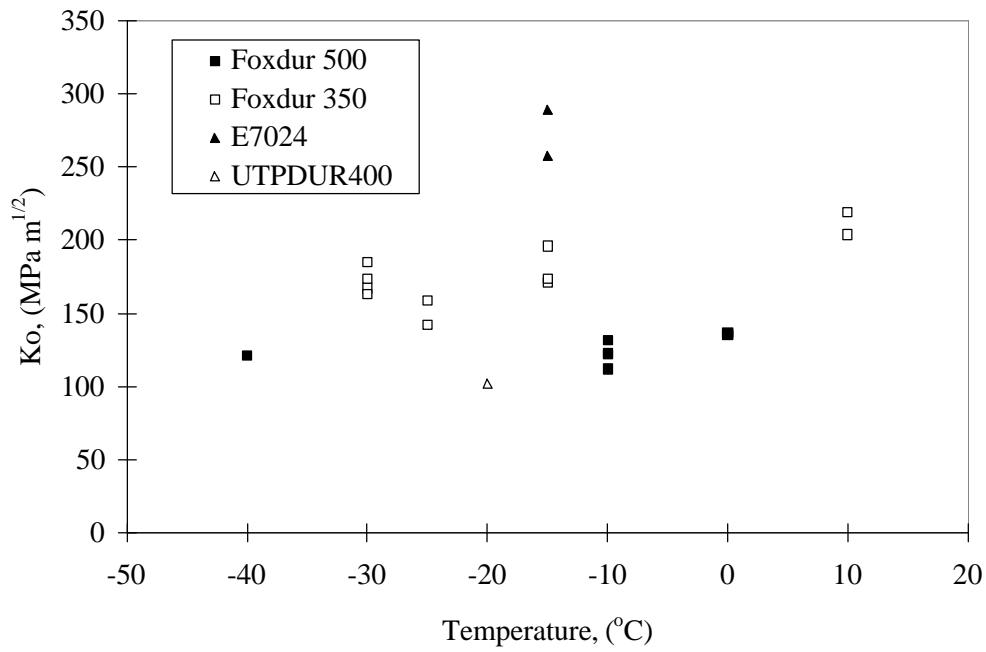


Figure 5.9: Stress Intensity Factor at Initiation vs Test Temperature for Various Brittle Weld Starters.

## 6. REFERENCES

- (1) E.J. Ripling: Communication to ASTM Full Thickness Crack Arrest Toughness Working Group, Oct., 1995
- (2) L.N. Pussegoda, L. Malik and J. Morrison: "Measurement of Crack Arrest Fracture Toughness of a Ship Steel Plate", Jour. of Testing & Evaluation, v.26, 1998, pp. 187-197.
- (3) P.B. Crosely and E.J. Ripling: "A Quality Control Test for Selecting Materials to Arrest Fast-running Full-thickness Cracks", JTEV, V.18, 1990, pp. 396-400.
- (4) ASTM E1221-96: Standard Test Method for Determining Plane-Strain Crack Arrest Toughness,  $K_{Ia}$ , of Ferritic Steels.
- (5) R.J. Bonenberger: "Development of a Chevron-Notched Crack-Arrest Specimen" Ph.D Thesis, University of Maryland, (1994)
- (6) L. Malik, L.N. Pussegoda, B.A. Graville, and W.R. Tyson: "Crack Arrest Toughness of a Heat Affected Zone Containing Local Brittle Zones", Transaction of the ASME, v.118, 1996, pp. 292-299.
- (7) 4th Quartely Report: "Crack Arrest Toughness of Steel Weldments" (SR-1384), Contract No. DTCG23-96-C-E 01061, September 23, 1997.
- (8) R.M. Denys and T. Lefevre: "Weld Metal Yield Strength Testing of Girth Welds", Final Report (Contract No. PR-202-9326), Prepared for The Welding Supervisory Committee of PRC International, Arlington, VA.
- (9) O.L. Towers: "Procedures for Fatigue Cracking Fracture Toughness Test Pieces, with Particular Reference to Weldments", The Welding Institute Research Bulletin, April 1982, pp. 112-120.
- (10) M.G. Dawes and B. Hayes: "Fracture Mechanics Compact Crack Arrest Testing of Weldments", Presented at Seminar on "Crack arrest concepts for failure prevention", TWI, Cambridge, U.K., Sept. 1995.
- (11) J.D.G. Sumpter: "Pop-in and Crack Arrest in HY80 Weld", Fatigue. Fract. Engng. Mater. Struct., v14, (1991), pp. 565-578

## **PART II – LARGE SCALE TESTS**

**Prepared by:**

**Dr. Stephen J. Kennedy and Mr. Yongqing Han  
Department of Civil and Environmental Engineering  
Carleton University, Ottawa, K1S 5B6**

### **ABSTRACT**

Flaws are always likely to exist in welded structures and are the source of the cracks that cause brittle fracture and failure, if the temperature and loading conditions are such that they cause unstable crack growth. The provision of tough steel with known crack arrest toughness characteristics is an effective method to prevent brittle fracture.

The main objective of this portion of the work was to conduct large-scale double tension tests to obtain Crack Arrest Toughness (CAT) data for correlation with the corresponding data from the full thickness Compact Crack Arrest (CCA) tests conducted according to a draft ASTM standard. Successful correlation would allow engineers to conduct relatively inexpensive tests to obtain representative toughness data, which in turn, would allow the prediction of crack propagation and crack arrest for ship and maritime structures.

Starter plate tests with double-side face grooves were developed to determine the conditions (starter load and temperature range) required to initiate a crack that had sufficient energy to propagate into the main plate of a large-scale double tension test section. The large-scale double tension test apparatus, the test specimen, the instrumentation and the test procedure were developed to accommodate a large-scale section measuring 500 mm by 2000 mm that could be subjected to loads up to 3500kN and temperatures of interests as low as  $-100^{\circ}\text{C}$ . Methods for determining the crack arrest toughness for the material in a variable stress intensity field with a temperature gradient were developed.

## **PART II – LARGE SCALE CRACK ARREST TESTS**

### **7. CRACK ARREST TESTS AND EVALUATION OF TOUGHNESS**

There are two principal design philosophies for the avoidance of brittle fracture:

- to design the structure such that crack initiation is prevented; and /or
- to specify fracture tough steels and to design the structure with details that will arrest brittle cracks.

The first requires considerable effort and does not guarantee that the brittle fracture will not occur during the service life of the structure. This is especially true for continuous all-welded steel structures, in which weld flaws, residual stresses, embrittled regions and stress concentrations exist and will be the source of fatigue cracks. Unexpected impact forces may also cause ruptures and tear cracks in the steel structures.

The provision of fracture-tough steels with appropriate structural detailing is the most practical means to minimize the number of cracks and to arrest the propagating cracks. This requires an understanding of fatigue, brittle fracture and methods for evaluating the crack arrest toughness of steel for conditions associated with the structure service life (varying temperatures and tensile stress fields). The crack arrest toughness can only be evaluated by the tests (small-scale tests or large-scale tests). A summary of these tests is presented in the following sections.

#### **7.1 Small-Scale Crack Arrest Tests**

The main objective of small-scale crack arrest tests is to provide a standardized and inexpensive method, which can be used to characterize the crack arrest toughness of a material. The most widely used tests are the Charpy-V-Notch test (CVN), the Nil-Ductility-Temperature Transition test (NDTT), the Dynamic Tear test (DT), the Double Cantilever Beam test (DCB), the Tapered Double Cantilever Beam test (TDCB) and the Compact Crack Arrest Test (CCA). The description of the test specimen and discussion for each type of test is given in Table 7.1 and Figure 7.1, respectively.

The CVN, NDTT and DT give an indirect measure of crack arrest toughness in the form of a temperature transition curve usually expressed in terms of absorbed energy versus temperature. Data from the remaining tests (load, strains and displacements) can be used to calculate the stress intensity factor at the arrest point (crack arrest toughness) using basic fracture mechanics.

Of this group, the CCA test has been standardized by ASTM since it is the most reliable and reproducible, and is not as affected as are the alternative test methods by the dynamics of crack propagation. The objective of CCA tests was to have the opportunity of applying fracture mechanics approach for crack arrest in a structural situation, under plane strain conditions (ASTM E 1221-96).

## 7.2 Large-Scale Crack Arrest Tests

Large-scale tests have been developed to study crack arrest toughness in a structural situation.

Note: The large-scale tests are generally conducted in conjunction with less expensive small-scale tests to establish correlations between these two. Of this group, the double tension test is considered to be the best for determining crack arrest toughness since:

- the dynamic effects and influence of the starter plate load are minimized;
- the main plate load (applied stress) and hence the stress intensity factor field can be controlled; and
- the test can be conducted under either isothermal temperature conditions or temperature gradient conditions.

A summary of five different large-scale test types including the geometry of the test specimen, the test description, the loading condition, the measurements and the data evaluation are given in Table 7.2 and Figure 7.2.

**Table 7.1: Summary of Small Scale Tests**

| Type of Test   | Description of Test   | Measurement and Discussion   |
|--|---|--|
| Charpy-V Notch (CVN) (ASTM E23-96)   | <ul style="list-style-type: none"> <li>• A pendulum mechanism is used to strike the test specimen illustrated in Figure 7.1(a) with a known mass and velocity to determine the energy required to cause brittle fracture.</li> <li>• A series of tests at different temperatures must be conducted to determine the transition temperature (temperature which initiates brittle fracture mode).</li> </ul>  | <ul style="list-style-type: none"> <li>• Although the test is fast, simple and relatively inexpensive to conduct, the energy absorbed by test specimen (for all specimens failed by brittle fracture) only gives a measure of the crack arrest toughness. Some empirical relationships have been developed but may not be applicable to all load cases.</li> <li>• The percentage of the fracture surface in shear and the corresponding lateral expansion at the specimen impact gives a measure of brittleness.</li> </ul> |
| Nil-Ductility Transition Temperature Test (NDTT) (ASTM E208)                   | <ul style="list-style-type: none"> <li>• Impact loads from a drop test are applied to a standard test specimen supported by the apparatus shown schematically in Figure 7.1(b). A brittle weld bead with a saw cut made on the face opposite of the face being struck is designed to initiate a crack on impact.</li> <li>• Maximum deformation is limited and tests are conducted at various temperature until crack propagation occurs.</li> </ul>  | <ul style="list-style-type: none"> <li>• Determination of lowest temperature when crack propagation in base metal does not occur.</li> </ul>   |
| Dynamic Tear Test (DT) (ASTM E604)   | <ul style="list-style-type: none"> <li>• Impact loads from a drop test are applied to standard specimens with dimension and the sharp notch geometry shown in Figure 7.1(c). Tests are conducted on specimens at various temperatures and the kinetic energy to cause fracture is recorded.</li> </ul>  | <ul style="list-style-type: none"> <li>• The measured energy versus temperature gives a temperature transition curve and serves as qualitative test to crack arrest toughness.</li> </ul>  |
| Double Cantilever Beam Test (DCB) & Tapered Double Cantilever Beam Test (TDCB) | <ul style="list-style-type: none"> <li>• The geometry of various types of test specimens are illustrated in Figure 7.1(d) and (e). There are no standard dimensions for either the DCB or the TDCB tests.</li> <li>• Blunt notches, chevron notch or fatigue cracks are used for crack initiation in both types. Face grooves are used to direct the crack growth along a known path, under plane strain.</li> <li>• A static load is applied to open and propagate a crack within the specimen. The crack mouth opening displacement is measured by clip gauge.</li> </ul> | <ul style="list-style-type: none"> <li>• The stress intensity factor at initiation and crack arrest toughness can be calculated from the data measured during the test.</li> <li>• This test method has not been standardized, as it may be susceptible to dynamic effects and as tests have shown unstable crack paths that tend to branch.</li> </ul>  |
| Compact Crack Test (CCA) (ASTM E1221-88/96)                                    | <ul style="list-style-type: none"> <li>• The geometry of the CCA test specimen is illustrated in Figure 7.1(f).</li> <li>• A brittle weld bead may be placed notch tip to promote crack initiation. Face grooves generally produce uniform crack fronts and stable crack path.</li> <li>• CMOD result from a wedge loading with split pins and is measured with a clip gauge.</li> </ul>  | <ul style="list-style-type: none"> <li>• Crack arrest toughness can be calculated as function of crack length and CMOD as defined by ASTM E1221-88/96. This test has been standardized since crack path is relatively stable. The dynamic effects have been determined to be small relative to other tests. The CCA gives the lower bound value of <math>K_{Ia}</math>.</li> </ul>   |

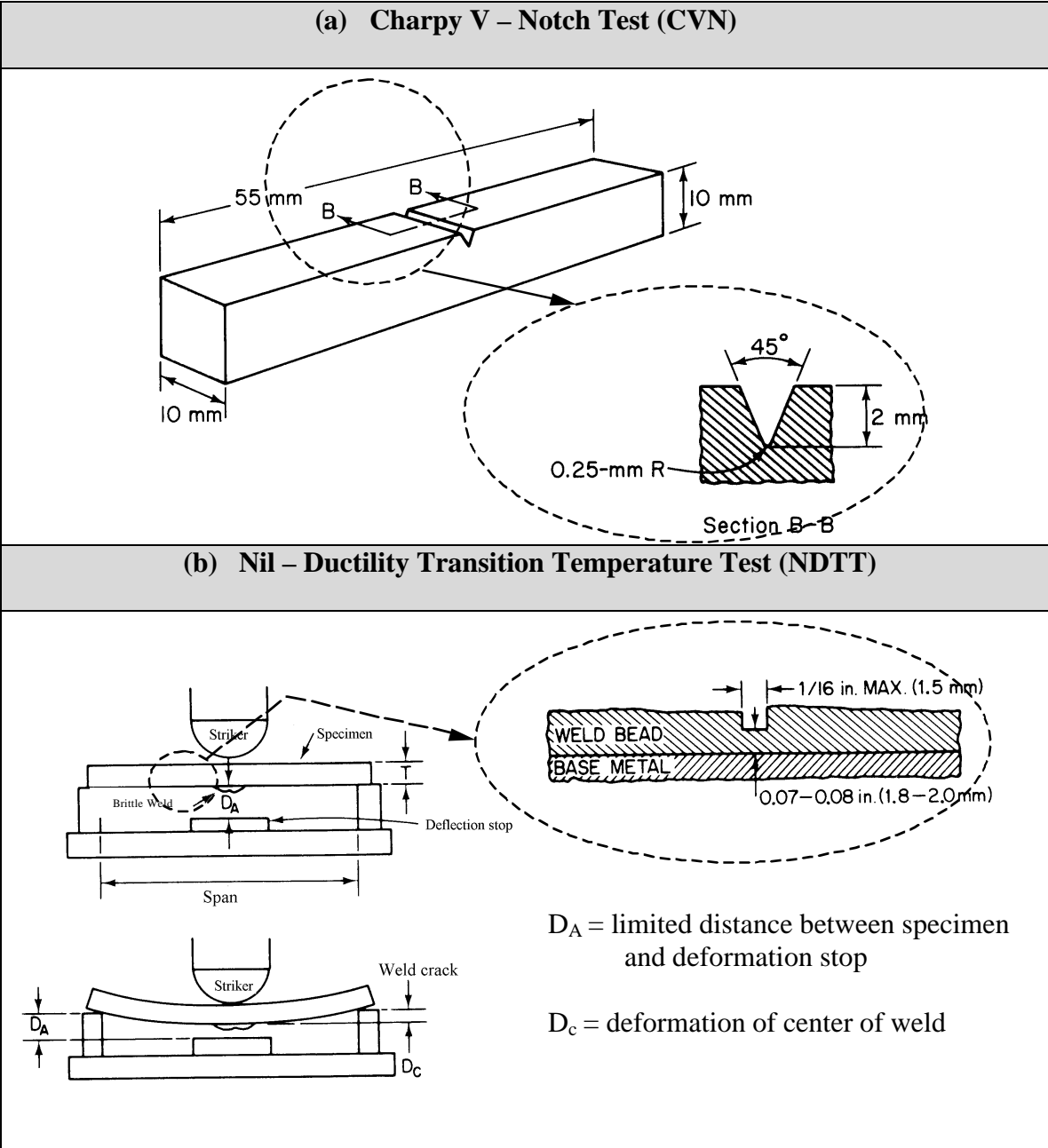


**Figure 7.1: Small-Scale Test Types**

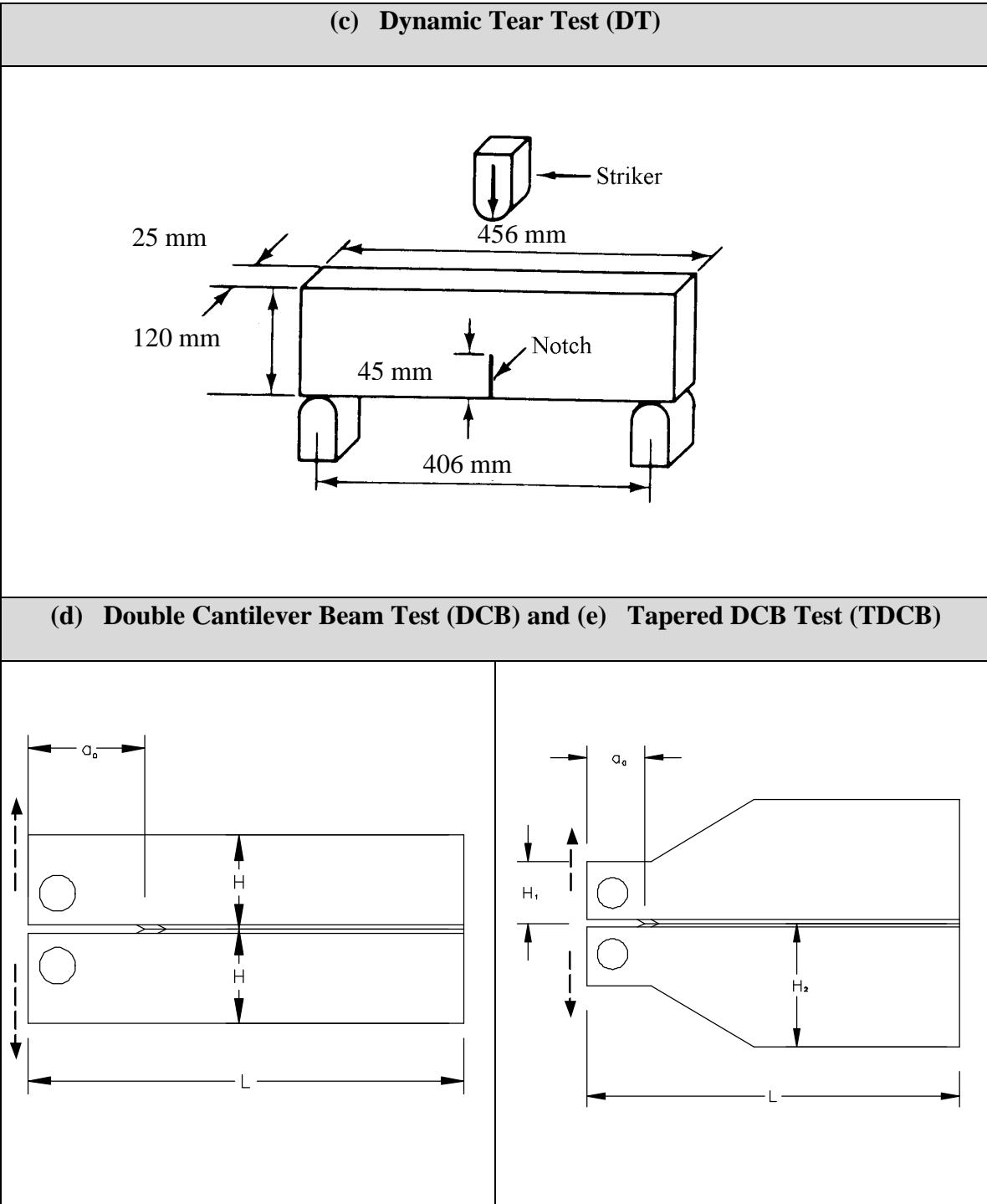


**Figure 7.1 (Cont'd): Small-Scale Test Types**

(f) Compact Crack Arrest Test (CCA)

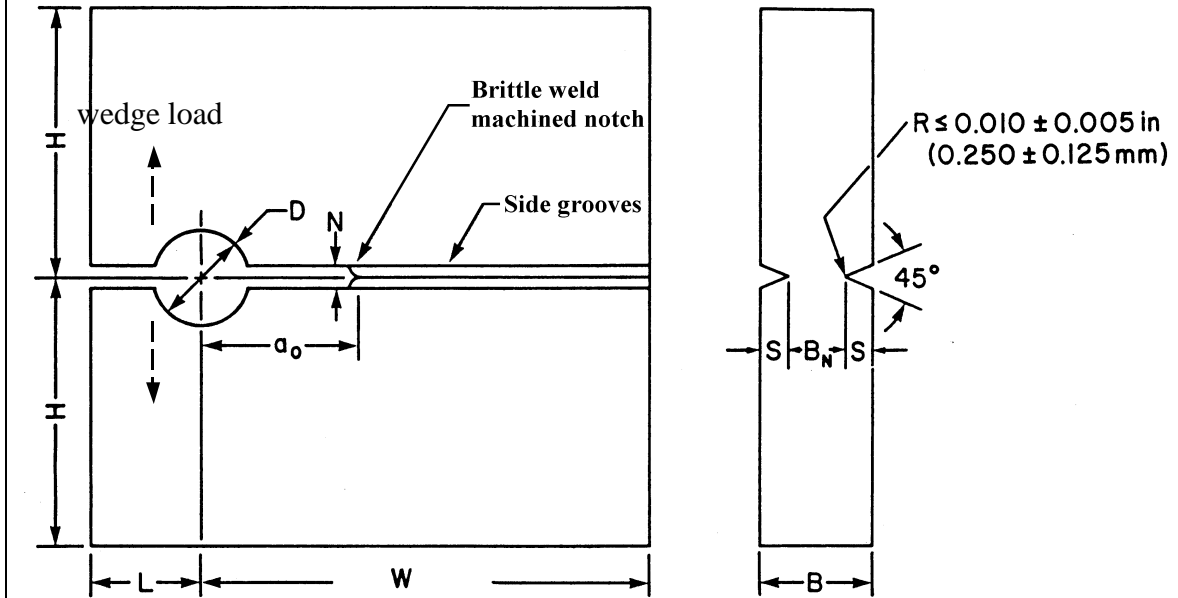
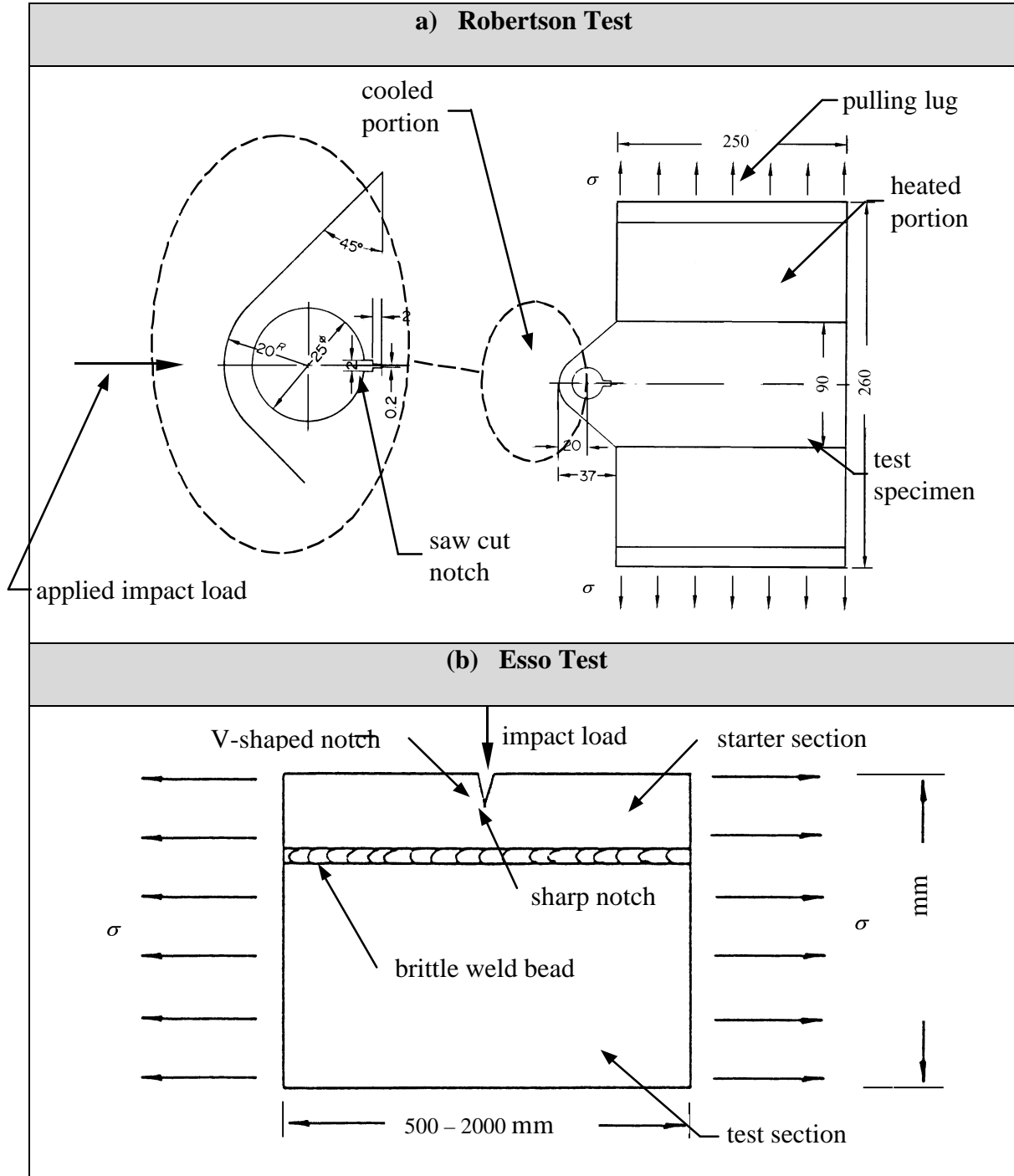


Figure 7.1 (Cont'd): Small-Scale Test Types

**Table 7.2: Summary of Large Scale Tests**

| Type of Test                   | Description of Test  | Measurement and Discussion   |
|--------------------------------|--|--|
| Robertson Test (1953)          | <ul style="list-style-type: none"> <li>The dimensions, sharp notch geometry and loading for the test specimen are illustrated in Figure 7.2 (a).</li> <li>The crack is initiated from impact load applied to the outstanding lug on one side as shown.</li> <li>Tests are conducted under either temperatures gradient or isothermal temperature condition.</li> </ul>   | <ul style="list-style-type: none"> <li>Temperature gradient, impact load, uniform transverse load and crack length are measured.</li> <li>The test gives the lowest temperature associated with crack arrest.</li> <li>The determination of the crack arrest is ambitious.</li> <li>The test gives qualitative data and is of limited value since impact load may influence the results.</li> </ul>  |
| Esso Test (1955)               | <ul style="list-style-type: none"> <li>The dimensions, sharp notch geometry and loading for the starter and test sections are illustrated in Figure 7.2(b).</li> <li>The brittle crack is initiated by driving a wedge into the V-shaped notch. This may be a pressed notch and placed close to brittle weld bead to promote the crack initiation.</li> <li>The test is conducted under isothermal temperature condition.</li> </ul> | <ul style="list-style-type: none"> <li>The test gives the lowest temperature associated with the crack arrest.</li> <li>The Esso test has not been used extensively since the test results may be affected by stress waves on the test plate. (This applies to all wide plate tests and is a function of the aspect ratio, i.e., L/W.)</li> </ul>  |
| Double Tension Test            | <ul style="list-style-type: none"> <li>The dimension, notch geometry and loading for the main and starter plate are illustrated in Figure 7.2(c).</li> <li>A pressed notch or brittle weld bead could be used to promote the crack initiation at notch tip.</li> <li>The test can be conducted under isothermal temperature or temperature gradient condition.</li> </ul>  | <ul style="list-style-type: none"> <li>The press notch yields the localized compressive residual stress in brittle region.</li> <li>Test results are only valid for tests in which cracks can be initiated and subsequently arrested in the main plate.</li> <li>The crack arrest toughness can be calculated using the displacement method or estimated from the empirical equation, which are a function of the measured crack length and applied stress.</li> <li>Starter load system isolation w.r.t. main load system.</li> </ul> |
| Dual Plate Double Tension Test | <ul style="list-style-type: none"> <li>The dimension, notch geometry and loading for the main, starter plate and brittle weld section are illustrated in Figure 7.2(d).</li> <li>Tests are usually conducted at low temperature.</li> </ul>  | <ul style="list-style-type: none"> <li>The test was specifically developed to simulate crack events in storage tanks so that the crack arrest toughness for these steels subject to low temperature could be evaluated.</li> <li>The crack arrest toughness is estimated from empirical equations, which are a function of applied stresses and crack length.</li> <li>Starter load system isolation w.r.t. main load system.</li> </ul>   |
| Short Crack Arrest Test (1982) | <ul style="list-style-type: none"> <li>The dimension, notch geometry and loading conditions for the starter and main plate for two different configurations are illustrated in Figure 7.2(e).</li> <li>The starter plate is welded to center of weld line to test plate on top of a brittle weld bead. A face groove machined on the opposite of the starter plate to create a stable crack path.</li> </ul>                         | <ul style="list-style-type: none"> <li>The test configuration minimizes the dynamic effects of stress waves and simplifies the calculation for crack arrest toughness, which is based on empirical formulation given as function of crack length and applied load.</li> <li>The bending effect in the test plate due to the starter load is not considered.</li> <li>Starter load system isolation w.r.t. main load system.</li> </ul>   |



**Figure 7.2: Large-Scale Test Types**

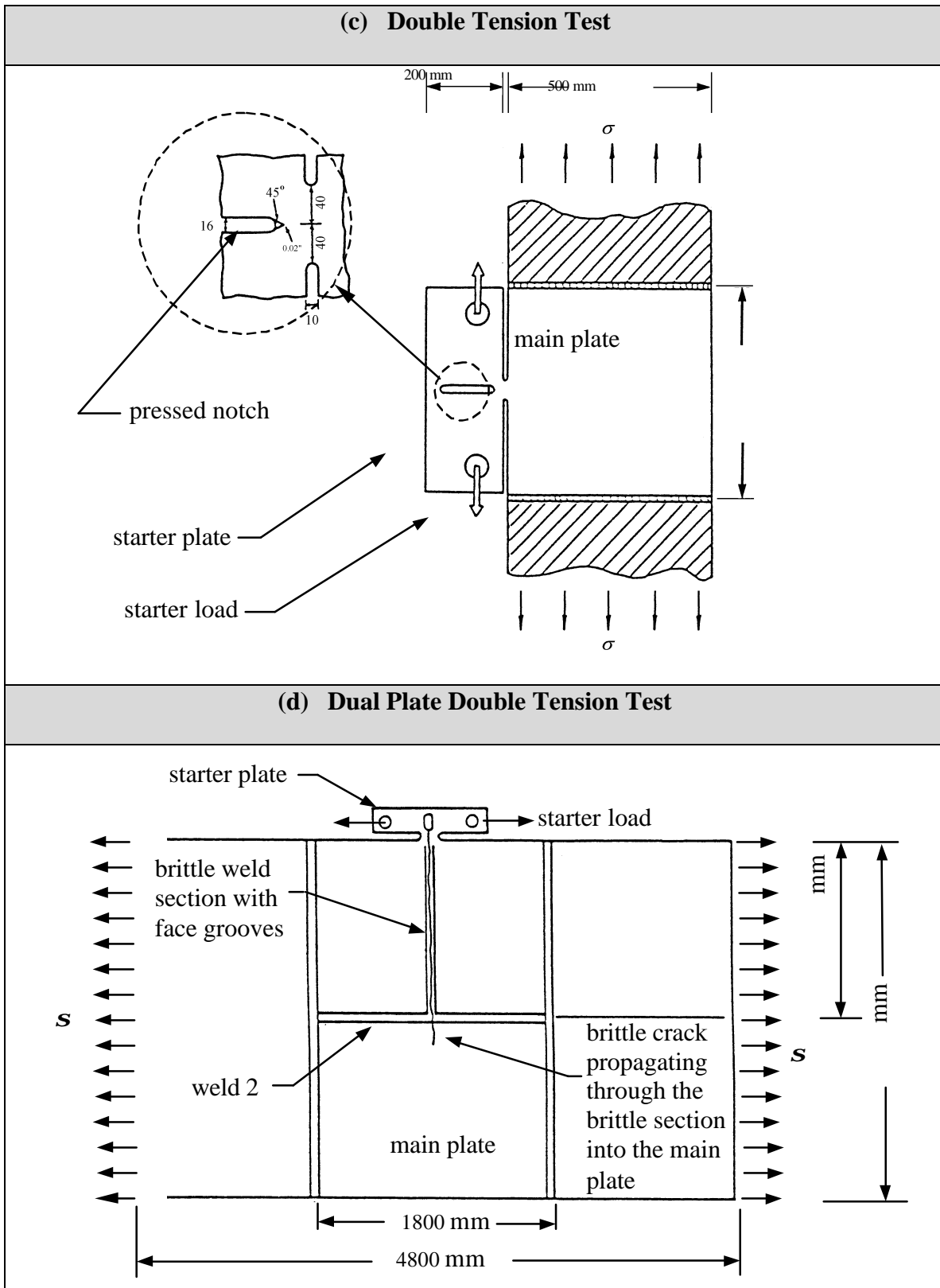


**Figure 7.2(Cont'd): Large-Scale Test Types**

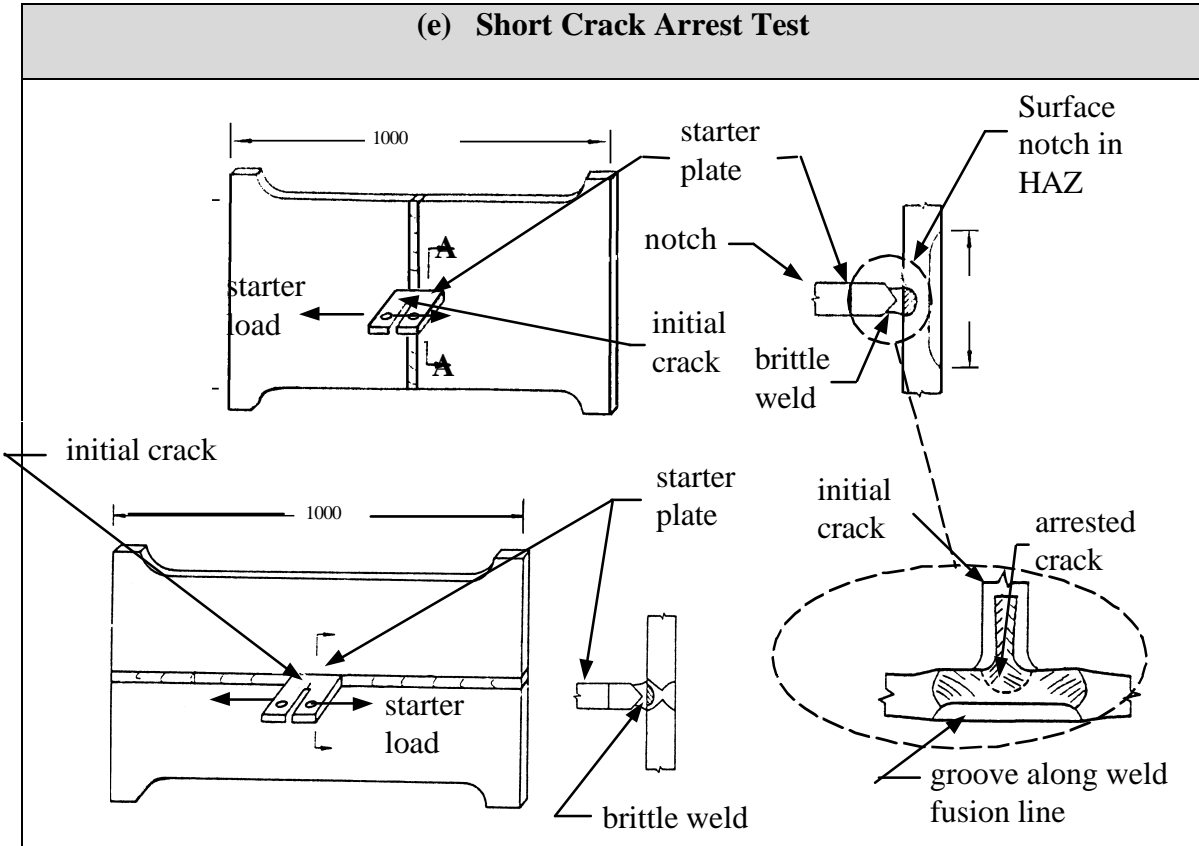


**Figure 7.2(Cont'd): Large-Scale Test Types**

### 7.3 Determination of $K_I$ by Finite Element Analysis (FEA)

For cracks loaded in tension, Mode I, the stress components and displacement at any arbitrary point “n” with respect to the crack tip as illustrated in detail in Figure 7.3, can be expressed as a function of its location relative to the crack tip in terms of polar coordinates, the stress intensity factor, Poisson’s ratio  $\nu$ , and the value  $k$ , and are given by Equations 7.1 (a) to (f) and 7.2 (a) to (c) respectively:

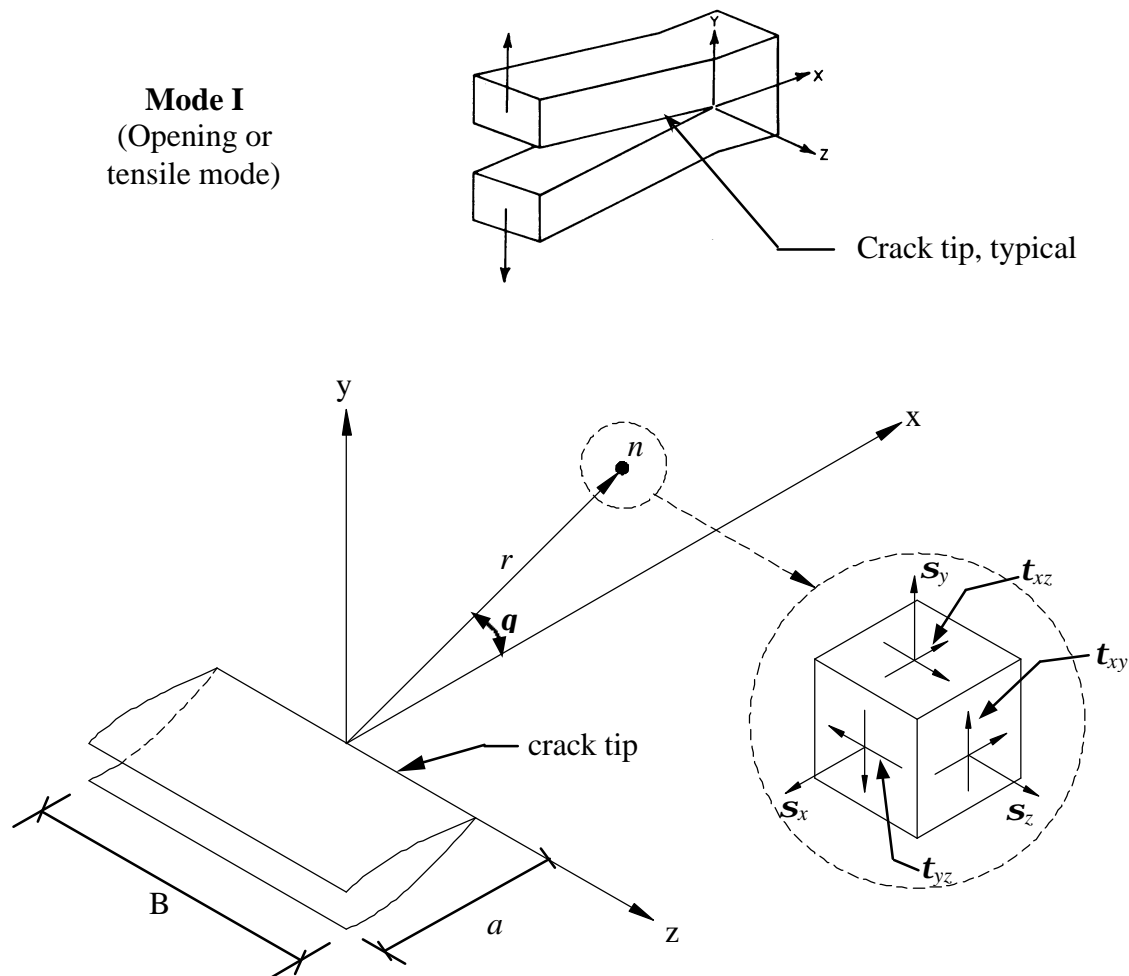


**Figure 7.3: Coordinate System and Stress Components Ahead of a Crack Tip**

$$\mathbf{s}_x = \frac{K_I}{\sqrt{2\mathbf{p}r}} \cos\left(\frac{\mathbf{q}}{2}\right) \left[ 1 - \sin\left(\frac{\mathbf{q}}{2}\right) \sin\left(\frac{3\mathbf{q}}{2}\right) \right] \quad 7.1 (a)$$

$$\mathbf{s}_y = \frac{K_I}{\sqrt{2\mathbf{p}r}} \cos\left(\frac{\mathbf{q}}{2}\right) \left[ 1 + \sin\left(\frac{\mathbf{q}}{2}\right) \sin\left(\frac{3\mathbf{q}}{2}\right) \right] \quad 7.1 (b)$$

$$\begin{aligned} \mathbf{s}_z &= 0 \quad (\text{for plane stress}) \text{ and,} \\ &= \nu (\mathbf{s}_x + \mathbf{s}_y) \quad (\text{for plane strain}) \end{aligned} \quad 7.1 (c)$$

$$\mathbf{t}_{xy} = \frac{K_I}{\sqrt{2\mathbf{p}r}} \cos\left(\frac{\mathbf{q}}{2}\right) \sin\left(\frac{\mathbf{q}}{2}\right) \cos\left(\frac{3\mathbf{q}}{2}\right) \quad 7.1 (d)$$

$$\mathbf{t}_{yz} = 0 \quad 7.1 (e)$$

$$\mathbf{t}_{zx} = 0 \quad 7.1 (f)$$

where,  $\mathbf{s}_x, \mathbf{s}_y, \mathbf{s}_z, \mathbf{t}_{xy}, \mathbf{t}_{yz}, \mathbf{t}_{zx}$  = stress components at any arbitrary point “n”.

$$u_x = \frac{K_I}{2\mathbf{m}} \sqrt{\frac{r}{2\mathbf{p}}} \cos\left(\frac{\mathbf{q}}{2}\right) \left[ \mathbf{k} - 1 + 2\sin^2\left(\frac{\mathbf{q}}{2}\right) \right] \quad 7.2 (a)$$

$$u_y = \frac{K_I}{2\mathbf{m}} \sqrt{\frac{r}{2\mathbf{p}}} \sin\left(\frac{\mathbf{q}}{2}\right) \left[ \mathbf{k} + 1 - 2\cos^2\left(\frac{\mathbf{q}}{2}\right) \right] \quad 7.2 (b)$$

$$u_z = 0 \quad 7.2 (c)$$

and where,  $u_x, u_y, u_z$  = displacement of any arbitrary point “n” in the x, y, z directions defined with respect to the crack tip as illustrated in Figure 7.3.

$\mathbf{n}$  = Poisson’s ratio

$\mathbf{m}$  = shear modulus

$\mathbf{k}$  =  $3 - 4\mathbf{n}$  ( for plane strain ) and,  
=  $(3 - \mathbf{n}) / (1 + \mathbf{n})$  ( for plane stress )

$K_I$  = stress intensity factor for Mode I

The stress intensity factor at the crack tip can be calculated for any given loading, plate geometry and crack length by the displacement extrapolation method or by the stress extrapolation method or by the energy release rate method (the latter expressions are not included on previous page), Chan et al (1990). For example, using the displacement extrapolation method;

- The stress intensity factor ( $K_I$ ) would be calculated for a series of points located at varying distances from the crack tip ( $r$ ) along the potential crack surface using Equation 7.2 and the displacement ( $u$ ) generated by finite element analysis (FEA);
- A tangent to the curve would be extrapolated back to the crack tip ( $r = 0$ ) as illustrated in Figure 7.4;
- The intercept with the dependent axis gives the stress intensity factor at the crack tip.

This series of calculations would be repeated for each crack length to generate a stress intensity factor graph for propagating cracks.

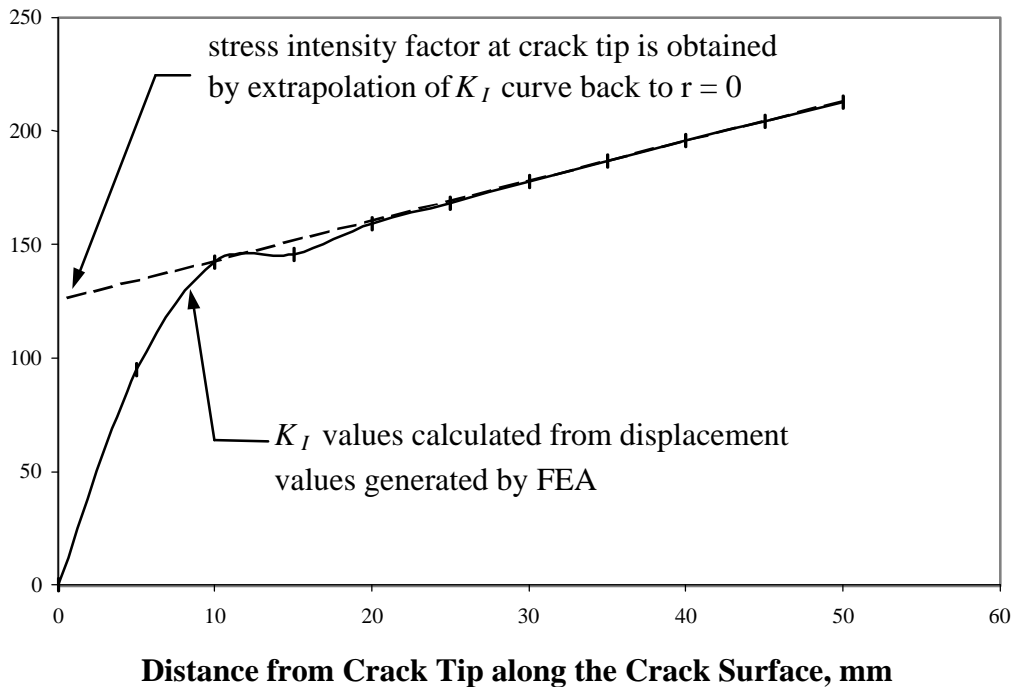
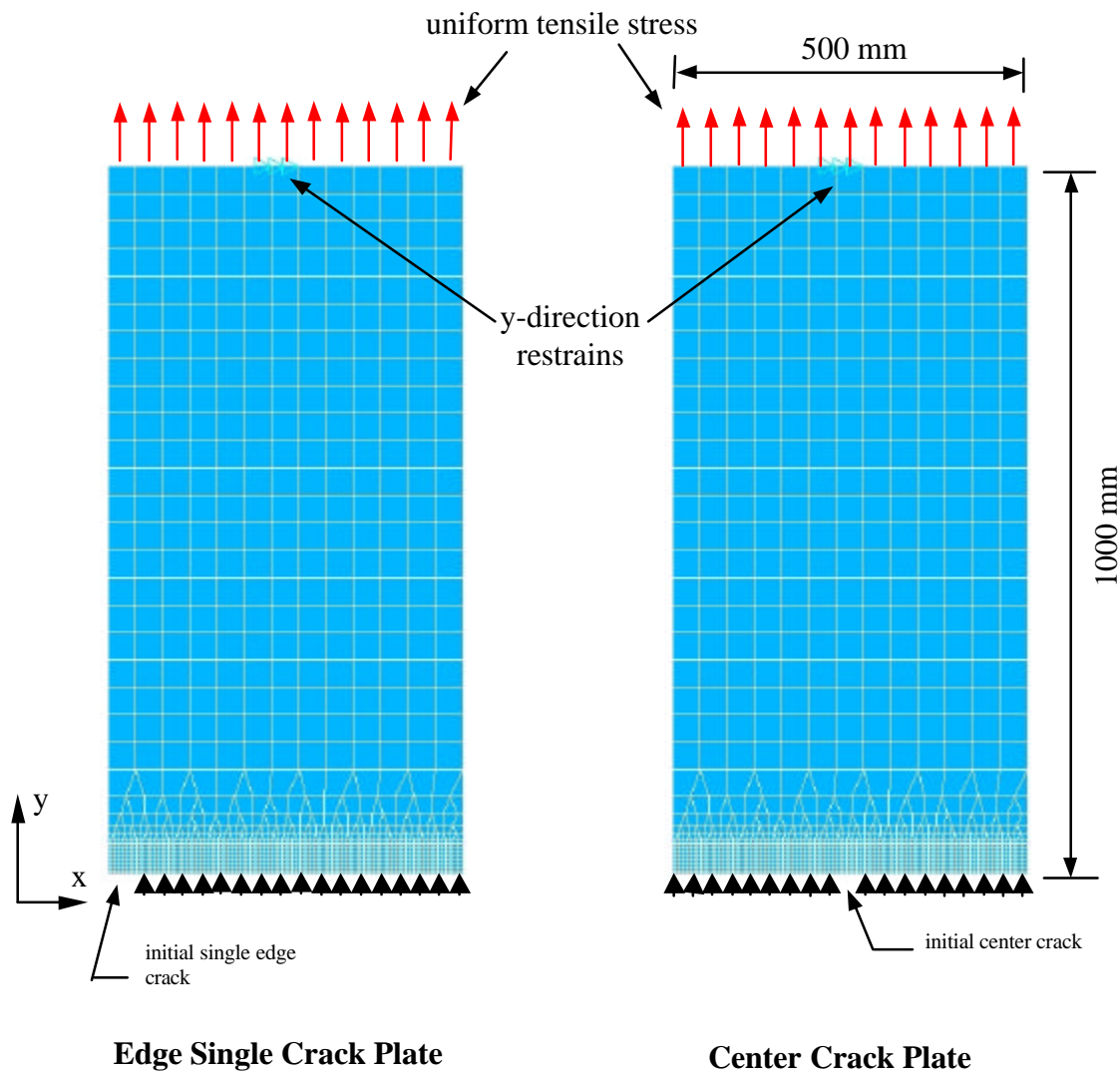


**Figure 7.4: Displacement Extrapolation Method**

Two finite plates with geometry similar to that for the large-scale test specimen with either an initial single-edge-crack (a) or a center-crack length (2a) of 30 mm, as illustrated in Figure 7.5, were analyzed to determine the stress intensity factor for propagating cracks for each of the three numerical methods. The calculated stress intensity factor (SIF) curves, for an applied uniform tensile stress of  $\sim 400$  MPa for each case, are plotted in Figures 7.6 and 7.7 along with the corresponding classical solution for an infinite plate. Both the stress and the displacement extrapolation method give good correlation for single-edge-cracks with any length. For an initial crack length of 30 mm, the ratio of the stress intensity factor of the displacement extrapolation method to the classical solution is 0.9913.

For the center crack model, the deviation of the stress intensity factor values evaluated by the displacement extrapolation method from those calculated by classical solutions, is related to the ratio of the crack length to the plate width. The small variation of the stress intensity factors at the initial crack length of 30 mm is again attributed to the difference in plate widths (finite (500mm) versus infinite). Notwithstanding, the corresponding ratio of the stress intensity factors was 1.0624. Chan et al. (1970) also concluded that the displacement extrapolation method would provide the best estimates of the stress intensity factor for any given load condition and crack geometry.



- Note, i) Two dimensional eight-node plane stress elements were used.  
 ii) Initial crack length was 30 mm for both cases.

**Figure 7.5: FEA Modeling for Standard Crack Geometry and Loading**

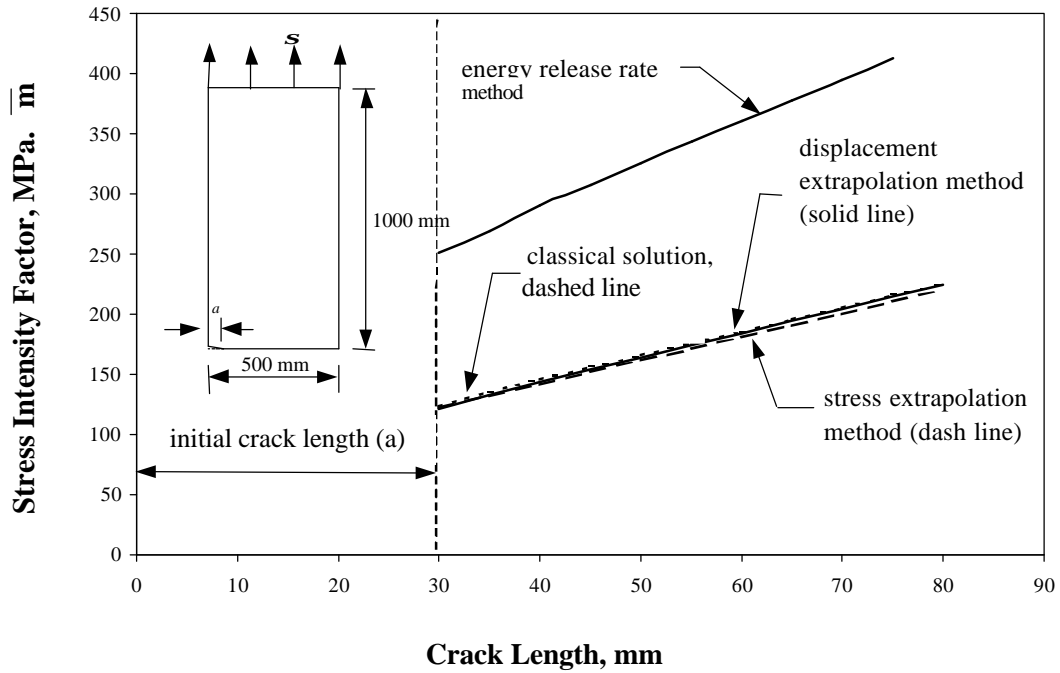


**Figure 7.6: Comparison of Stress Intensity Factors for a Single-Edge-Crack in a Finite width Plate Subjected to Uniform Tension ( ~ 400 MPa)**

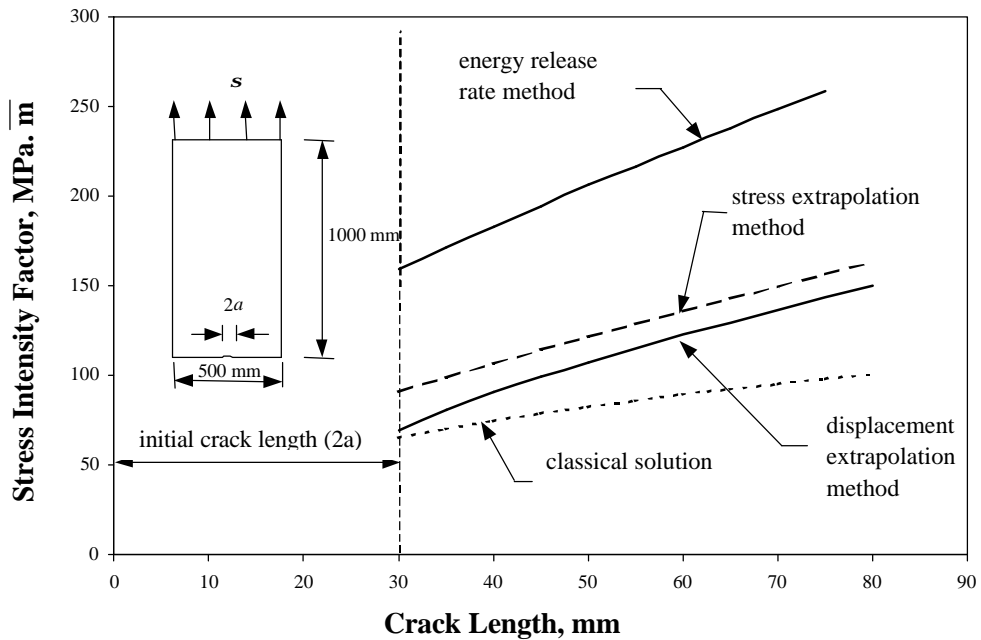


**Figure 7.7: Comparison of Stress Intensity Factor for a Center-Crack in a Finite width Plate Subjected to Uniform Tension ( ~ 400 MPa)**

## **8. SMALL-SCALE TEST PROGRAM**

### **8.1 General**

Small-scale tests give a measure of the crack arrest toughness of a material with respect to any given temperature. From this data, the temperature transition curves and the crack arrest toughness of the steel or weld (with prescribed welding procedures) can be determined and compared to the specified toughness values, to determine the acceptability of the material for a given application. The test data may be used for design or they may be used to conduct toughness or safety assessments of welded structures such as ship hulls, bridges, storage tanks and pressurized containers. Small-scale tests produce data that is generally more qualitative than quantitative, since the loading is generally indirect and the specimens are not tested in a uniform or gradient tensile stress field indicative of real loading conditions.

A series of small-scale tests have been conducted by Fleet Technology Limited as part of this investigation to characterize the crack arrest toughness for a butt weld joining ship steel plate to define the experimental parameters (notch geometry, temperature, stress field) for the large-scale test. A description of the plate and weld material characteristics, small-scale tests and results are given in detail in Part I.

The work described in this section builds on this data and extends it to the developments of the large-scale test program. In particular, this section describes the finite element analyses conducted for all valid small-scale CCA tests to determine the crack arrest toughness values so that direct comparisons could be made between established numerical methods and the corresponding values calculated from the expressions stated in the ASTM Standard E1221-96. The numerical methods are then applied to nonstandard test specimen geometries, and boundary and load conditions. This section also describes the starter plate tests conducted as a subset of the large-scale test series to define the notch geometry, temperature conditions and starter loads that would generate a successful crack propagation event, which is defined as crack propagation along the weldment with sufficient energy to propagate into the main plate. Finite element analyses were also conducted to determine the corresponding stress intensity factors distributions and the crack initiation toughness values associated with these tests.

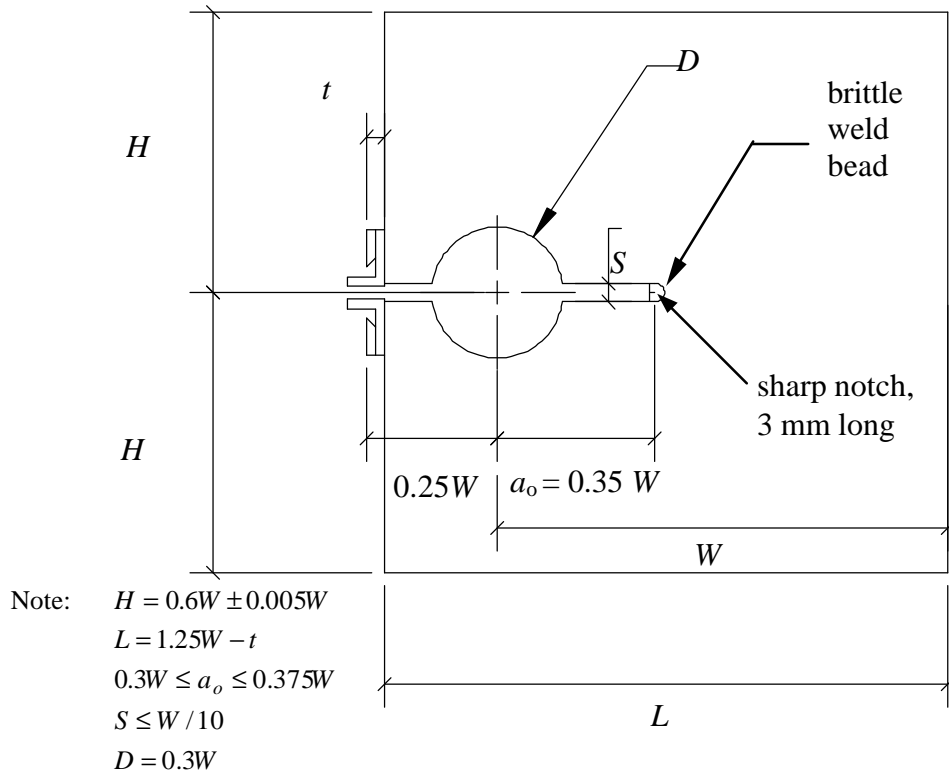
## 8.2 Finite Element Analysis of Compact Crack Arrest Tests

To compare the toughness of the weld material from the successful CCA tests with those from the starter plate tests or from the large-scale double tension tests, a correlation between the crack arrest toughness evaluated according to Crosley & Ripling (1990) must be made with the corresponding  $K_a$  values calculated using the displacement method and the results of finite element analyses based on the data from the CCA tests (CMOD and crack length).

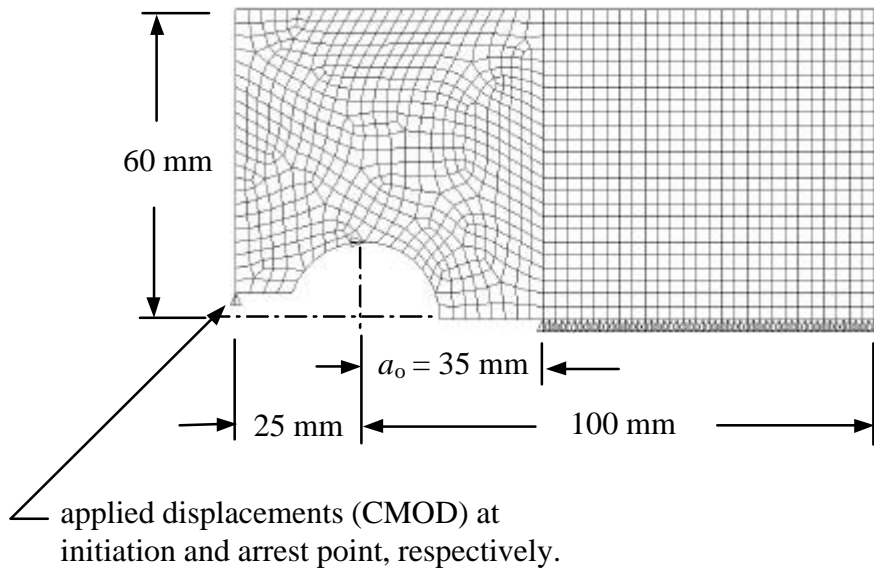
A 2-dimensional solid model replicating the CCA test specimen geometry, shown in Figure 8.1, was developed. Elastic analyses were performed for each successful test listed in Table 8.1 and the stress intensity factor at the arrest point (crack arrest toughness) was calculated. These values are illustrated in Figure 8.2 as open circles and triangles and correspond to the solid shapes for the  $K_a^*$  values, plasticity corrected crack arrest toughness, calculated according to the equations given by Crosley & Ripling (1990). The corresponding crack arrest toughness values evaluated from the results of the finite element analysis by displacement method are higher than these with the average increase of 1.387 and 1.291 for  $-10^\circ\text{C}$  and  $0^\circ\text{C}$ , respectively. Ideally, the comparison would have been values of  $K_a$  instead of  $K_a^*$  from experimental data. However,  $K_a$  determined by FEA is still higher.

**Table 8.1: CCA Test Results and FEA Results**

| Test Temperature    | Test Identification | $K_a^*$<br>( $\text{MPa}\sqrt{m}$ ) | $K_a$ , by FEA<br>( $\text{MPa}\sqrt{m}$ ) |
|---------------------|---------------------|-------------------------------------|--|
| $-10^\circ\text{C}$ | W2(2)-2             | 102.3                               | 126.8                                      |
|                     | W2(3)-6             | 90.8                                | 119.0                                      |
|                     | W2(1)-4             | 78.6                                | 105.1                                      |
| $0^\circ\text{C}$   | W2(1)-1             | 120.7                               | 172.7                                      |
|                     | W2(1)-2             | 112.8                               | 148.2                                      |
|                     | W2(1)-3             | 89.7                                | 127.3                                      |



(a) dimensions of full-thickness CCA test specimen



(b) 2-dimensional finite element model

**Figure 8.1: Compact Crack Arrest Test Specimen and Analytical Model**

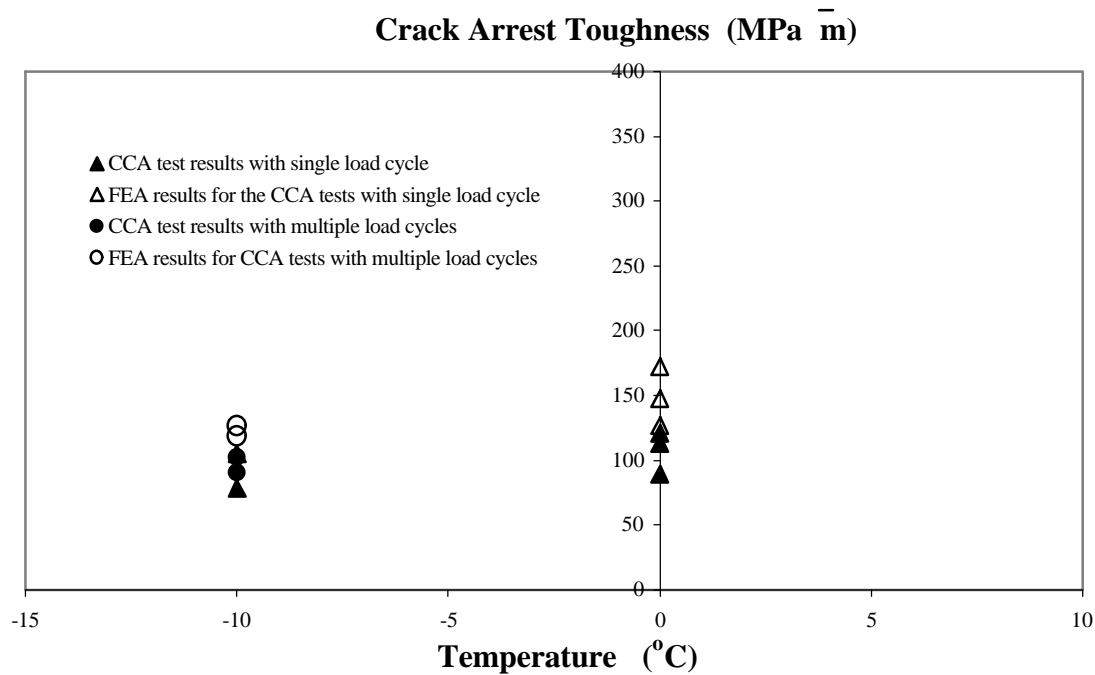


**Figure 8.2: Comparison of Crack Arrest Toughness Values Evaluated by Crosby & Ripling (1990) and the Displacement Method**

### 8.3 Finite Element Analysis of Starter Plate Tests

#### 8.3.1 General

It was anticipated at the onset of the small-scale test program that the CCA tests would demonstrate the best crack starter method to be used in the double tension test and to give appropriate crack arrest toughness values to characterize the fracture toughness of the weldment being investigated. These tests demonstrated that the crack starter methods have to match the arrest toughness of the test material. Accordingly, crack starter methods were developed as part of the starter plate test series, which simulated more closely the plate and notch geometry of the large-scale double tension test.

Four starter plate tests with two different crack starter methods were conducted to determine which method would be the most effective for the large-scale double tension test. The first method involved embrittlement of the weld metal by lateral compression through the thickness by up to 15%. The concept of through thickness compression was to use a significant portion of the strain energy density of the material (through the net section) through plastic deformation to make it brittle. In principal, the embrittlement of the weld metal section at the crack tip in the starter plate should generate favourable crack initiation and growth conditions, making it possible to conduct the large-scale double tension test under isothermal conditions and have the crack terminate in the tougher weld metal in the main plate outside the embrittled weld region.

The second method provides double-side face grooves made on either side of the weld in the starter plate over a length that the initial crack needs to be propagated. The grooves create a state of plane strain through the net section (induces brittle behaviour), and reduce that section which locally increases the stress intensity factor. The combination of these two effects drives the crack to propagate along the desired plane (center of weld). Since the stress intensity factor value at the crack tip is higher than that of a plate without a reduced section (double-side grooves), and since the large-scale double tension test has an increasing stress intensity factor field for propagating cracks, the large-scale test with this crack starter method are ideally conducted under a temperature gradient. The remaining portion of this section presents the FEA and the test results for both crack starter methods.

### 8.3.2 Lateral Compression of the Weld

Based on the results from the CCA tests conducted by Fleet Technology Limited, Malik et. al. (1996) and Pussegoda et. al. (1998), the weldments for two starter plate tests (*STP1* and *STP2*) were laterally compressed with hardened cylinders. The indentations reduced the thickness locally to the values of 10% and 15%, respectively.

Pictures of the test setup for the lateral compression of the weld and an end view of starter plate *STP2* with 15% compression are shown in Figure 8.3(a) and (b), respectively. Although a significant portion of the strain energy density for the net section is used by lateral compression, the material surrounding this compressed or plastic zone remains elastic and restrains the plastified material from lateral extension due to Poisson effect, placing a portion of this zone into residual compression across the potential crack face.

This residual compression across the interface was verified by a nonlinear FEA of the lateral compression event on a quarter model of starter plate, weldment, and cylinder group as shown in Figure 8.4. The mesh density, the loading, and the boundary condition are also shown in this figure. Contact elements were used between the hardened cylinder (considered rigid for analysis purposes) and the weldment surfaces to provide the proper interaction between two as the indentation was applied. The von Mises strain and normal stresses across the potential crack face for a plate subject to 15% compression are shown in detail in Figure 8.5 and 8.6 for the area bounded by dash line in Figure 8.4.

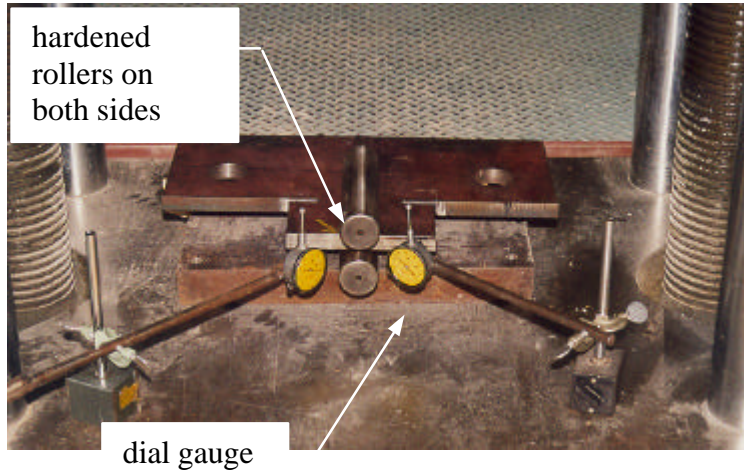
Figure 8.6 clearly shows a significant von Mises strain (strain energy density) that extends from the mid-thickness of the plate to the edge of the plate in the region of the last point of contact between the indenter and the plate. This band does not lie along the potential crack face and may cause the crack to diverge from the desired path. Figure 8.5 clearly illustrates the residual compression across the potential crack face through approximately 40% of the thickness extending from surface to the middle of the plate. Cracks do not propagate through residual compression zones. However, there are significant tensile normal stresses on the outside surface between the weld metal and parent plate. Brittle cracks may propagate along this interface if a crack runs into this zone.

The question still remains, whether or not, the effects of embrittlement outweigh the effects of residual compression producing an effective crack starter method. This can only be answered by tests.

The dimensions of the starter plate specimen, the notch geometry, the lateral compression and the location of the strain gauges are illustrated in Figure 8.7(a). The test specimen was installed in the 1700 kN Tinius Olsen testing machine as shown in Figure 8.7(b). The notch and the starter crack detail including the blunt and sharp cracks are shown in Figure 8.7(c). The instrumentation (strain gauges and thermocouples) was connected to the data acquisition system. The local temperature control chamber was installed and liquid nitrogen was pumped into the chamber to bring the steel to the test temperature.

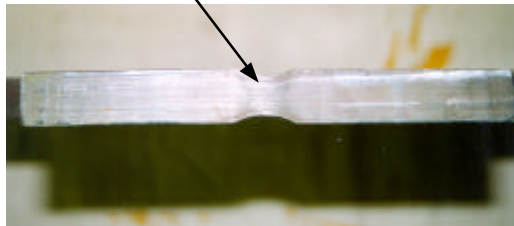
For the starter plate *STP1*, with a 10% lateral compression and initial temperature of  $-10^{\circ}\text{C}$ , a crack could not be initiated even with a starter load of 900 kN. The test specimen was removed, laterally compressed to 15% and re-tested at the temperature of  $-20^{\circ}\text{C}$ . The ductile branching cracks propagated a very short distance out of the compression zone away from the tip of sharp crack at a load of 850 kN, as illustrated in Figure 8.8. This test was considered unsuccessful.

The second starter plate test *STP2* with a lateral compression of 15% was tested at  $-40^{\circ}\text{C}$ . The ductile branching cracks developed at a load of 831 kN and propagated right across the width of specimen along the heat-affected zone as shown in Figure 8.9. The crack evaded the compression zone and fractured through the region where significant normal tensile stresses and von Mises strains exist (not of the region of interest). This test was also considered unsuccessful and clearly indicates that the lateral compression is not a viable crack starter method.



(a) Lateral Compression Setup

15% lateral compression by hardened roller



(b) Deformation through the Thickness of Plate

**Figure 8.3: Test Setup of Lateral Compression of Weld and the Lateral Deformation after the 15% Compression**

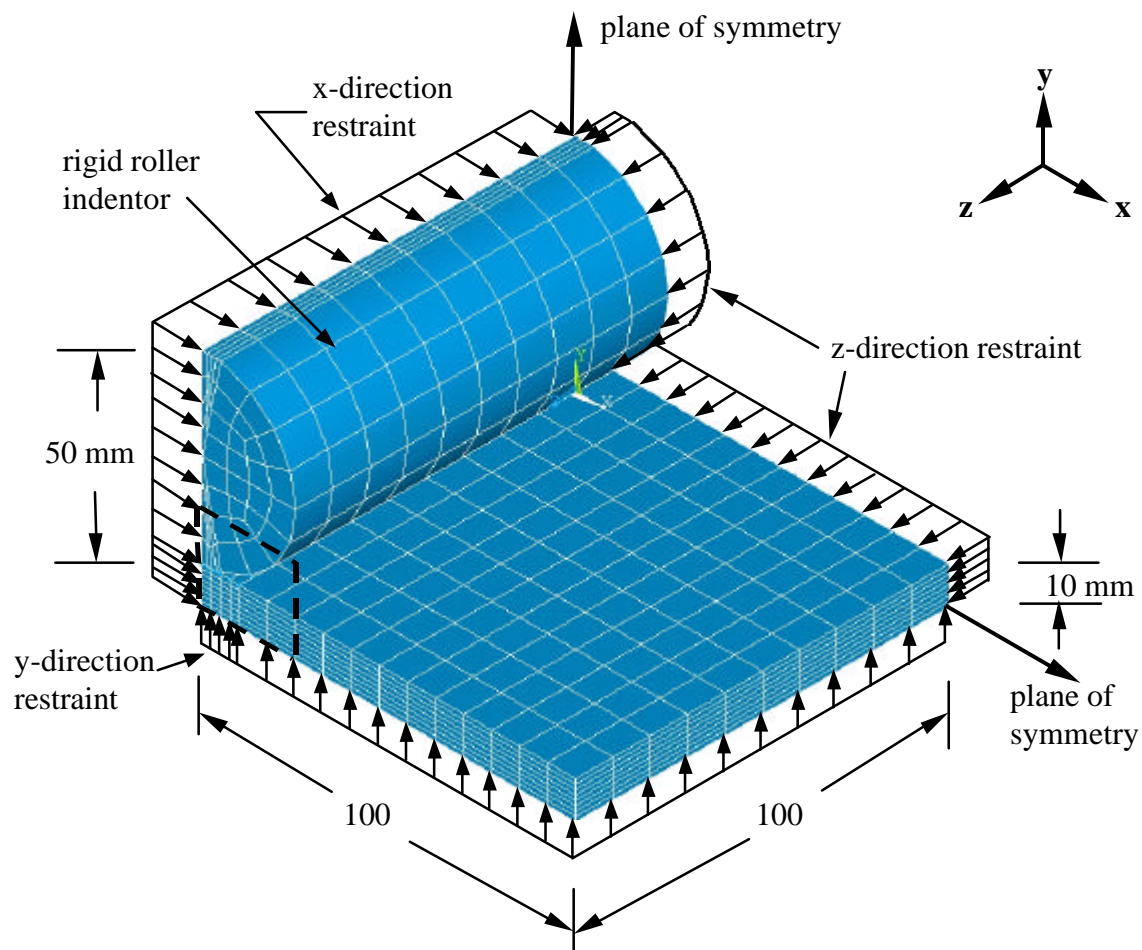


**Figure 8.4: 3-Dimensional FEA Model for Lateral Compression Indented by a Rigid Steel Roller**

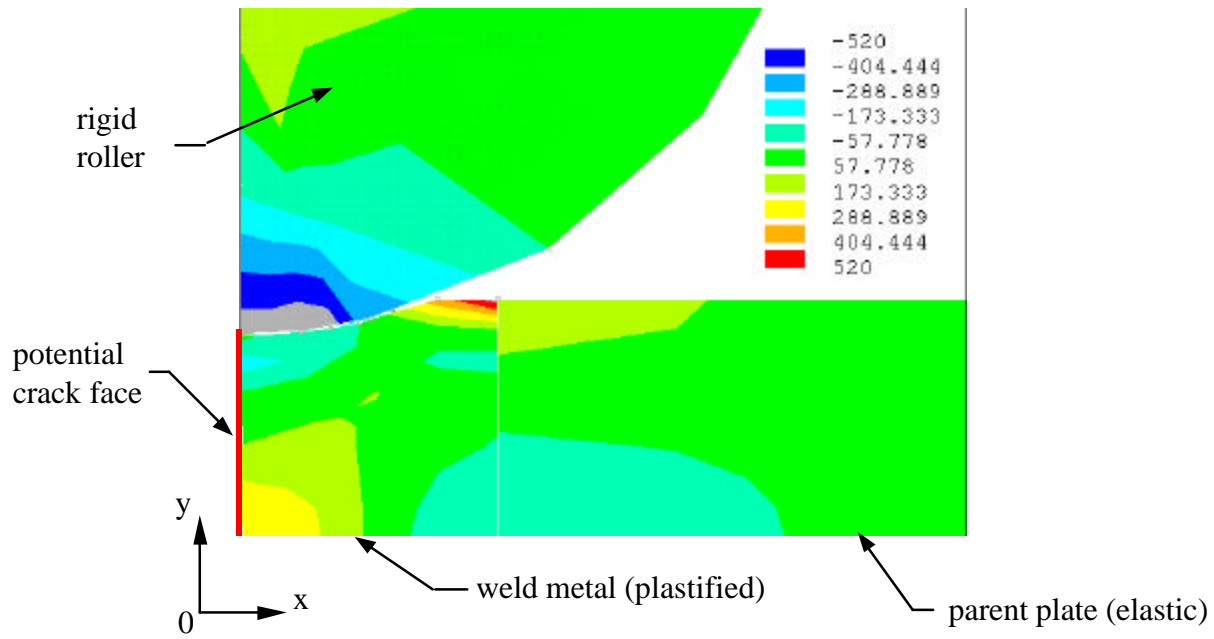


**Figure 8.5: X-Direction Stress across the Potential Crack Face, 15% Lateral Compression**

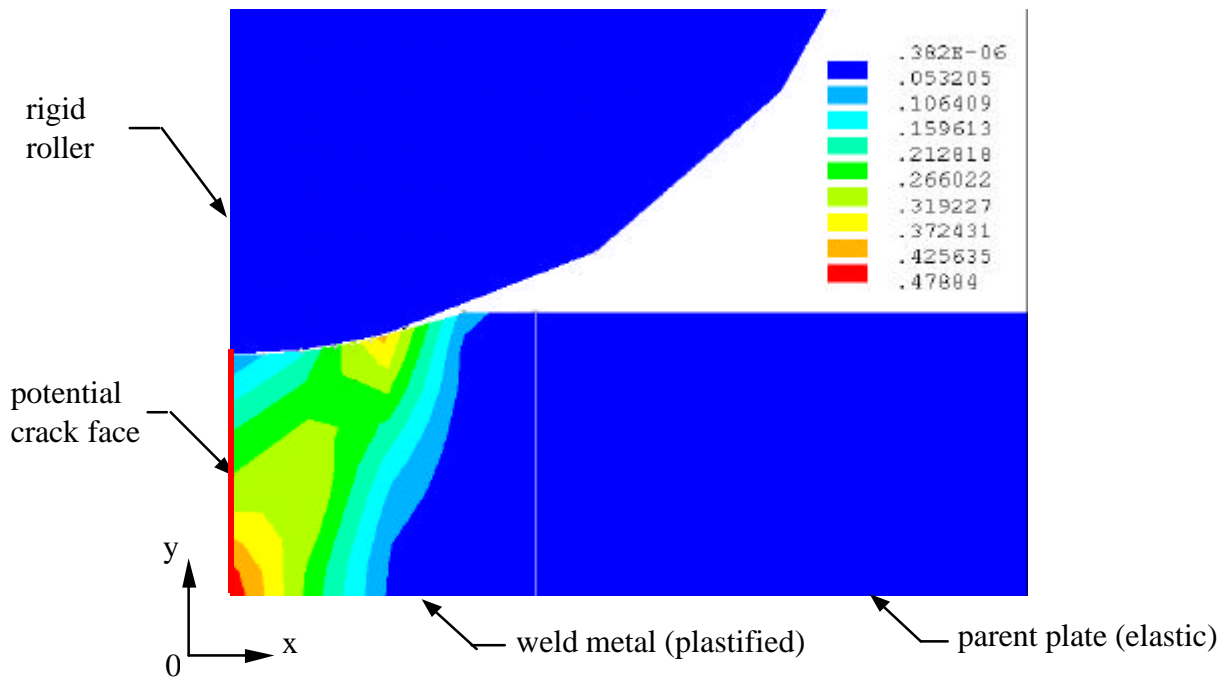
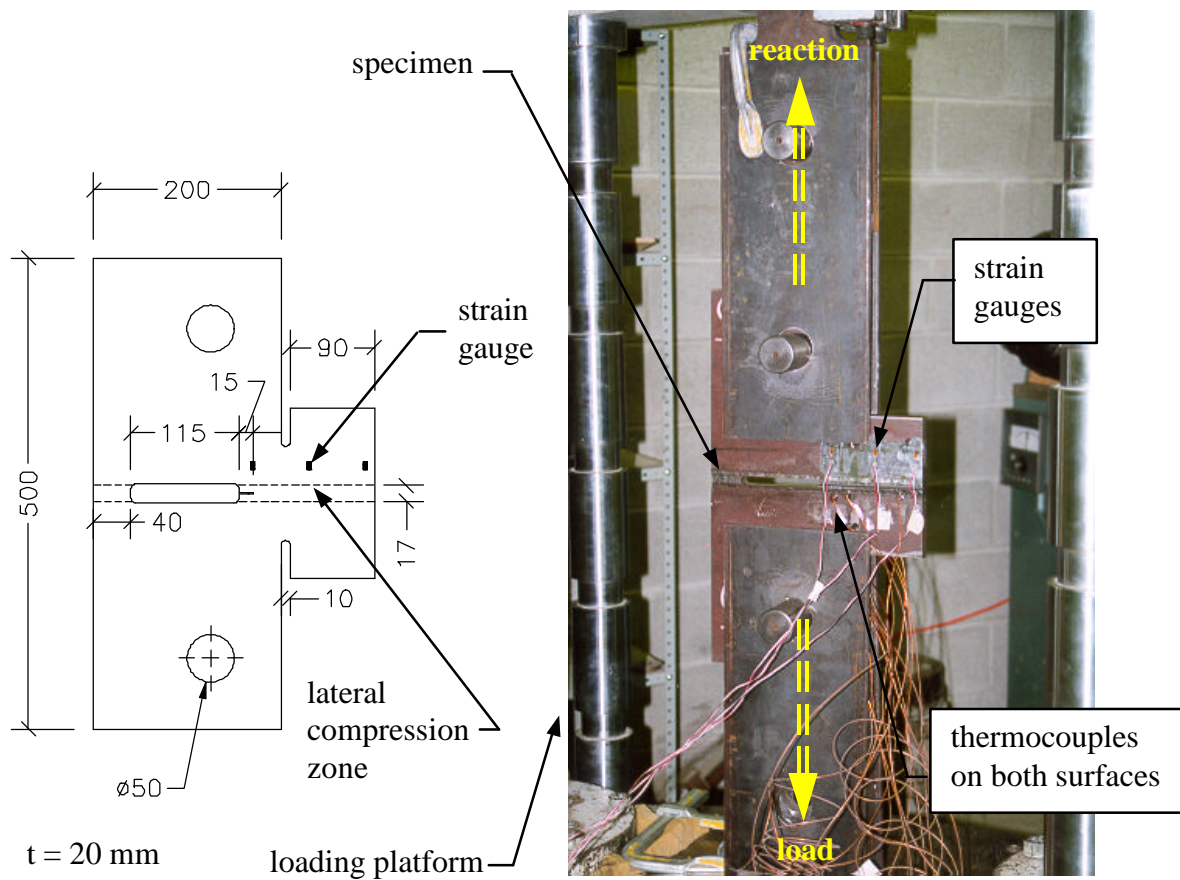
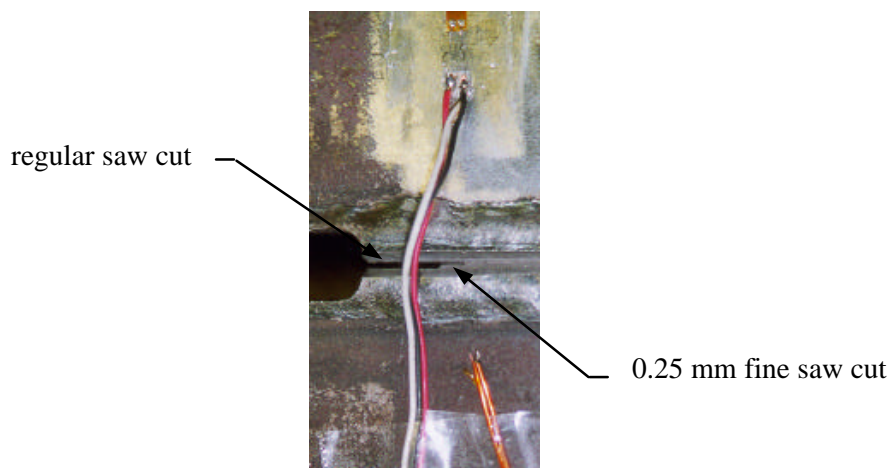


**Figure 8.6: von Mises Strain, 15% Lateral Compression**



**(a) Dimensions and Notch Geometry**

**(b) Test Setup**



**(c) Notch Detail**

**Figure 8.7: Starter Plate Test Setup**

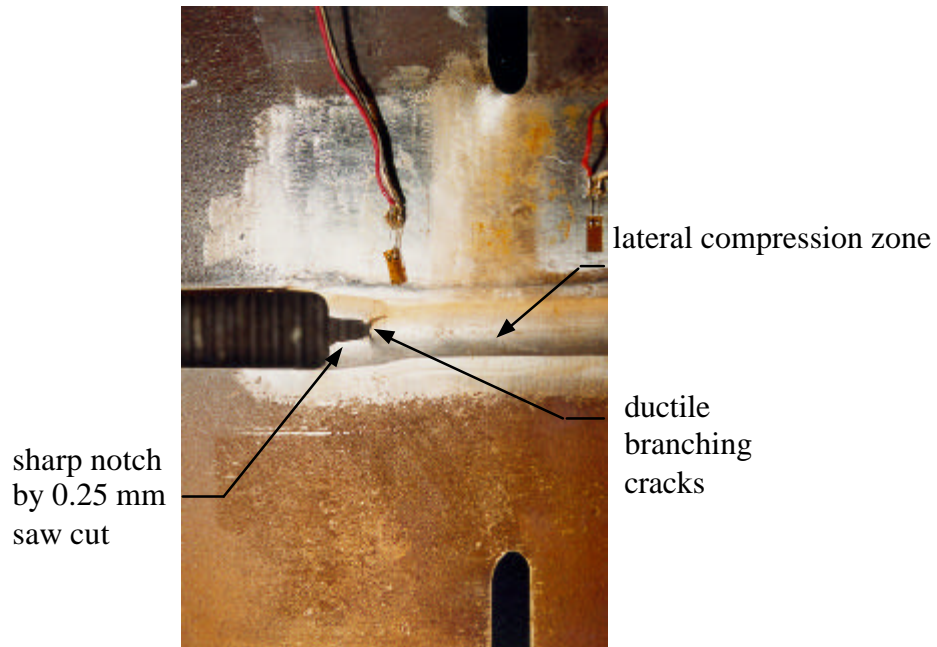


**Figure 8.8: Ductile Branching Crack – Starter Plate Test, *STP1***

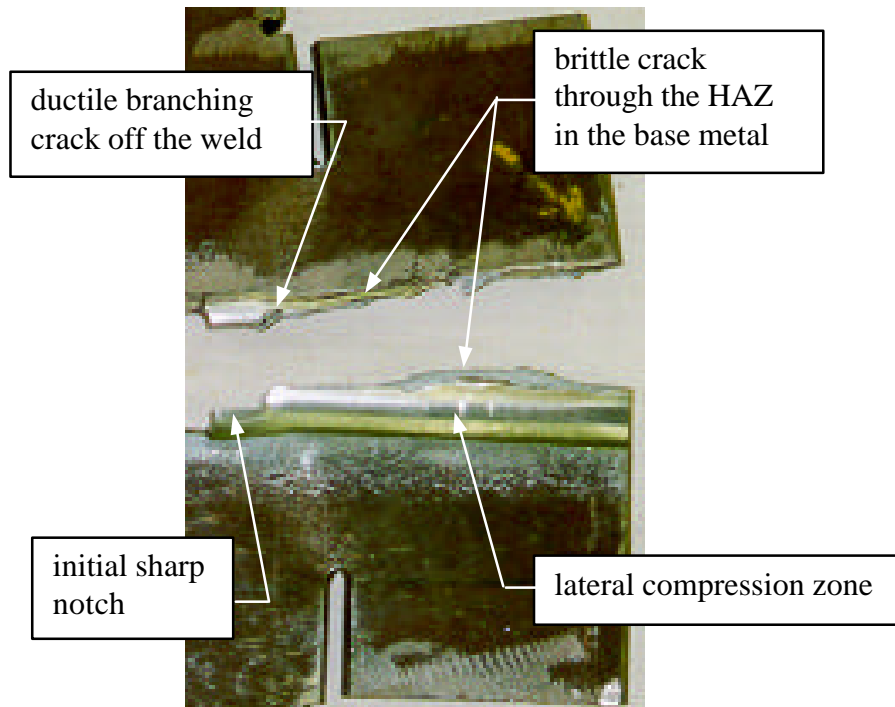


**Figure 8.9: Crack Location – Starter Plate Test, *STP2***

### 8.3.3 Double-Side Face Grooves

A three-dimensional solid FEA model was developed for starter plates with double-side face grooves and is shown in Figure 8.10. Elastic analyses were conducted for a starter load of 700 kN (applied by a 50 mm diameter pin) with varying crack lengths and two different groove depths, 3 mm and 5 mm, to evaluate the stress intensity factor as a function of the crack propagation and the depth of groove. The stress intensity factor corresponding to the fracture load obtained from the tests gives the crack initiation toughness. At the end of the groove there is a transition zone, 4mm in length, in which the groove depth diminishes to zero. The free surfaces had zero normal stress and the load application at the pin hole was based on a distributed load.

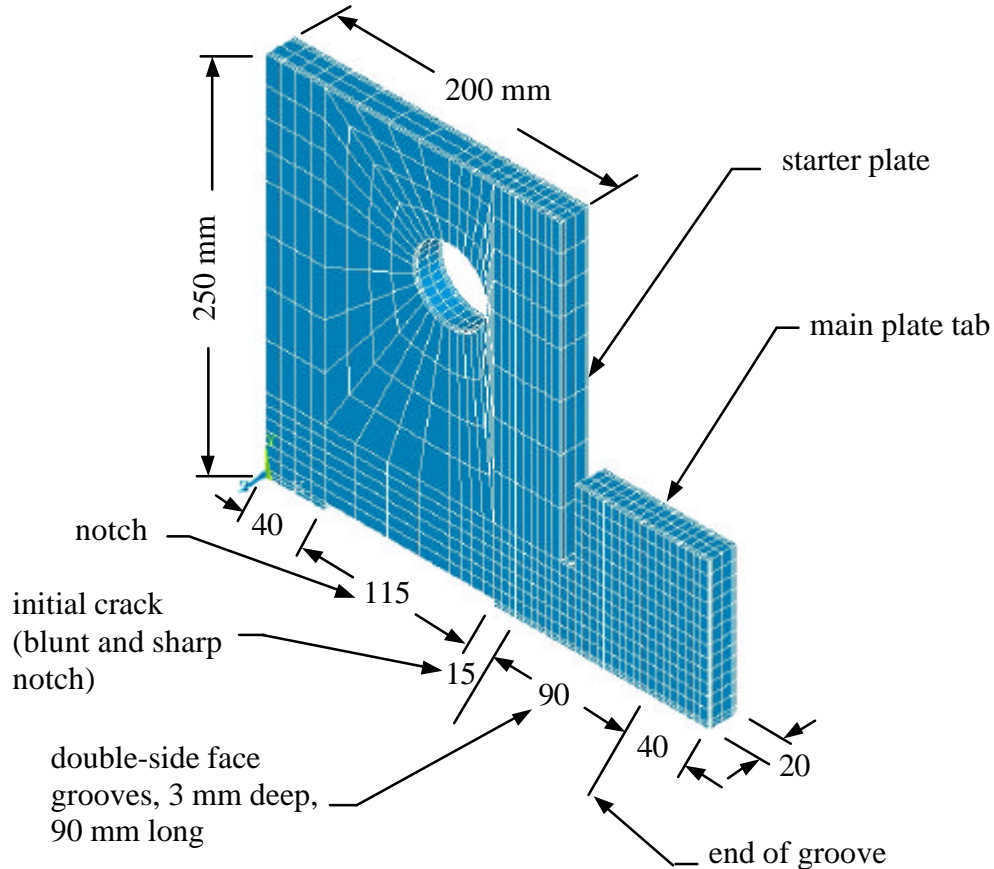


**Figure 8.10: Double-Side Face Groove Finite Element Model**

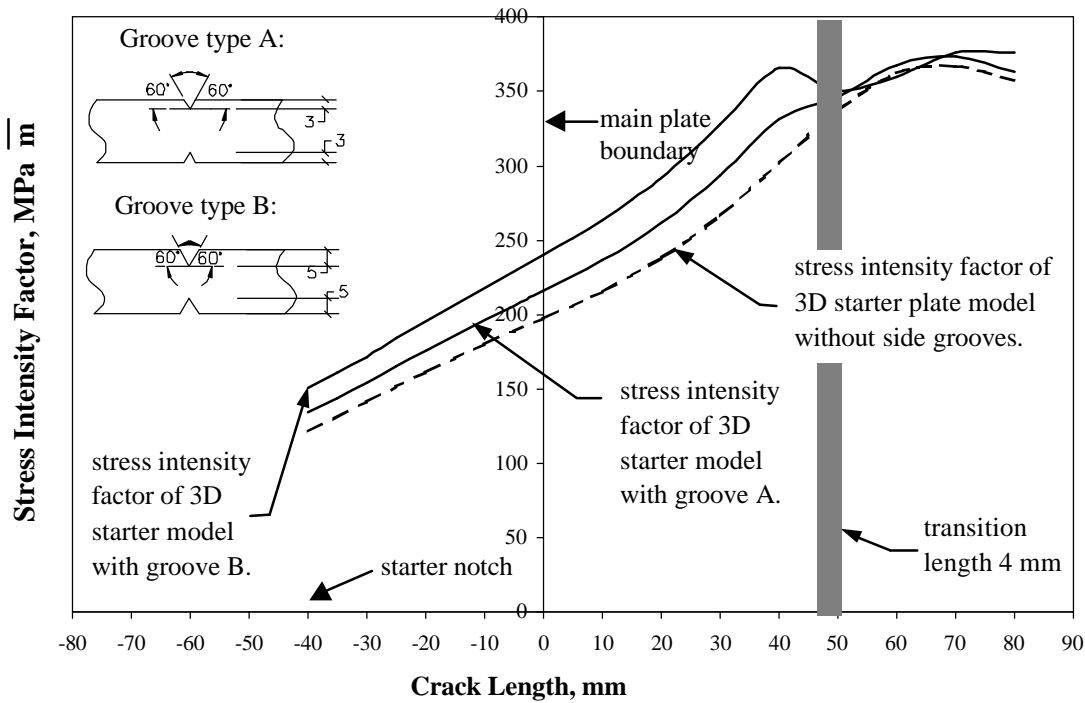


**Figure 8.11: Stress Intensity Factor versus Depth of Grooves**

The average stress intensity factor values were calculated using the displacement extrapolation method. The results of these analyses are illustrated in Figure 8.11 along with the comparable curves of the calculation for a full thickness starter plate without double-side face grooves. The shaded vertical band indicates the transition length. As illustrated, with increasing groove depths, the stress intensity factor value also increases, and maps onto the full thickness plate curve shortly after the transition zone. For starter plates with increasing depths of the double-side face grooves, the load required to initiate the cracks will be smaller (inversely proportional to the increase in the stress intensity factor) for any given temperature. The analyses also confirm that the material along the potential crack face is in a state of the triaxial tension. The starter crack position and boundary of the main plate are shown in Figure 8.11 relative to the abscissa.

Two starter plate tests *STP3* and *STP4* with 3 mm deep double-side face grooves (groove type A), as shown in Figures 8.11 and 8.12, were conducted at temperatures of  $-42^{\circ}\text{C}$  and  $-10^{\circ}\text{C}$ , respectively. The test procedure was the same as that for the other starter plate tests. For *STP3*, a brittle crack was initiated at load of 403 kN and propagated approximately 80mm. This resulted in a relaxation of the load system and an apparent drop in the applied load. The load was then increased to 410 kN, at which the crack propagated completely through the main plate tab along the groove. The corresponding fracture surface is illustrated in Figure 8.13(a).

For *STP4*, as the specimen was loaded, the crack popping sounds were heard at 680 kN and 710 kN. At a load of 841 kN, the crack propagated through the main plate tab. As previously described, the double-side face grooves cause the material through the net section to become more brittle and forces the crack to propagate along the groove. The corresponding fracture surface is illustrated in Figure 8.13(b). Examination of the crack surfaces for both *STP3* and *STP4* revealed straight crack fronts with no apparent tunneling. The crack initiation toughness associated with *STP3* and *STP4* are  $77 \text{ MPa}\sqrt{\text{m}}$  and  $159 \text{ MPa}\sqrt{\text{m}}$ , respectively.

In conclusion, the double-side face grooves caused a brittle fracture through the net section and force the crack to propagate along the groove as intended. This crack starter method was therefore used for large-scale double tension tests. Based on this limited data, it is anticipated that the temperature of  $-20^\circ\text{C}$  in the starter plate region for the double tension test will correspond to a crack-initiating load of approximately 700 kN. This load level should provide sufficient energy to propagate the crack into the main plate.

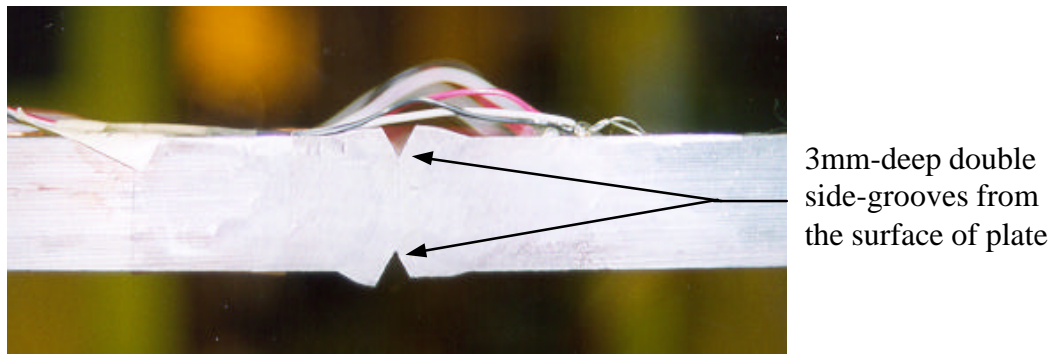
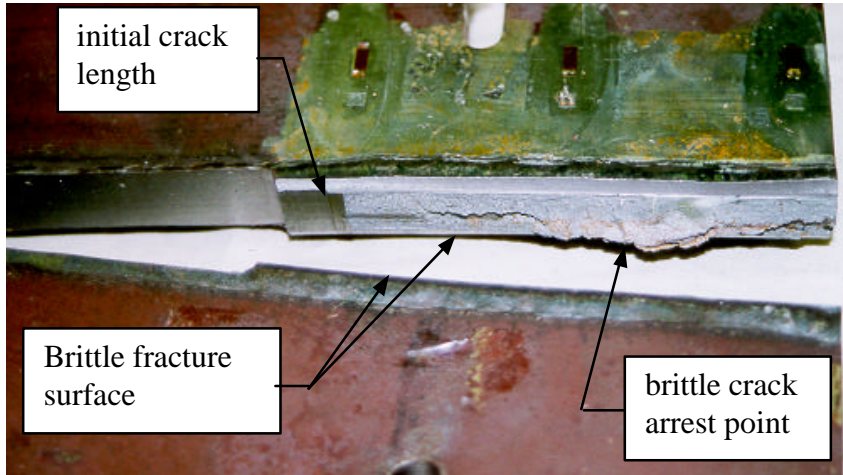
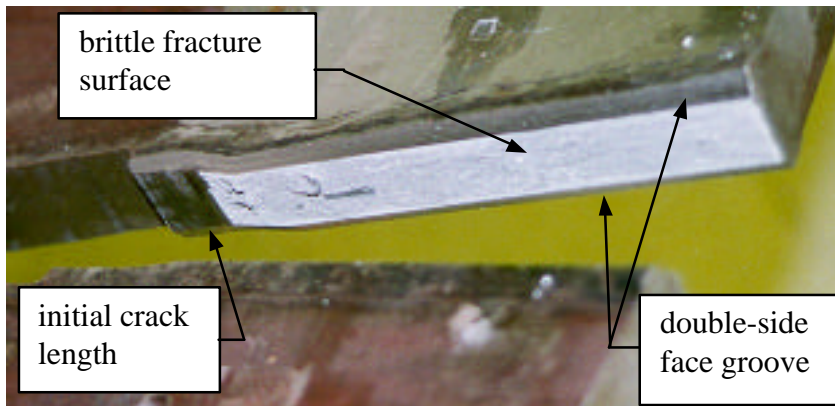


**Figure 8.12: Side View of Double-Side Face Grooves**



(a) Starter Plate Test, STP3



(b) Starter Plate Test, STP4

**Figure 8.13: Crack Surfaces for Starter Plate**

## 9. LARGE-SCALE DOUBLE TENSION TEST PROGRAM

### 9.1 Objective and Scope

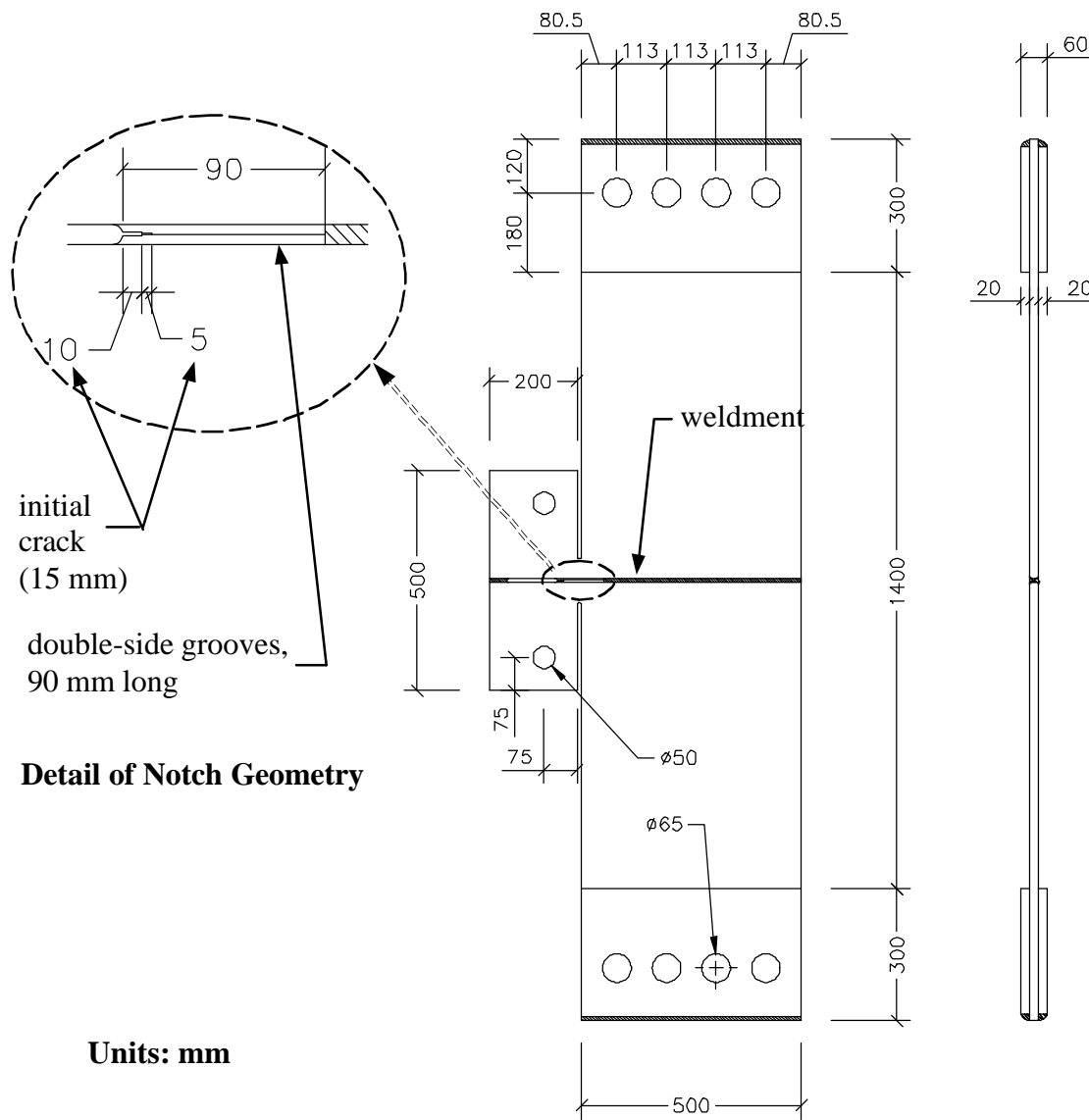
The objectives of this investigation were to design the test apparatus for the large-scale double tension test specimen shown in Figure 9.1, to outline the testing procedure; to develop the instrumentation and analytical tools to determine the crack arrest toughness of weldments; and to conduct the corresponding series of large scale tests to complete a matrix of crack arrest toughness values for varying temperature and tensile stress fields in the main plate. In addition, a series of finite element analyses were conducted on 3-dimensional solid models of the large-scale double tension test with double-side grooves to determine the stress intensity factor curves (evaluated using the displacement extrapolation method) as a function of the crack length, the starter load and the main plate tensile load. This method would then be used to determine both the crack initiation toughness and the crack arrest toughness of the weld metal.

Details of the test apparatus, the instrumentation, the test procedure, the discussion of the interpretation of the results of the large-scale tests and the discussions of all corresponding analyses are given in the following sections.

### 9.2 Stress Intensity Factor Curves and Data Interpretation

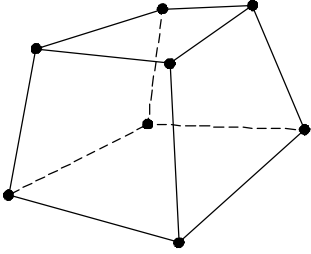
A series of elastic analyses were performed using the finite element analysis program, ANSYS 5.4, to determine the stress intensity factor curves as a function of the crack length, the starter load and the main plate load, for the large-scale double tension test specimen in Figure 9.1. The corresponding 3-dimensional solid FEA model of half of the specimen taken about the line of symmetry consists of 11490 elements and 14630 nodes, and is illustrated in Figure 9.2. SOLID45 elements were used for both the parent steel plate and for the weld metal. A description of the SOLID45 element's characteristics is given in Table 9.1.

The boundary conditions, the loading and the elastic material properties are summarized in Figure 9.3. The test load will be introduced and taken out of the main plate through four pins in a thickened section at either end of the specimen. To verify that this loading could be modeled by uniform load across the end of the specimen without changing internal force distribution along the weld, FE analyses were conducted on the full-section for both sections. As anticipated, no differences were found, hence the simpler loading case was used for the main plate and is illustrated in Figure 9.3. The load distributed on the starter plate approximates the pin-load on the hole and is statically equivalent to the starter plate load. Along the line of symmetry, the nodes were restrained from the displacement in the  $y$ -direction. Three additional nodes, as indicated in Figure 9.3, were restrained from the displacement in the  $x$  and  $z$ -directions to restrict rigid body rotations without restricting deformation along the line of symmetry. The reaction forces at the bottom of the main plate were modeled, with appropriate stiffnesses of the restraint connections.



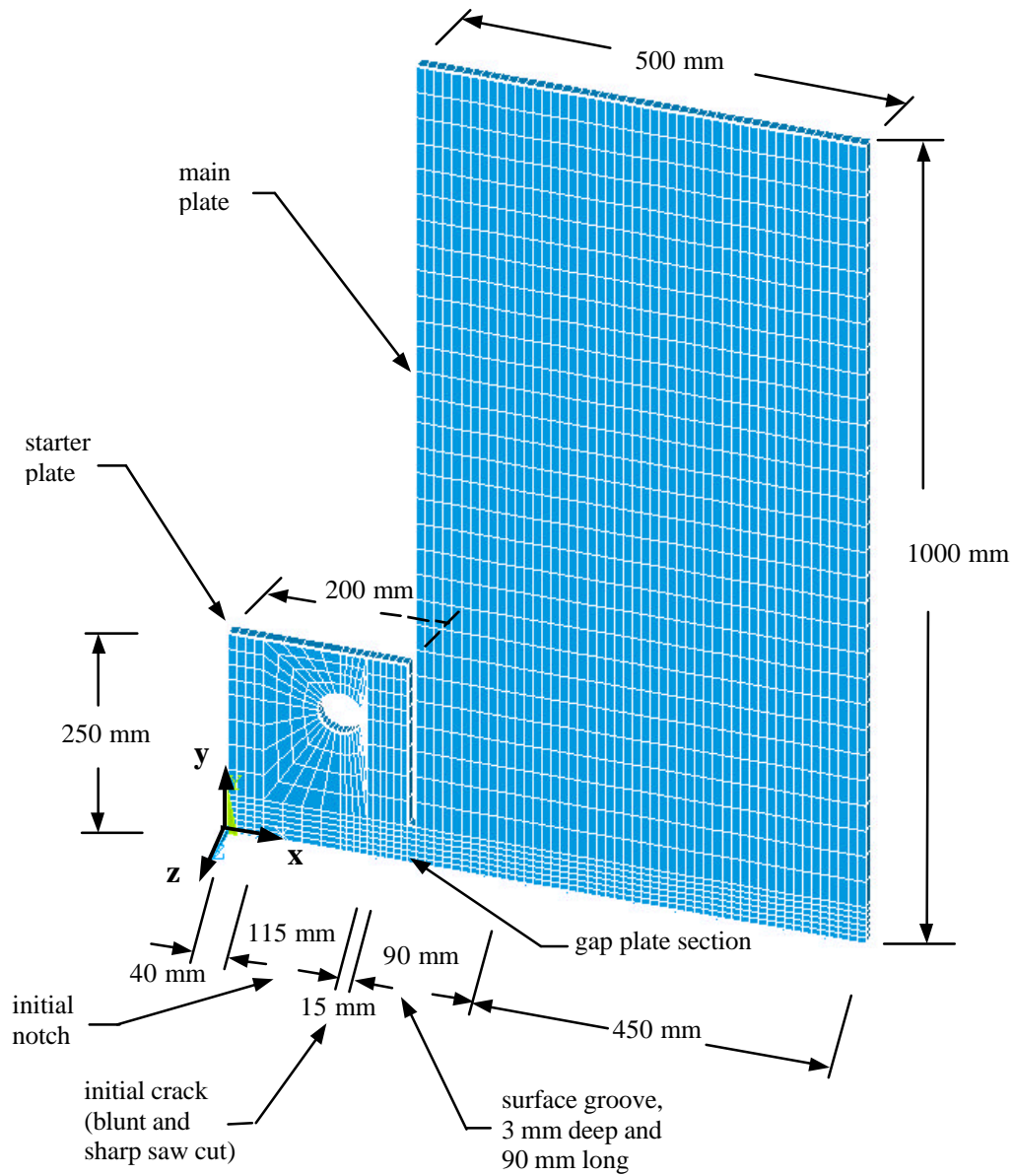
**Figure 9.1: Large-Scale Double Tension Test Specimen with Double-Side Grooves**

**Table 9.1: SOLID45 Element Description**

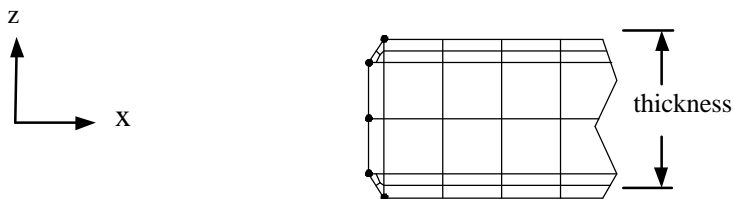
| Element Geometry  | Element Characteristics  |
|---|--|
|  <ul style="list-style-type: none"> <li>• 8 Corner nodes</li> <li>• 3D Space</li> <li>• DOF: Translation in <math>x</math>, <math>y</math>, and <math>z</math>-Directions</li> </ul> | <p style="text-align: center;"><b>SOLID45</b></p> <ul style="list-style-type: none"> <li>• Models three-dimensional solid structures;</li> <li>• The element has plasticity, large strain, and stress-stiffening capabilities;</li> <li>• Steel and weld characteristics are modelled as linear elastic material which is defined by the modulus of elasticity and Poisson's ratio.</li> </ul> |

For this particular example, a series of FEA were conducted with the anticipated starter load of 700 kN required to initiate the crack in conjunction with five different main loads which give normal tensile stress in main plate equal to  $0.0s_{sy}$ ,  $0.25s_{sy}$ ,  $0.4s_{sy}$ ,  $0.5s_{sy}$ , and  $0.625s_{sy}$  where  $s_{sy}$  is specified as yield strength of parent main plate steel. For each combination of the starter load and the main plate load, a series of analyses were conducted releasing the  $y$ -direction displacement restraint of the nodes along the potential crack face simulating the crack propagation. For each of these analyses, the displacement method was used to calculate the stress intensity factor. The results of this series of analysis give the set of stress intensity factor curves illustrated Figure 9.4. Each curve required 17 analyses. Also shown on this figure are the locations of the crack tip, the gap plate section (transition plate section between the starter and main plates), the start of the main plate, the transition zone, and the end of the double-side face grooves.

The initial stress intensity factor for this group of curves ranges from  $142 \text{ MPa}\sqrt{m}$  to  $150 \text{ MPa}\sqrt{m}$ , which is in the anticipated range of the crack initiation toughness of a starter plate with a temperature of  $-20^\circ\text{C}$  as interpolated from starter plates *STP3* and *STP4*.

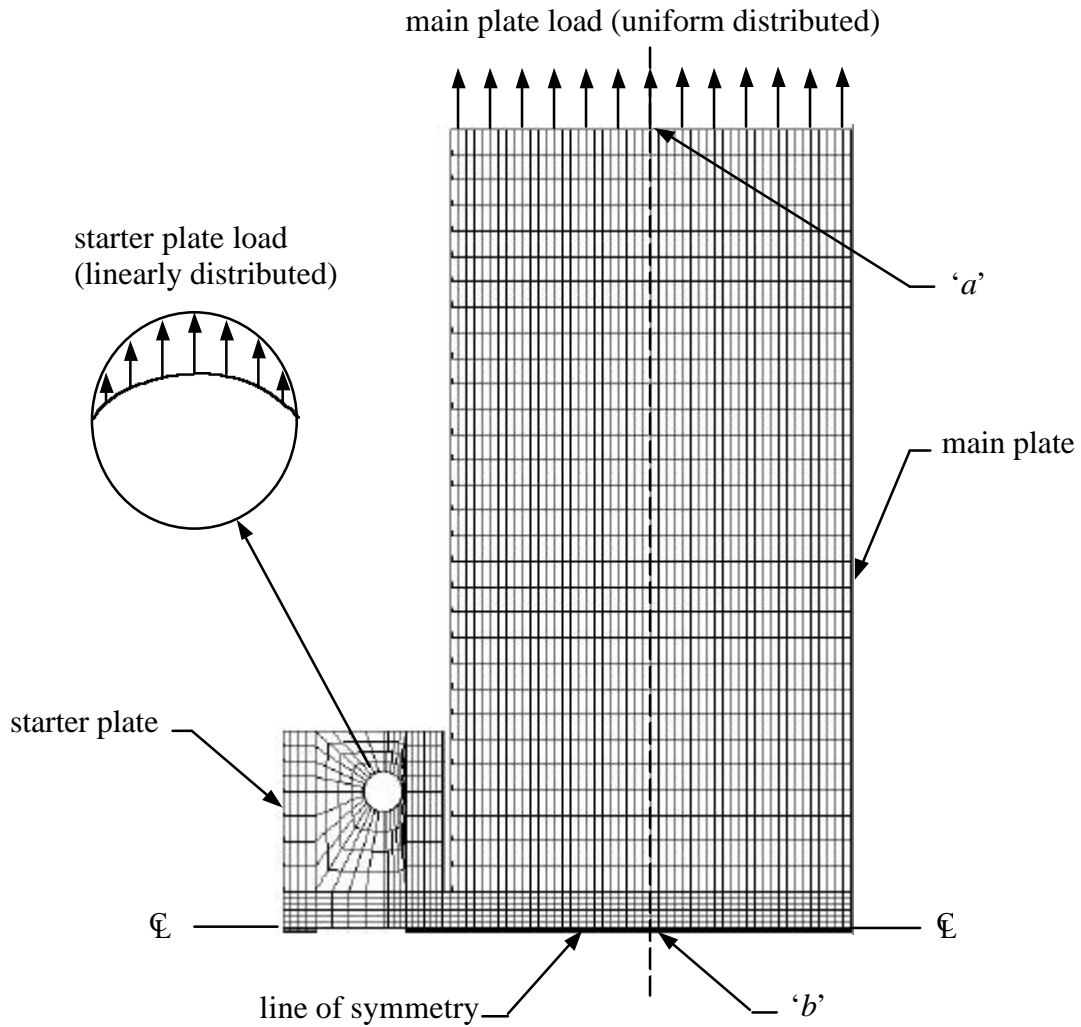


(a) Dimension and Mesh of Large-Scale Specimen



(b) Detail Illustrating Elements through the Thickness in the Groove region

**Figure 9.2: FEA Model for Large-Scale Test Specimen with Face Grooves**



|   |   |
|---|---|
| <p><b>Material Properties</b></p> <ul style="list-style-type: none"> <li>Elastic material properties for steel and weld metal.</li> <li><math>E_s = 200500 \text{ MPa}</math></li> <li><math>E_w = 210000 \text{ MPa}</math></li> <li><math>\nu = 0.286</math></li> </ul> | <p><b>Model Properties</b></p> <ul style="list-style-type: none"> <li>Number of Nodes = 14630</li> <li>Number of Element = 11490</li> </ul>   |
| <p><b>Loading</b></p> <ul style="list-style-type: none"> <li>Uniformly distributed load across the end of specimen as shown above</li> <li>Equivalent distributed pin-load as shown in detail above</li> </ul>  | <p><b>Boundary Condition</b> (see Figure 9.2)</p> <ul style="list-style-type: none"> <li>y-direction constraints across the centerline of weld</li> <li>x and z-direction constraints on point 'a' and z-direction constraint on point 'b'</li> </ul> |

**Figure 9.3: Details of FEA Model for Large-Scale Test Specimen**

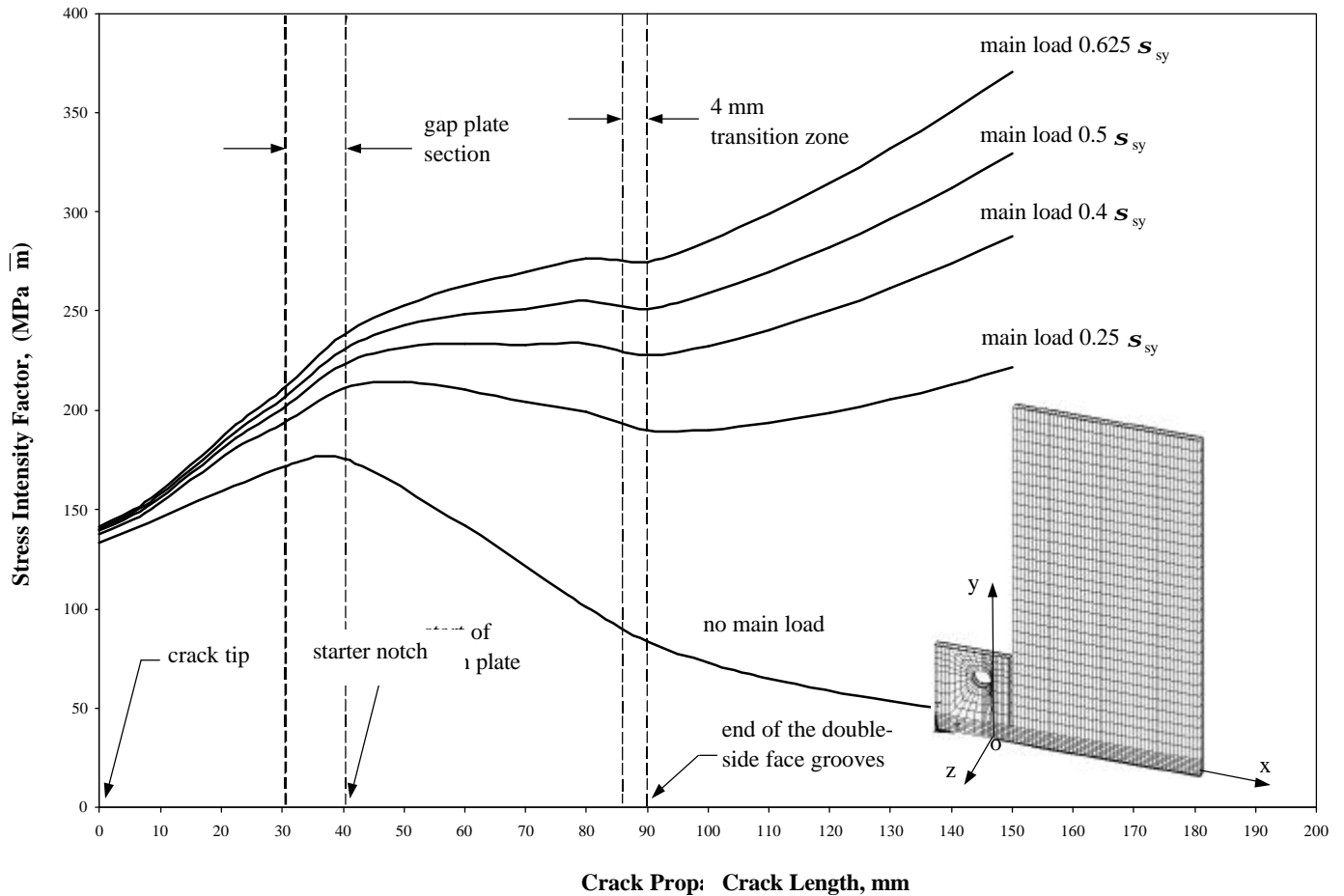


**Figure 9.4: Stress Intensity Factor versus Crack Propagation as predicted by FEA**

Because of the double-side grooves, all curves show an increasing stress intensity factor as the crack propagates through the starter plate into the main plate, and have slopes greater than any other portion of the curve. With the exception of the two curves associated with no load in the main plate and the curve with a tensile normal stress of  $0.25s_{sy}$ , the others show an increasing stress intensity factor field as the crack propagates through the main plate.

There are only two distinct sets of testing conditions in which the cracks can be arrested in the main plate. The first set involves tests conducted under isothermal conditions in which the crack arrest toughness value is constant as illustrated by the horizontal dashed-dotted line for the stress intensity factor graph in Figure 9.5.

At a starter plate load of approximately 700 kN, the stress intensity factor at the crack tip exceeds the crack arrest toughness and the crack propagates until the stress intensity factor curve falls below the crack arrest toughness value as indicated by point 'a' on the stress intensity factor curve for a main plate load of zero. The magnitude of the crack arrest toughness value will be equal to the stress intensity factor value for the measured crack length, which should coincide with point 'a' depending on the distance it takes for the crack arrest itself.

The second set of test conditions involve the tests in which the test specimen is subjected to a temperature gradient (the starter plate to the main plate) as shown in Figure 9.5. The corresponding potential crack arrest toughness curve can be drawn and overlaid (dashed double dotted line) on the stress intensity factor curves as indicated in the figure. The shape of this curve or family of curves for varying tensile stress fields can only be determined by tests and has yet to be determined. Two known crack arrest toughness values of 117 and 149.4 MPa $\sqrt{m}$  for temperatures of  $-10^{\circ}\text{C}$  and  $0^{\circ}\text{C}$ , respectively, are plotted on this curve with triangle symbols.

For example, for any given test load conditions, the measured starter load required to propagate a crack into the main plate and load in the main plate, the stress intensity factor curve can be calculated using the displacement extrapolation method and the data from an appropriate finite element analysis. The measured crack length indicated by point 'b' is coincident with the point at which the calculated stress intensity curve falls below the crack arrest value of the material, as illustrated for the stress intensity factor curve associated with a main plate load of  $0.5S_{sy}$ . The crack arrest toughness value for that magnitude of tensile stress field is equal to the SIF at this point for the given temperature.

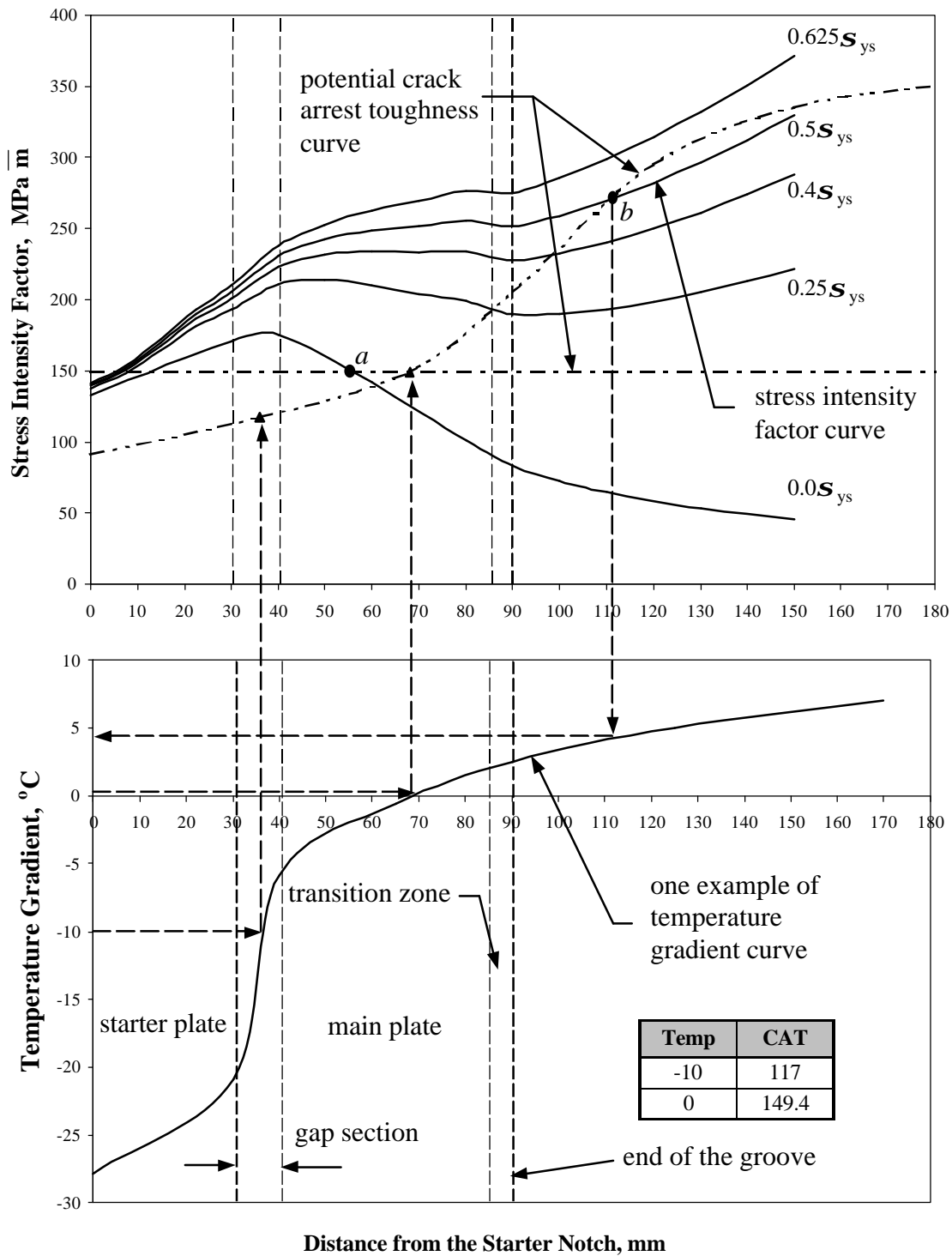


**Figure 9.5: Data Interpretation and Design**

## 9.3 Large-Scale Double Tension Tests

### 9.3.1 Test Specimen Description

Seven large-scale double tension test specimens, as illustrated in Figure 9.1, were flame cut, welded and machined by Fleet Technology Limited (FTL). The specimens were cut from ship steel plate (used for small scale testing) with the rolling direction coinciding with long dimension of the test specimen. The plate was manufactured to ABS Grade DH36 with 20 mm nominal thickness. The full penetration groove weld was made with multiple passes along the line of symmetry of test specimen as previously described in Section 4.1. The welding parameters are presented in Appendix A and the characterization of the weld is given in Section 4.1. The notch geometry and double-side grooves for the large-scale double tension tests are identical to those developed for the starter plate tests.

### 9.3.2 Test Set-Up

The schematic diagram of the test specimen in the load frame along with the 500T and 200T hydraulic actuators, the end restraints, the load plates, the high-strength rods, the distributed beams, the couplers and the turnbuckle are illustrated in Figure 9.6. The instrumentation, the temperature control chamber and the data acquisition systems are not shown for clarity.

The 200T and 500T actuators can be controlled independently of each other and displaced by load control or stroke control. The starter load is applied by the 200T actuator on the top of the stiffened distributing beam through another series of distributing beams, high-strength plates and pins to the starter plate. This mechanism is self-aligning and ensures that the load is applied vertically and parallel to the length of the test specimen. The remaining components consisted of a stiff transition plate, a turnbuckle and a base plate-fixture to transmit the force from the starter plate to the strong floor. The 500T actuator is used to apply a uniform tensile normal stress to the main plate through a coupler, and stiff transition plate and four pins to the test specimen. Pins are also used to transmit the reaction force to the main base plate and then to the strong floor. Both sets of pins have been aligned vertically and horizontally to ensure that the load is transmitted into the main plate with out bending about either principle axis of its cross-section. An assembled view of the test specimen with the temperature control chamber is shown in Figure 9.7.

Figure 9.8 illustrates a section view of the temperature control chamber. A 25 mm thick section of Styrofoam is used as an internal insulation to separate chamber 1 and chamber 2. Two independent liquid nitrogen distribution pipes, single pipes located on either side of the test specimen, were used to distribute the liquid nitrogen uniformly in each chamber. The outlet holes are 3 mm in diameter and are located uniformly along the pipe at 30 mm intervals. Each pipe is fed from a separate liquid nitrogen tank with its own temperature pressure control valve so that the temperatures in each chamber can be controlled independently.

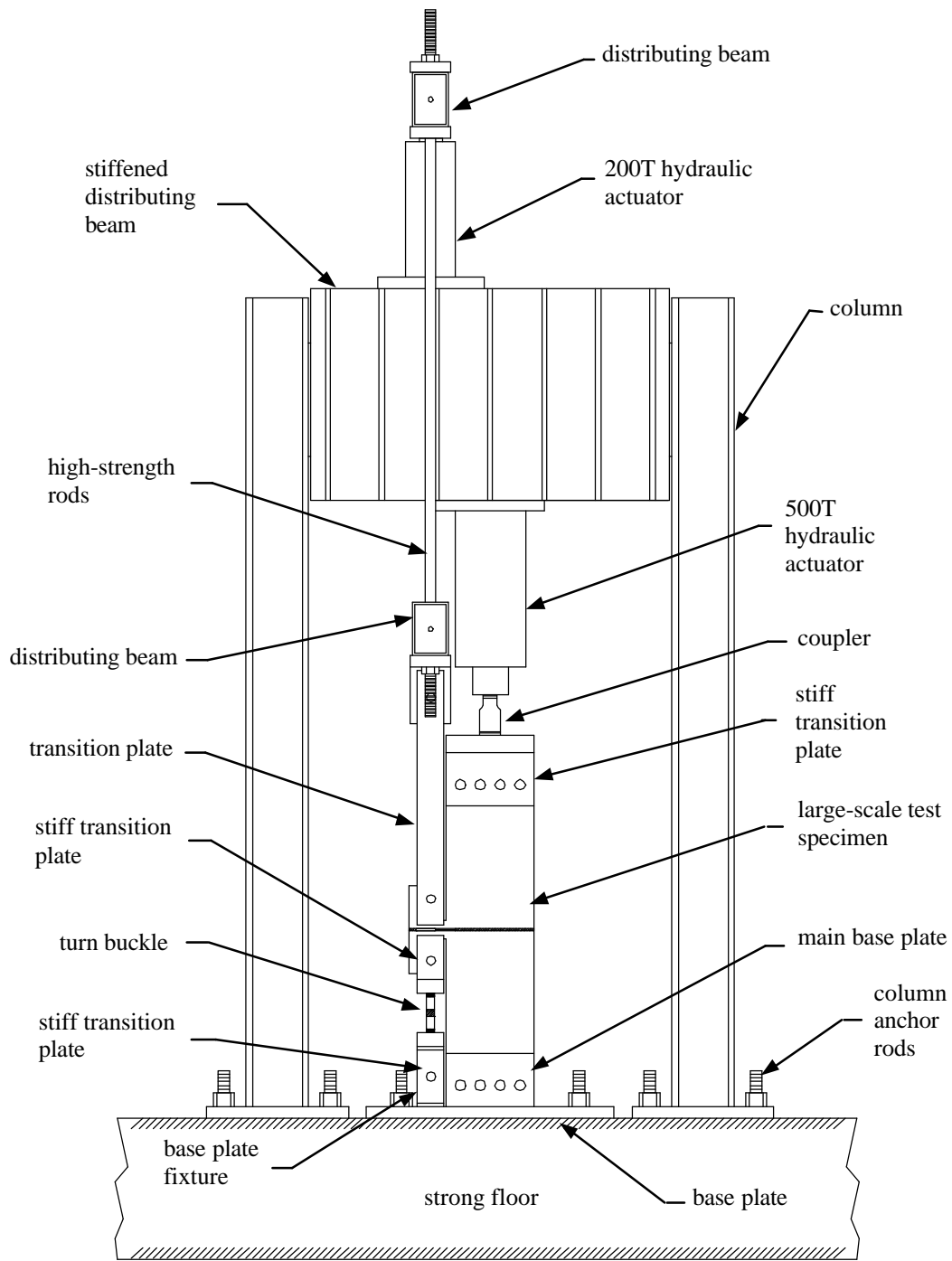


**Figure 9.6: Schematic Diagram of the Double Tension Test In Load Frame**

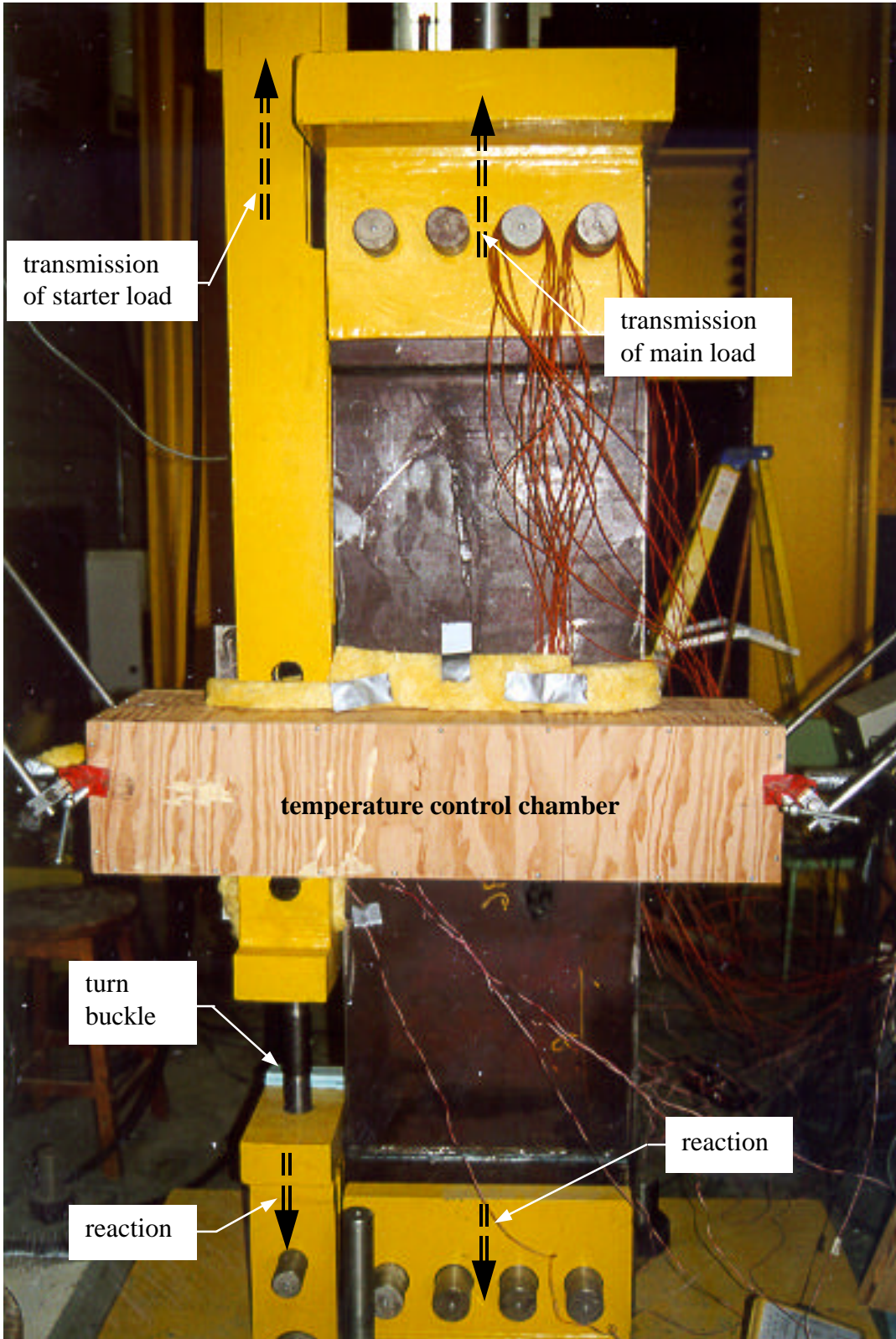


**Figure 9.7: Assemble View of Large-Scale Test**

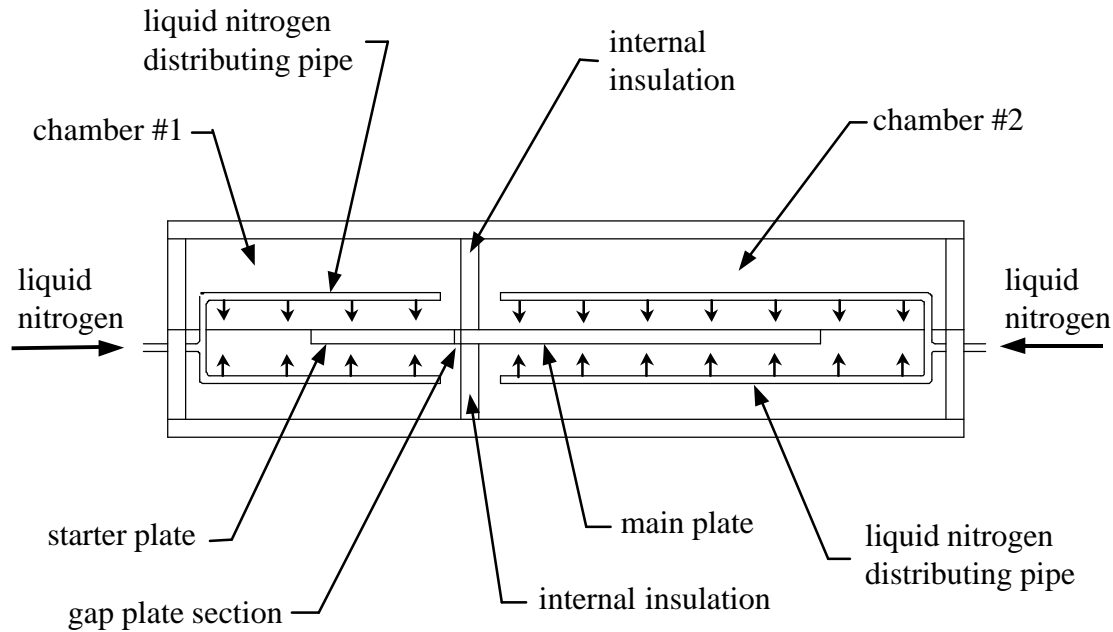


**Figure 9.8: Section View of the Temperature Control Chamber**

### 9.3.3 Instrumentation

Two different data acquisition systems were used to measure the applied load, the strains and the temperatures. The loads, the strains and the temperatures were determined by the pressure transducers, 13 strain gauges and 30 thermocouples with locations and identification numbers illustrated in Figures 9.9 (photograph of specimen with thermocouples, strain gauges and cooling pipes) and 9.10.

The high speed *Gauge Scope* data acquisition has six channels and was used to measure the two loads and the strain response from four strain gauges with numbers 1 to 4. The system is set to record 45000 readings over the period of 0.25 of a second when one of strain gauges is triggered by a 392 *me* drop that results from the strain release due to a crack propagation event. Strain gauge number 1 is the trigger gauge.

The nine strain gauges (numbers 5 to 13) have been located at a distance of 45mm from the centerline of the weld to measure the strains. This series of strains gives a distribution across the width of the main plate, which can be used to estimate the crack length.

Figure 9.11 illustrates a typical series of strain distributions for the initial condition and for different crack propagation lengths (just entering the main plate, end of the double sided groove and 100 mm into the main plate) as determined by finite element analysis.

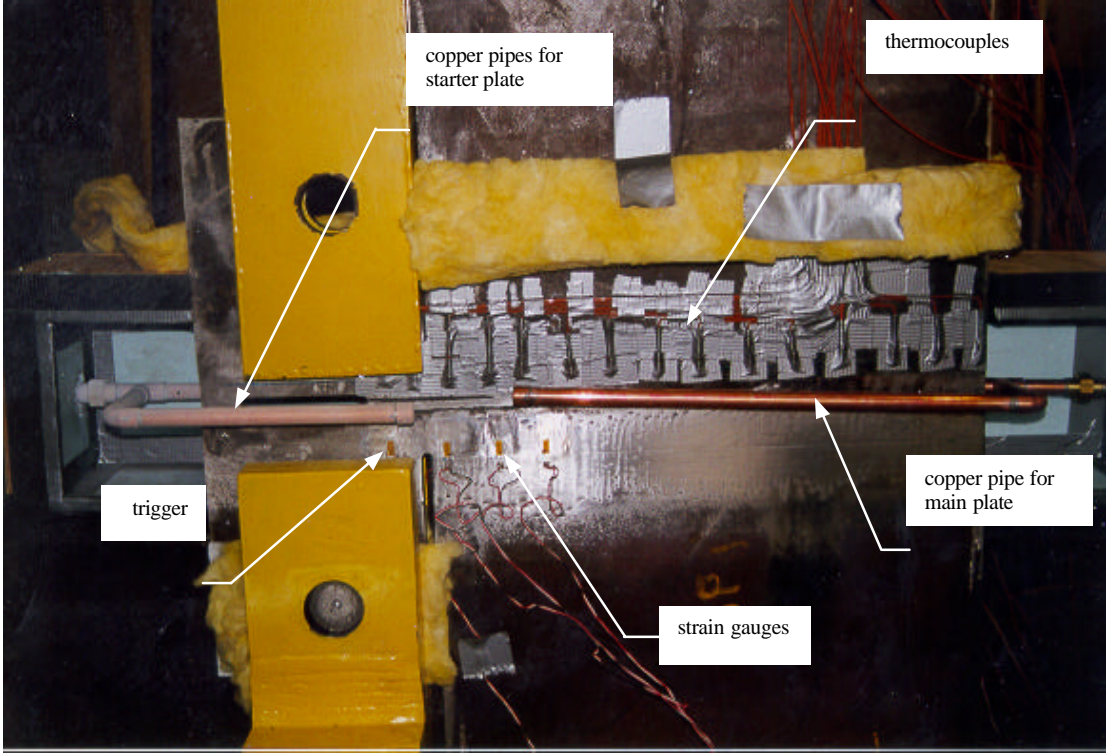


**Figure 9.9: Thermocouples, Strain Gauges and Cooling Pipes**

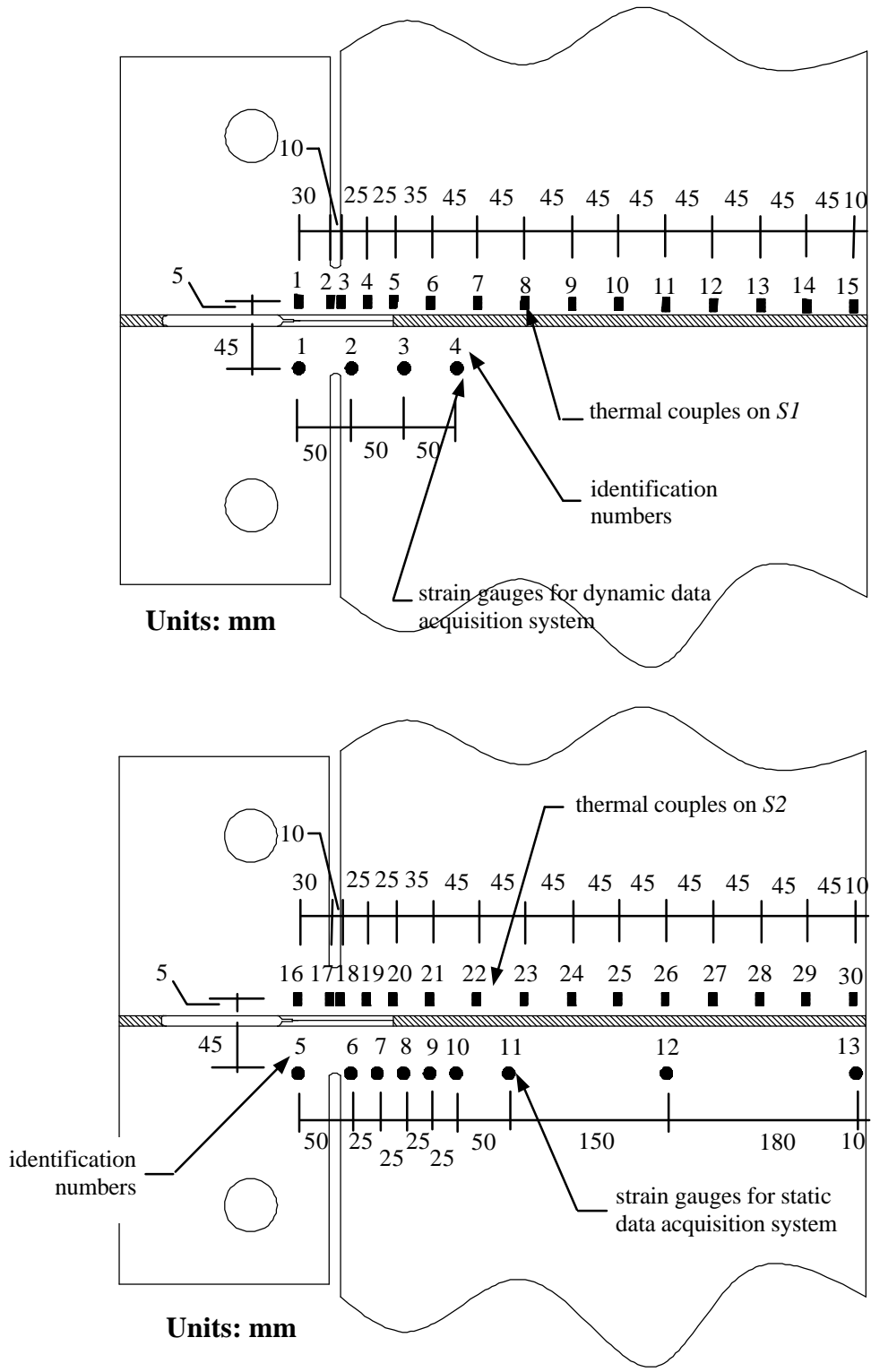
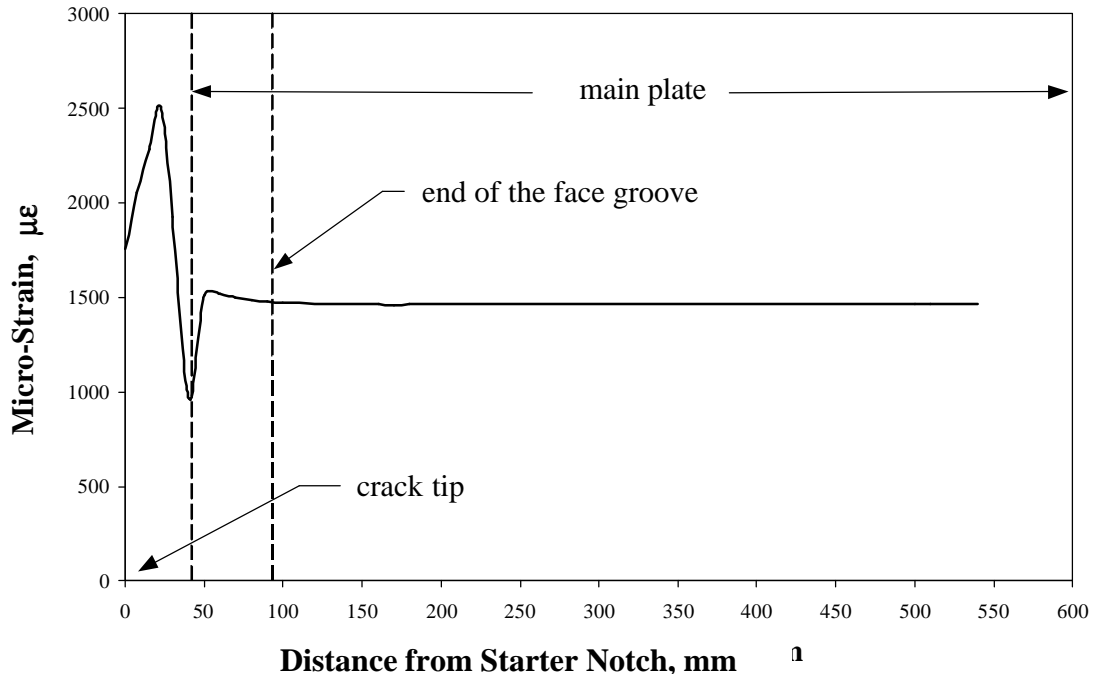
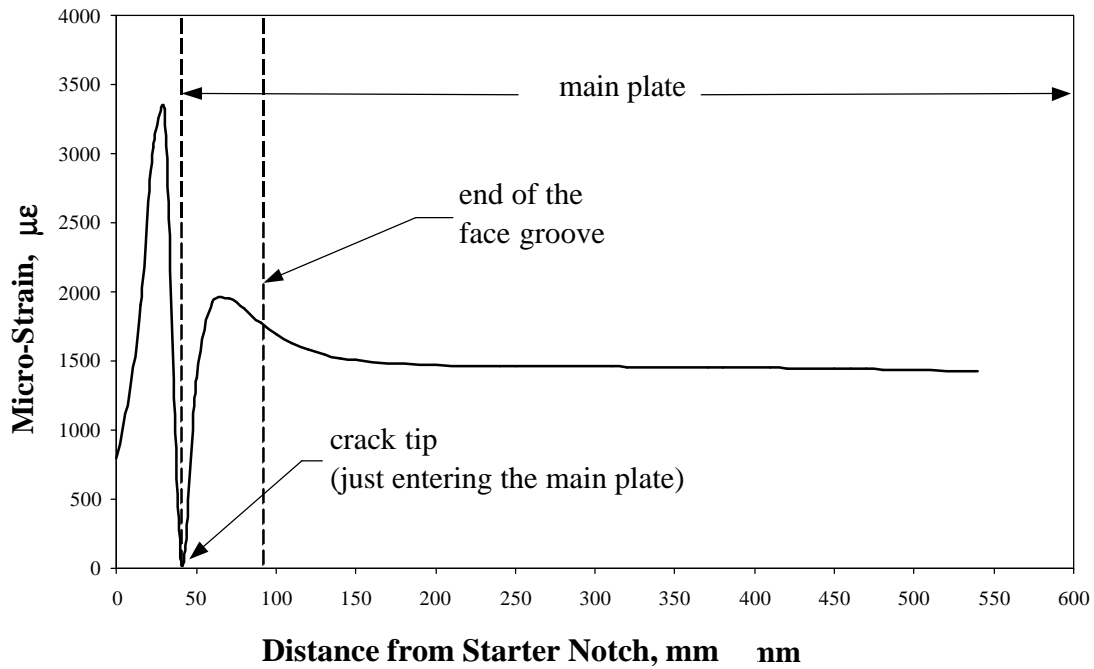


**Figure 9.10: Location and Identification of Strain Gauges and Thermocouples on the Two Sides of the Specimen (S1, S2)**

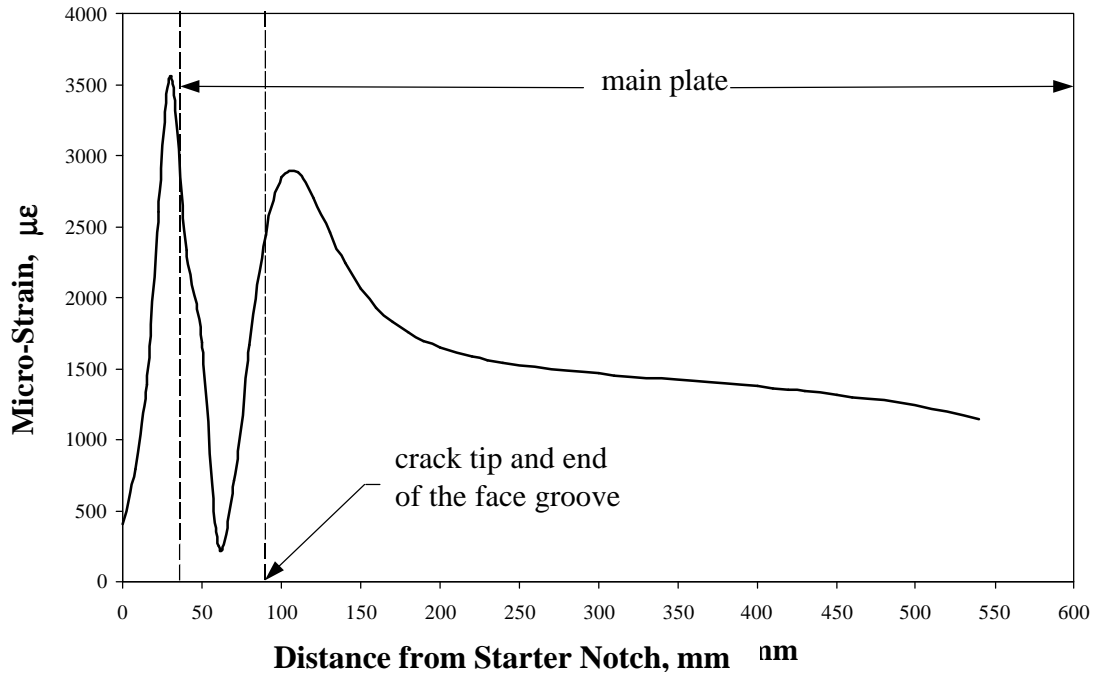


(a) Strain Distribution without Crack Initiation

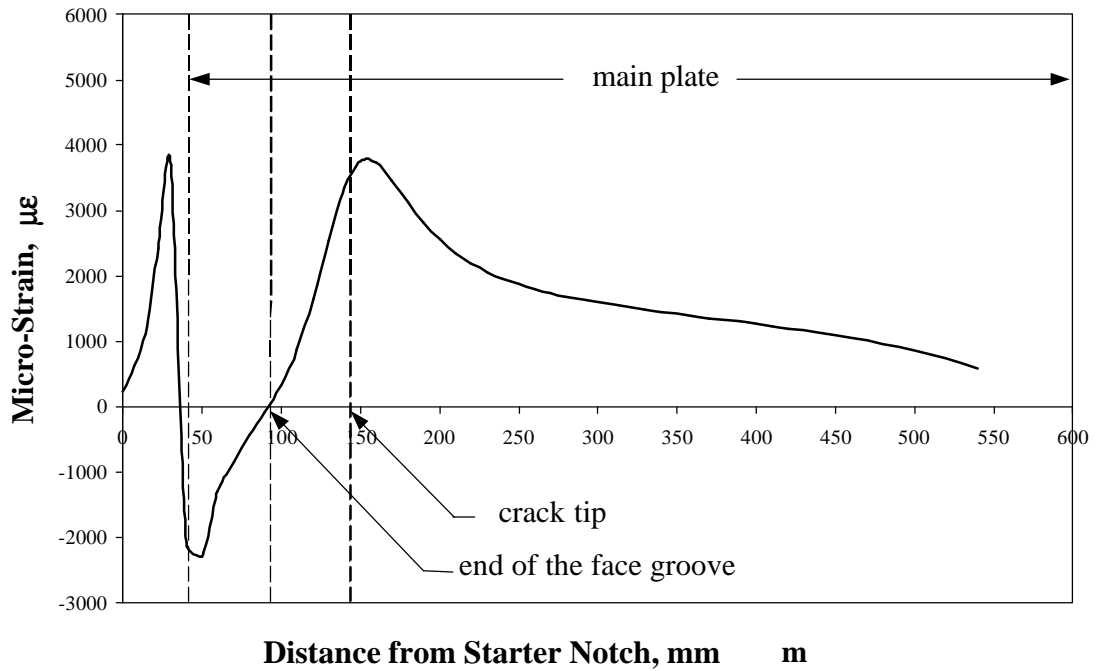


(b) Strain Distribution with Crack just Entering the Main Plate

Figure 9.11: Strain Distributions for Varying Crack Lengths



(c) Strain Distribution with Crack Reaching the end of Face Groove



(d) Strain Distribution with Crack Propagating 100mm into Main Plate

Figure 9.11 (Cont'd) - Strain Distributions for Varying Crack Lengths

### 9.3.4 Measurement of Temperature Gradients

A series of steady temperatures were measured prior to conducting the first large-scale test to establish the effectiveness of the internal insulation barrier and to ensure that the temperature in both chambers can be controlled and repeated. Each of three steady state temperature curves associated with temperatures of  $-20^{\circ}\text{C}$  to  $0^{\circ}\text{C}$ ,  $-20^{\circ}\text{C}$  to  $-10^{\circ}\text{C}$  and  $-10^{\circ}\text{C}$  to  $10^{\circ}\text{C}$  in chamber 1 and 2 respectively are illustrated in Figure 9.12. The temperature variation curves had a gradient that extended approximately 150 mm from the crack tip into the main plate. The internal insulation barrier effectively isolated the two chambers with a significant temperature drop (gradient) from one side to the other. The temperature control chamber provided the conditions required to initiate a crack run within the starter plate while maintaining a shallow temperature gradient in the main plate.

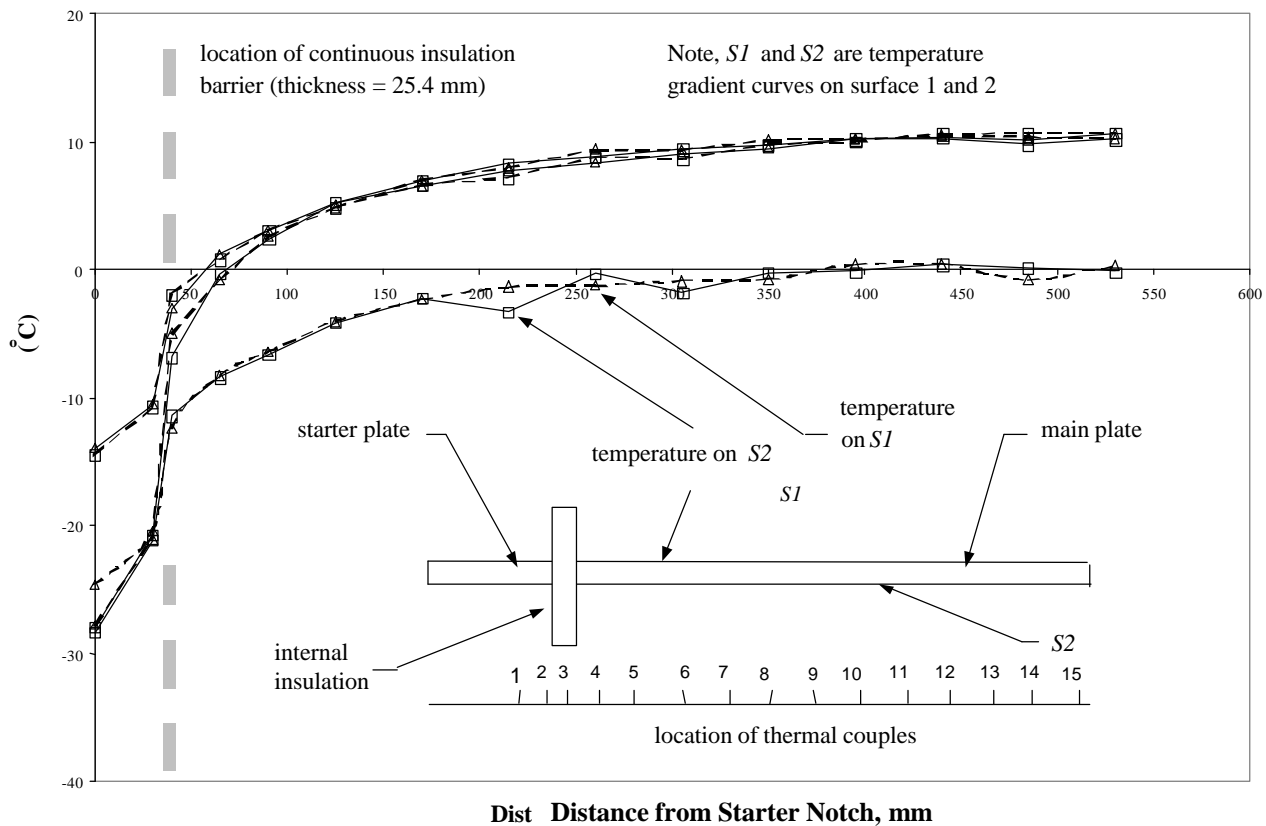


**Figure 9.12: Temperature Gradient Curves**

### 9.3.5 Large-Scale Double Tension Test Summary

Seven large-scale tests were conducted with a variety of starter load systems, temperatures and starter crack geometries in an attempt to initiate and propagate cracks from the starter plate into the main plate. The test identification codes, conditions, results, loading mechanisms and comments for each test are summarized in Table 9.2. Tests are identified with alphanumeric tags that indicate large-scale plate (LSP3) and the numeric order in which the plates were tested. The three different starter load systems, direct tension, articulating load mechanism, and edge crack open displacement (load arms located in the plane of the test specimen and welded to starter plate) associated with each test are identified in the table with the coloured cells green, purple and blue. Discussions about the modifications to the load systems and test conditions follow. Relevant pictures, diagrams, and results from additional finite elements analyses have been included.

Fracture classification was done based on a “structural” perspective, that is, based on crack event duration. In general, the first short (5 to 20 mm) crack propagation event took place along the groove, i.e., plane strain type. On a macroscopic scale, using conventional fracture classification terminology, these first events would be “brittle”. The second event, at higher applied load, occurred in most cases in the “shear mode”, called that because of its orientation with respect to the long range 2D stress field. It has been called “brittle shear” because the fracture surface is flat with respect to the plate thickness. As the fractures were not cut out, these definitions were made with limited access to the fracture face.

**Table 9.2: Large-Scale Double Tension Test Summary**

| Test ID | Test Conditions  | Test Results   | Comments and Modifications  |
|---------|--|--|---|
| LSP1    | <ul style="list-style-type: none"> <li>Notch and crack geometry identical to the starter plate STP4 with double-side face grooves, a 15 mm long initial crack (10 mm blunt saw cut and 5 mm sharp saw cut)</li> <li>testing temperature of -20°C and 10°C for the starter plate and the main plate, respectively.</li> <li>Direct tension loading</li> <li>Load sequence:               <ol style="list-style-type: none"> <li>3000 kN was applied to the main plate, with the starter plate disconnected;</li> <li>starter plate connected and made fast with the turnbuckle</li> <li>starter plate load applied monotonically till a crack propagation event occurred</li> </ol> </li> </ul> | <ul style="list-style-type: none"> <li>brittle crack propagated approximately 10 mm along the weldment at a load of 740 kN</li> <li>during continued loading a brittle shear failure occurred through the gap plate section (i.e., the 10 mm gap between starter and main plate) at 800 kN</li> <li>brittle fracture illustrated in Figure 9.13 (a), (b)</li> <li>Crack Arrest Toughness (CAT) value cannot be calculated</li> </ul> | <ul style="list-style-type: none"> <li>The deviation of the fracture from its initial path through to the gap plate may be the result of excessive localized shear induced by differential shear which in turn is a function of the loading sequence.</li> <li>finite element analysis replicating the load sequence clearly illustrated the shear distortion and excessive shear stress between plates (equal to or greater than shear yield) in the fracture region, as illustrated Figure 9.14</li> <li>A modified load sequence was developed to minimize differential shear</li> </ul> |

Table 9.2 (Cont'd) - Large-Scale Double Tension Test Summary

| Test ID | Test Conditions   | Test Results   | Comments and Modifications   |
|---------|---|--|--|
| LSP2    | <ul style="list-style-type: none"> <li>Notch and crack geometry identical to the starter plate STP4 with double-side face grooves, a 15 mm long initial crack (10 mm blunt saw cut and 5 mm sharp saw cut)</li> <li>testing temperature of -20°C and 10°C for the starter plate and the main plate, respectively.</li> <li>Direct tension loading</li> <li>Modified load sequence as per Table 9.3</li> </ul>   | <ul style="list-style-type: none"> <li>brittle crack propagated 15 mm to 20 mm along the weld at 700 kN</li> <li>during continued loading a brittle shear failure occurred through the gap plate at 810 kN.</li> <li>brittle fracture illustrated in Figure 9.17</li> <li>CAT value can not be calculated</li> </ul>   | <ul style="list-style-type: none"> <li>Since the failure mode and loads were essentially identical to the previous test, further modifications (listed in Table 9.4) were required to improve the possibility of a successful crack propagation event</li> </ul>   |
| LSP3    | <ul style="list-style-type: none"> <li>Modified notch and crack geometry with double-side face grooves, a 35 mm long initial crack (30 mm blunt saw cut and 5 mm sharp saw cut)</li> <li>Ligament width decreased to 20mm</li> <li>Thermal barrier permanently shifted 50mm into the main plate</li> <li>testing temperature of -40°C and 0°C for the starter plate and the main plate, respectively.</li> <li>Direct tension loading</li> <li>Modified load sequence with target starter and main plate loads of 400 kN and 3000 kN, respectively.</li> </ul>          | <ul style="list-style-type: none"> <li>brittle crack propagated 15 mm along the weld at 413 kN</li> <li>during continued loading a brittle shear failure occurred through the gap plate at 558 kN</li> <li>CAT value can not be calculated.</li> <li>measurements indicated that 70% of applied starter load was transferred through the starter plate to the passive restraint (turnbuckle mechanism)</li> </ul>  | <ul style="list-style-type: none"> <li>consistent failure mode and shear distortion through gap plate</li> <li>the articulating starter load system illustrated in Figures 9.18 and 9.19 was developed to provide equal outward displacement of the pins that join the load system to the starter plate, the application of direct tension equal and opposite across the potential crack path and uniform opening of that crack, while minimizing the interaction with the load and deformation of the main plate</li> </ul> |
| LSP4    | <ul style="list-style-type: none"> <li>Notch and crack geometry identical to the starter plate STP4 with double-side face grooves, a 15 mm long initial crack (10 mm blunt saw cut and 5 mm sharp saw cut)</li> <li>testing temperature of -40°C and 0°C for the starter plate and the main plate, respectively.</li> <li>articulating load mechanism</li> <li>the ligament adjacent to the notch was cut through to decrease the load required to promote crack propagation modifying the problem to an edge crack problem</li> <li>main plate load 2569 kN</li> </ul> | <ul style="list-style-type: none"> <li>initial ligament length of 20 mm; at a actuator load of 1176 kN or a starter load of 530 kN the loading arms experienced localized yielding at the pin connection near the column</li> <li>the ligament was cut through and the test restarted</li> <li>a brittle crack propagated 5 to 10 mm at a starter load of 181 kN</li> <li>brittle crack propagated 200 mm into the main plate, but deviated from the weld metal, at 214 kN</li> <li>refer to Figures 9.21, 9.22</li> </ul> | <ul style="list-style-type: none"> <li>crack deviation may be caused either by local weld flaws, unequal loading above and below, by a varying temperature field along the length of the test specimen (varying crack arrest toughness), and/or by local plastification at the crack tip during the initial loading</li> <li>the liquid nitrogen streams emitted by the cooling system were directed at the weld and would project downward due gravity</li> </ul>   |

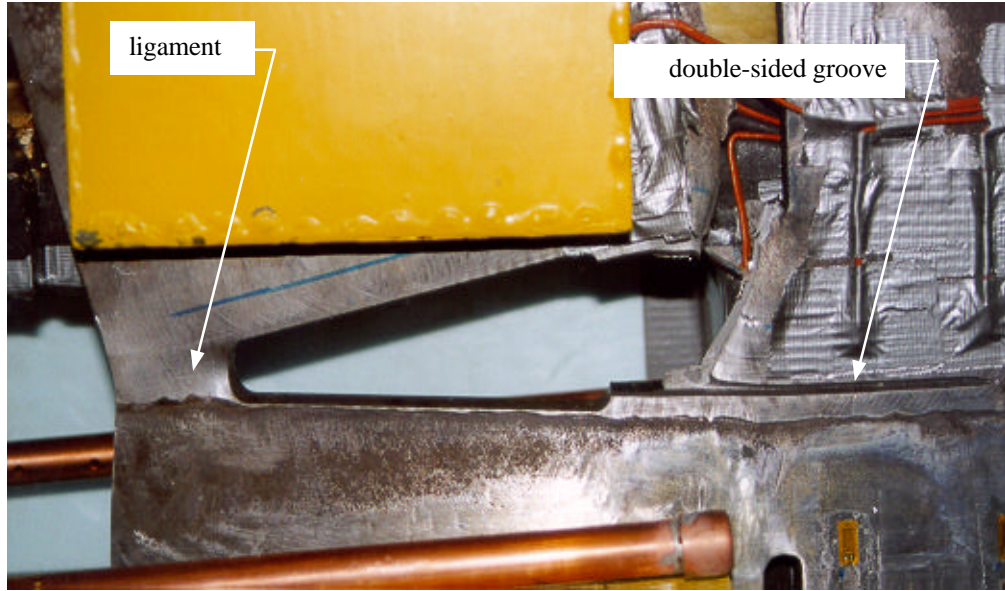
Table 9.2 (Cont'd) - Large-Scale Double Tension Test Summary

| Test ID | Test Conditions   | Test Results   | Comments and Modifications  |
|---------|---|--|---|
| LSP5    | <ul style="list-style-type: none"> <li>Notch and crack geometry identical to the starter plate STP4 with double-side face grooves, a 15 mm long initial crack (10 mm blunt saw cut and 5 mm sharp saw cut); ligament cut through</li> <li>testing temperature of -44°C and 0°C for the starter plate and the main plate, respectively.</li> <li>articulating load mechanism</li> <li>main plate load 2527 kN</li> </ul> | <ul style="list-style-type: none"> <li>a brittle crack propagated approximately 10 mm along the weld at a starter load of 177 kN</li> <li>brittle crack propagated 130 mm into the main plate, but deviated from the weld metal, at 248 kN</li> <li>refer to Figures 9.23</li> </ul> | <ul style="list-style-type: none"> <li>previous test conditions repeated to determine whether the crack deviation was systematic or random</li> <li>measurements of the friction forces, starter loads, and outward displacement for both loading arms were essentially the same</li> <li>no conclusions as to whether small deviations were sufficient to cause crack deviation</li> <li>temperature gradient along the length is the most likely cause for crack deviation</li> <li>temperature control chamber modified to double pipe system (separated vertically by 100mm)</li> </ul> |
| LSP6    | <ul style="list-style-type: none"> <li>Notch and crack geometry identical to the starter plate STP4 with double-side face grooves, a 15 mm long initial crack (10 mm blunt saw cut and 5 mm sharp saw cut); ligament cut through</li> <li>testing temperature of -44°C and 0°C for the starter plate and the main plate, respectively.</li> <li>articulating load mechanism</li> <li>main plate load 2557 kN</li> </ul> | <ul style="list-style-type: none"> <li>brittle crack propagated 40 mm into the main plate, but deviated from the weld metal, at 271 kN</li> <li>refer to Figures 9.24,9.25</li> </ul>  | <ul style="list-style-type: none"> <li>double pipe system illustrated in Figure 9.24</li> <li>thermal barrier located 50mm into main plate</li> <li>holes in piping system adjusted upward (projects liquid nitrogen stream into chamber and not directly onto the test specimen) to provide uniform cooling of chamber, refer to Figure 9.26</li> <li>starter load system must be the cause of systematic crack deviation away from intended path</li> <li>modified load system required</li> </ul>  |
| LSP7    | <ul style="list-style-type: none"> <li>Notch and crack geometry identical to the starter plate STP4 with double-side face grooves, a 15 mm long initial crack (10 mm blunt saw cut and 5 mm sharp saw cut); ligament cut through</li> <li>testing temperature of -47°C and 0°C for the starter plate and the main plate, respectively.</li> <li>Edge crack open displacement load system</li> </ul>                     | <ul style="list-style-type: none"> <li>brittle crack propagated 10mm along the weldment at 115 kN</li> <li>arrested in starter plate</li> <li>continue loading produced ductile tearing and deformation of gap plate</li> <li>refer to Figure 9.28</li> </ul>                        | <ul style="list-style-type: none"> <li>edge crack open displacement load system illustrated in Figure 9.28</li> <li>temperature gradient curves illustrated in Figure 9.27</li> <li>insufficient energy to propagate crack into main plate</li> <li>requires more strain energy (larger load, center crack detail similar to STP4)</li> <li>suggested modification given in recommendations</li> </ul>  |

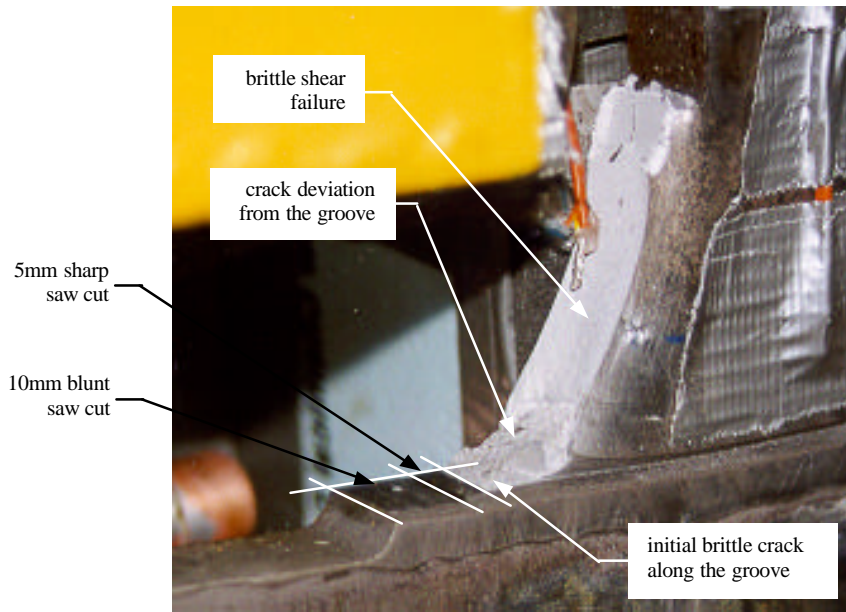
### 9.3.6 Test LSP1 Discussion

The first large-scale double tension test *LSP1* with the same notch and crack geometry as starter plate STP4 (double-side face grooves and a 15 mm long initial crack (10 mm blunt saw cut and 5 mm sharp saw cut)) was tested with temperature of  $-20^{\circ}\text{C}$  and  $10^{\circ}\text{C}$  for the starter plate and the main plate, respectively. Temperatures were stabilized after 2 to 3 hours of cooling. A 3000 kN load was applied to the main plate with the starter plate disconnected. The starter plate was then connected and made fast with the turnbuckle and a direct tension load applied monotonically with the 200T actuator until a crack propagation event occurred. Initially, a brittle crack propagated approximately 10 mm along the weldment at a load of 740 kN. The starter plate load was then increased and a brittle shear failure occurred across the gap plate at 800 kN as illustrated in Figure 9.13 (a) and (b). The cracks deviated from the weldment and did not enter into the main plate, hence a crack arrest toughness value could not be determined.

The deviation of the fracture from its initial path through to the gap was the result of excessive localized shear that may have been induced by differential shear between the starter and main plates, which in turn would be a function of loading sequence. The displacement along the length of the test specimen and the corresponding shear stress associated with the application of a main plate load of 3000 kN and then subsequently starter load of 700 kN are shown in Figures 9.14. The figure clearly illustrates that shear distortion between the starter plate and the main plate, and the large shear stress (equal to or greater than shear yield) in the fracture region.

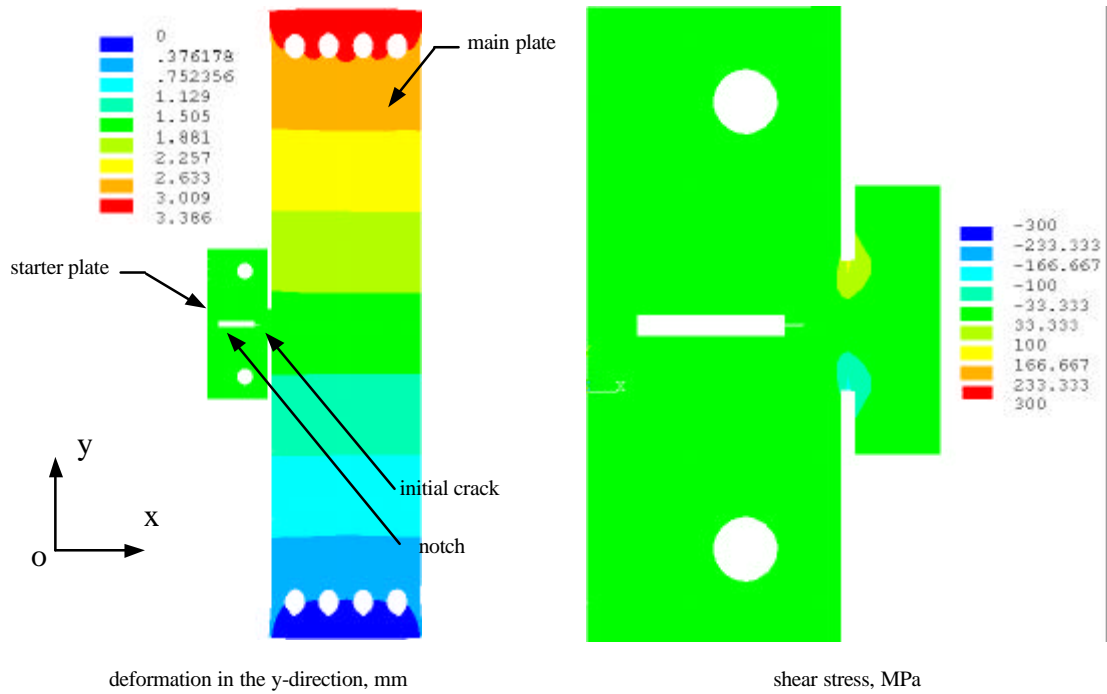


(a) Side View of Crack Propagation

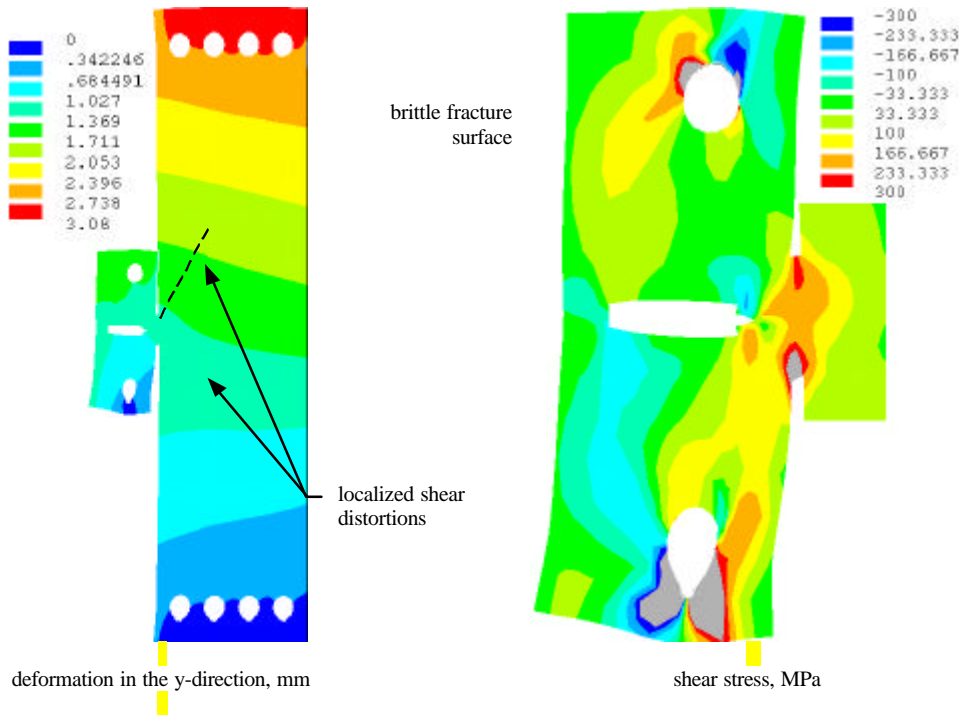


b) Brittle Crack Surface

**Figure 9.13: Brittle Crack Propagation**



**Load Step 1: Main load = 3000 kN; starter load mechanism unconnected**



**Load Step 2: Main load = 3000 kN; starter load = 700 kN**

**Figure 9.14: Deformation and Shear Stress Contours, LSP1**

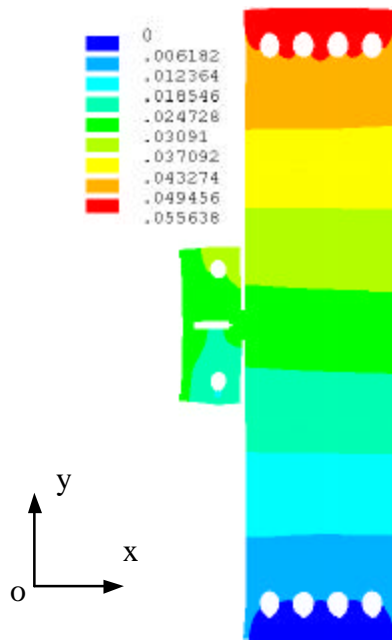
### 9.3.7 Modified Load Sequence

Recognizing this failure mode and verifying its occurrence analytically resulted in a re-definition of the load sequence to minimize the shear distortion along the length of the weldment and the shear stresses in the gap plate section associated with the failure of the first specimen. After alignment of the test specimen, connection of the data acquisition, and establishment of the ambient temperature for both the starter plate and the main plate, the first load step is to make the specimen fast with all the connections in the load reaction systems. The second load step is to apply a small initial contact starter load and main load in proportion to the relative stiffness for both the starter plate and the main plate. The remaining load increments, which bring the starter load and main load to their target values, will be applied in the same ratio. If the crack is not initiated, then additional load can be applied to the starter plate alone. In the absence of any crack extension, this small increment in the starter load should have little effect in increasing the shear stresses in the region where the first specimen failed. The effects of the modified load sequence given in Table 9.3 on the gap plate region, as illustrated by the y-direction deformations in the starter and main plates and shear stresses across the gap plate in Figures 9.15 and 9.16, respectively, clearly demonstrate that the displacements were kept relatively uniform along the weldment and that shear deformations were minimized.

The load was applied to the upper end of both the starter and main plates as per the test. The lower connection points of the main plate were in full contact and attached to rigid elements of very short length. The elastic deformation of these elements under the applied loads was small (negligible for the main plate). The starter plate lower connection points were modeled together with the elasticity of the two plates.

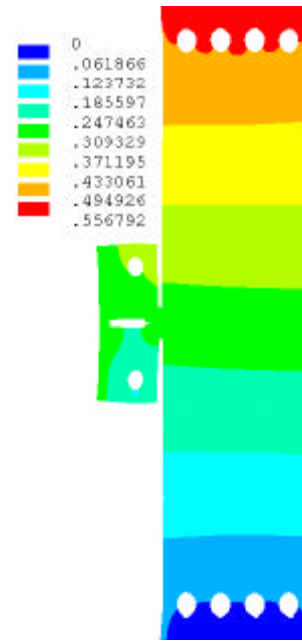
**Table 9.3: Modified Load Sequence**

| <b>Load Steps</b> | <b>Starter Load<br/>(kN)</b> | <b>Main Load<br/>(kN)</b> |
|-------------------|------------------------------|---------------------------|
| 1                 | 10                           | 50                        |
| 2                 | 100                          | 500                       |
| 3                 | 200                          | 1000                      |
| 4                 | 300                          | 1500                      |
| 5                 | 450                          | 2000                      |
| 6                 | 600                          | 2500                      |
| 7                 | 700                          | 3000                      |
| 8                 | 840                          | 3000                      |



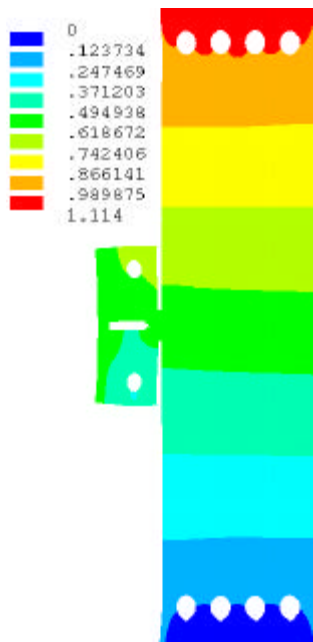
Load Step 1

**Step 1: Main load = 50 kN  
Starter load = 10 kN**



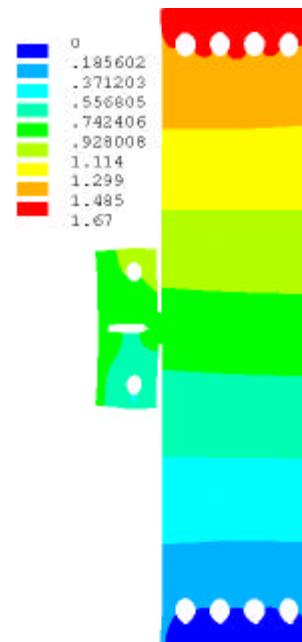
Load Step 2

**Step 2: Main load = 500 kN  
Starter load = 100 kN**



Load Step 3

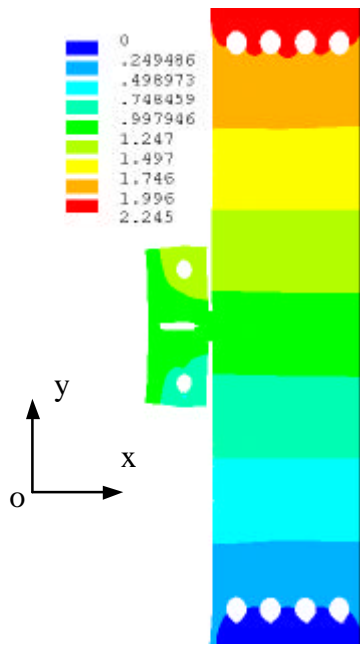
**Step 3: Main load = 1000 kN  
Starter load = 200 kN**



Load Step 4

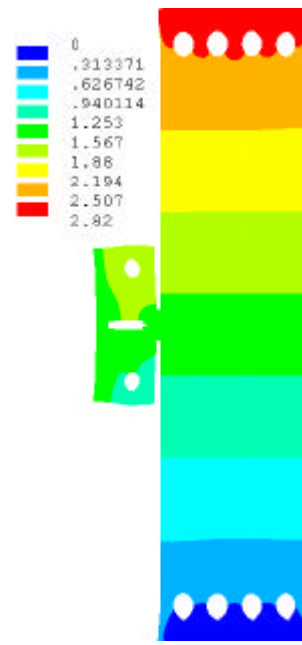
**Step 4: Main load = 1500 kN  
Starter load = 300 kN**

**Figure 9.15: Deformation in the y-direction, Modified Load Sequence**



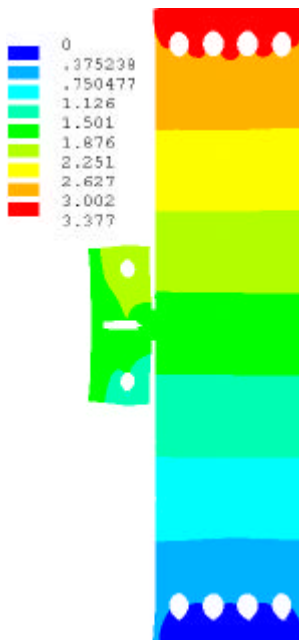
Load Step 5

**Step 5: Main load = 2000 kN  
Starter load = 450 kN**



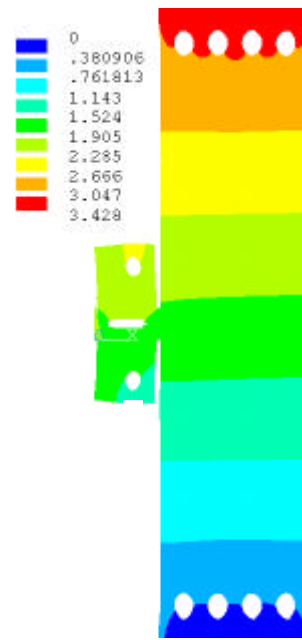
Load Step 6

**Step 6: Main load = 2500 kN  
Starter load = 600 kN**



Load Step 7

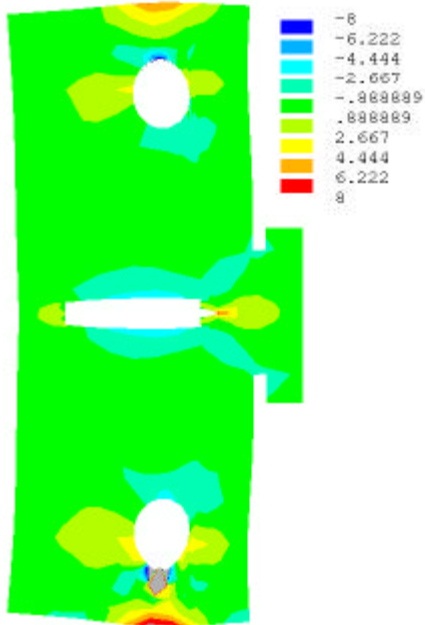
**Step 7: Main load = 3000 kN  
Starter load = 700 kN**



Load Step 8

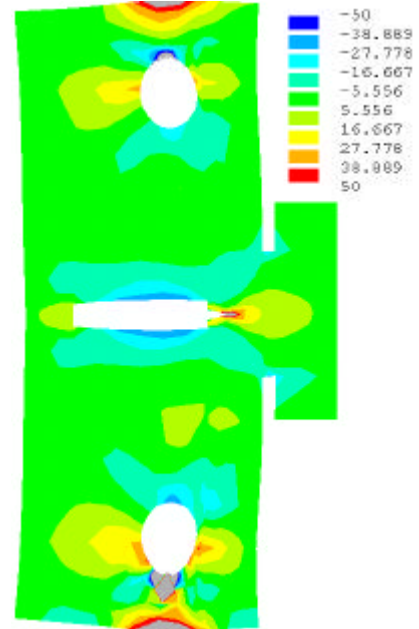
**Step 8: Main load = 3000 kN  
Starter load = 840 kN**

Figure 9.15 (Cont'd) - Deformation in the y-direction, Modified Load Sequence



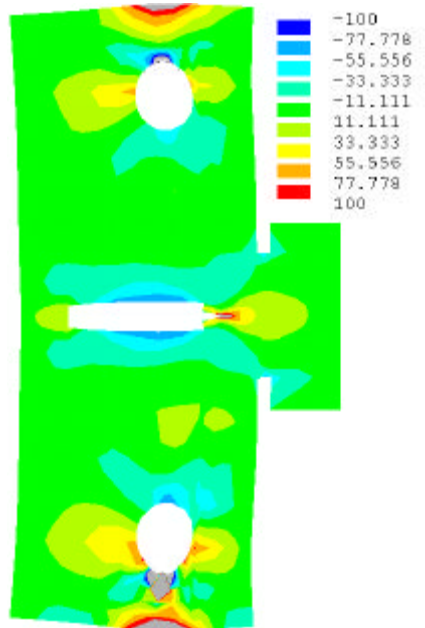
Load Step 1

**Step 1: Main load = 50 kN  
Starter load = 10 kN**



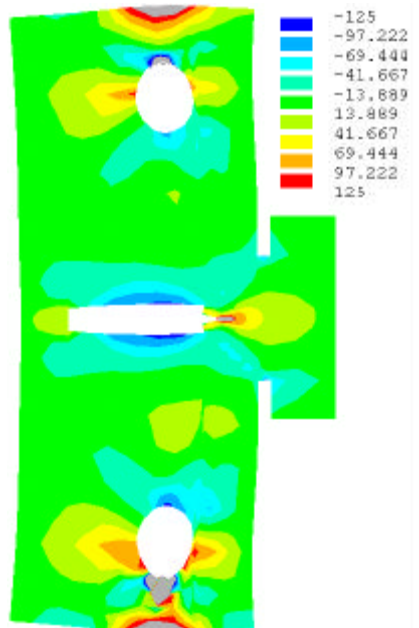
Load Step 2

**Step 2: Main load = 500 kN  
Starter load = 100 kN**



Load Step 3

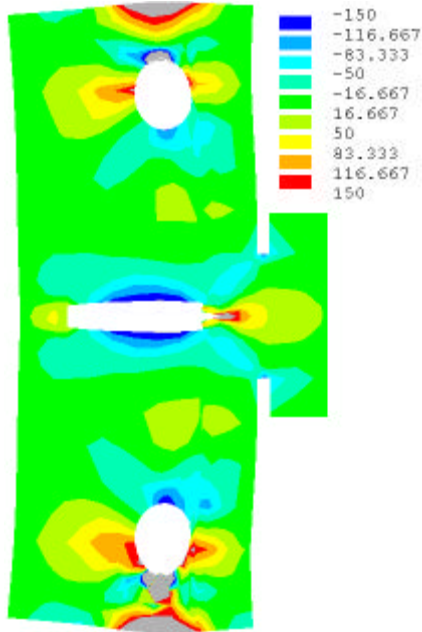
**Step 3: Main load = 1000 kN  
Starter load = 200 kN**



Load Step 4

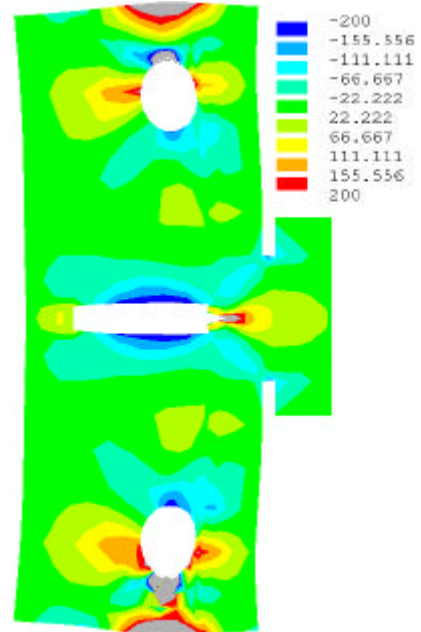
**Step 4: Main load = 1500 kN  
Starter load = 300 kN**

**Figure 9.16: Shear Stresses across the Gap Plate, Modified Load Sequence**



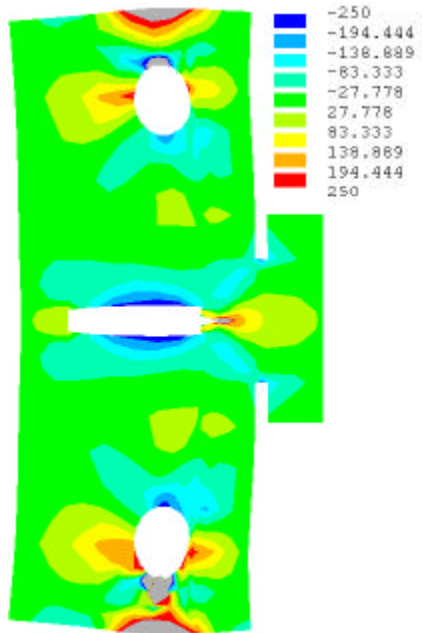
Load Step 5

**Step 5: Main load = 2000 kN  
Starter load = 450 kN**



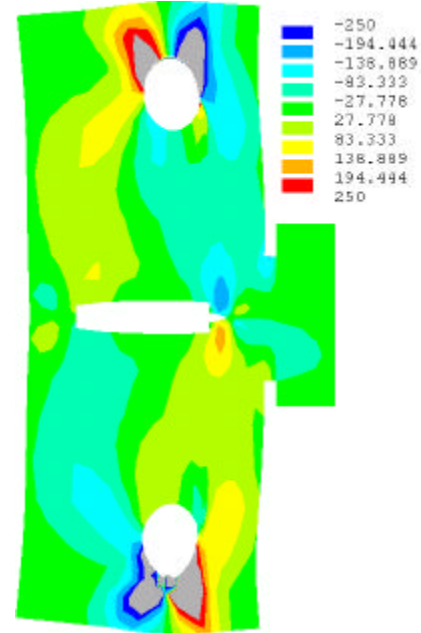
Load Step 6

**Step 6: Main load = 2500 kN  
Starter load = 600 kN**



Load Step 7

**Step 7: Main load = 3000 kN  
Starter load = 700 kN**



Load Step 8

**Step 8: Main load = 3000 kN  
Starter load = 840 kN**

Figure 9.16 (Cont'd) - Shear Stresses across the Gap Plate, Modified Load Sequence

### 9.3.8 Test LSP2 Discussion

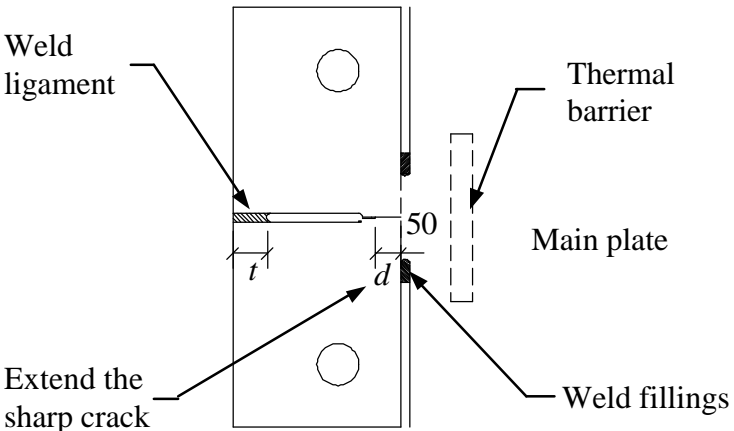
Based on the analysis of load sequence, the second large-test LSP2 loaded according to load steps listed in Table 9.3. The specimen configuration, notch geometry, initial crack details and ambient temperature for the starter and main plates remain the same as first test. The failure mode was similar to the first with the initial brittle crack (15mm to 20 mm along the weldment) forming at a starter plate load of 700 kN. The picture shown in Figure 9.17 clearly illustrates the shear distortion in the gap plate above the double-sided groove. The brittle shear failure in the gap plate occurred at 810 kN. The passive restraint provided by turnbuckle below the starter plate was not effective in opening the crack uniformly.

To increase the possibility of propagating the crack a into the main plate beyond the double-sided grooved section, the test conditions and local geometry for the third large scale test specimen LSP3 were modified according to the highlighted options given in the summary in Table 9.4 which lists the desired effects associated with each modification.



**Figure 9.17: Results of Fracture for LSP2**

**Table 9.4: Modifications to Promote Crack Propagation and Corresponding Effects**

| Modification   | Effects  |
|--|--|
| Draft of Configuration of Starter Plate  |    |
| Extend Sharp Notch   | <ul style="list-style-type: none"> <li>Extend the sharp crack to the edge of gap to reduce the effect of decreasing K values caused by relaxation in the starter load as the crack propagates;</li> </ul>  |
| Decrease width of ligament, $t$  | <ul style="list-style-type: none"> <li>Decreasing the length of ligament (from 40mm to 20 mm) opposite to the end of crack tip allows this material to plastify prior to shear-yielding in the gap region, which yields better crack opening geometry;</li> </ul>  |
| Shift thermal barrier and increase brittleness of material for the region local to the initial propagating crack | <ul style="list-style-type: none"> <li>Move the thermal barrier into the main plate, 50mm away from the edge region;</li> <li>Decreases the crack arrest toughness locally ensuring a minimum crack propagation length into the main plate (ambient temperatures in the starter and main plates were reduced to <math>-40^{\circ}\text{C}</math> and <math>0^{\circ}\text{C}</math>, respectively);</li> </ul> |
| Add weld in gap region (Option)  | <ul style="list-style-type: none"> <li>Add weld material into gap shown by the shaded area in above figure, to increase the shear capacity;</li> </ul>   |

### 9.3.9 Test LSP3 Discussion

LSP3 was tested with these modifications and a load sequence (similar in concept to that for LSP2) modified to match stiffnesses and target loads of 400 kN (anticipated load to cause the initial brittle crack) and 3000 kN in the starter and main plates, respectively. The failure sequence and mode were essentially as before, with a 15mm long single brittle crack propagation event occurring at 413 kN, which was followed by brittle shear failure with continued loading across the gap plate at 558 kN.

Consistent failure modes and shear distortions through the gap plate for the first three large scale tests led to the joint decision to redesign the starter load system apparatus to minimize its interaction with the loading and deformation of the main plate. With this objective, the articulating starter load system illustrated schematically and in assembled views in Figures 9.18 and 9.19, respectively, was designed to provide:

- equal and opposite tension across the potential crack path while minimizing unwanted restraint and friction from the load system (the latter must be measured and its effects quantified); and
- uniform opening of potential crack (equal outward displacement of the pins that join the load system to the starter plate).

Even with slots to allow movement of the upper and lower arms without unwanted restraint, sliding friction will develop along the steel contact surfaces. The magnitude of applied load (vertical), frictional force (horizontal) and vertical displacements of the upper and lower loading arms were measured for the next series of tests, LSP4, LSP5 and LSP6. Additional finite element analyses were conducted to determine the effects of friction force on the stress intensity factor distribution for original notch and crack geometry. A direct comparison of like load conditions, 700 kN load in the starter plate and an average applied tensile stress of  $0.625s_{sy}$  for the main is illustrated in Figure 9.20. Within the first 20 mm of crack propagation there is no influence. The slope of the curve diminishes slightly, but remains essentially constant, until the crack propagates into the main plate. Subsequently, the stress intensity factor shows a marginal decrease to the end of the double-sided grooves, after which it remains relatively constant. The interpretation of crack arrest toughness would be conducted as previously describe with the analysis including the measured friction forces in both loading arms.

#### 9.3.10 Test LSP4 Discussion

Test LSP4, with the new articulating loading system, was conducted using the same initial temperature conditions, notch geometry, ligament length and main plate load as in test LSP3. As expected, the articulating load system simply shifted upwards like distorting a parallelogram, and the slots accommodated relative horizontal movement. The actuator load was increased to 1176kN, a starter load of 530kN. The loading arms started to experience localized yielding at the pin connection near the column. The test was stopped and the specimen unloaded. Based on discussions with the project team, it was decided to cut the ligament through creating an edge crack condition. The large-scale test specimen LSP4 was reloaded and at a starter load of 181kN a 5 mm to 10 mm brittle crack propagated along the weldment as illustrated in Figure 9.21. At 214kN the brittle crack propagated a further 200mm, into the lower part of the main plate. This crack deviation may be have been caused by:

- local weld flaws,
- unequal loading to the starter plate above and below the region of interest, or by
- a varying temperature field above and below the region of interest (varying crack arrest toughness or resistance to crack growth)

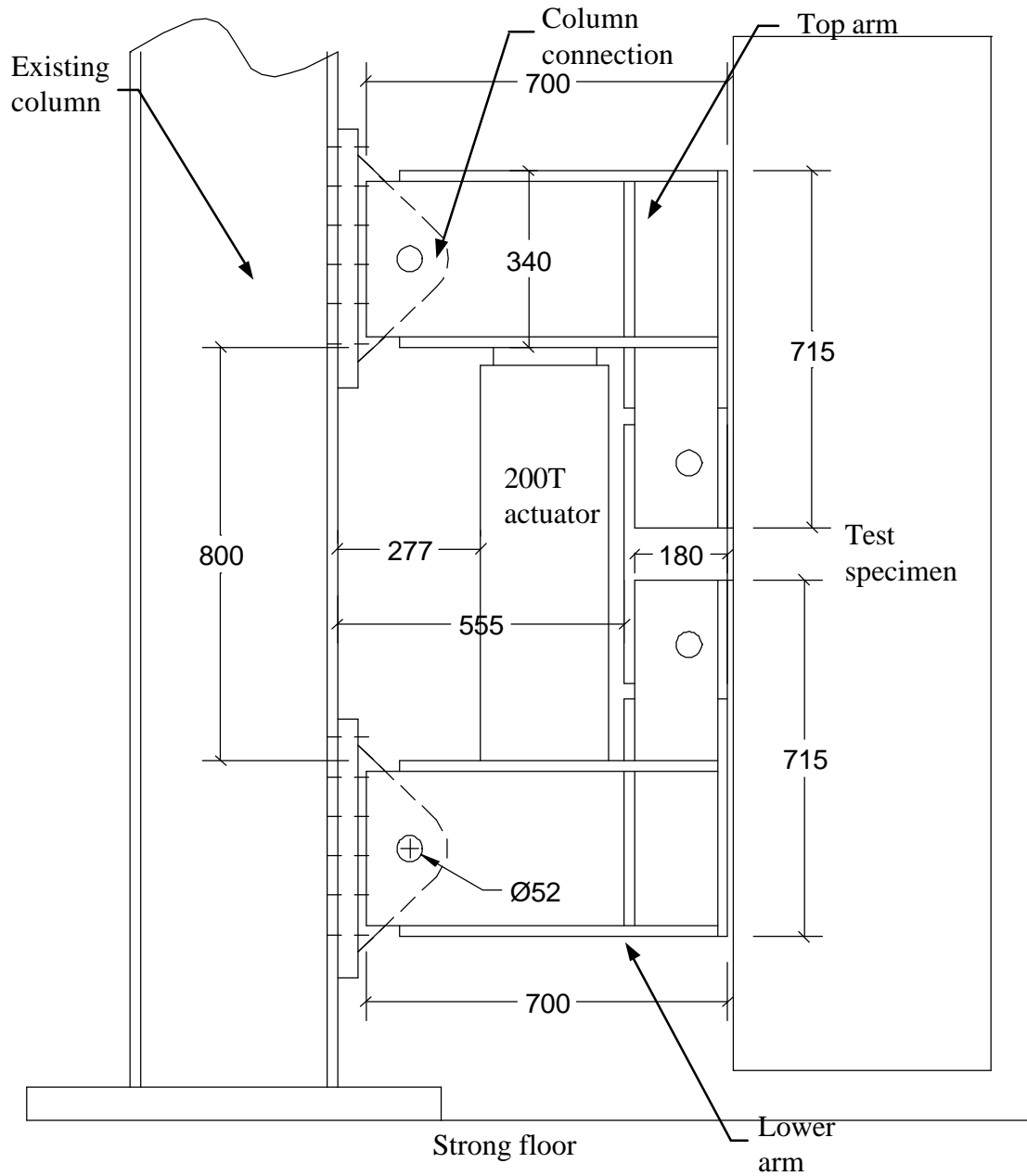


**Figure 9.18: Schematic Diagram of Articulating Starter Loading System**

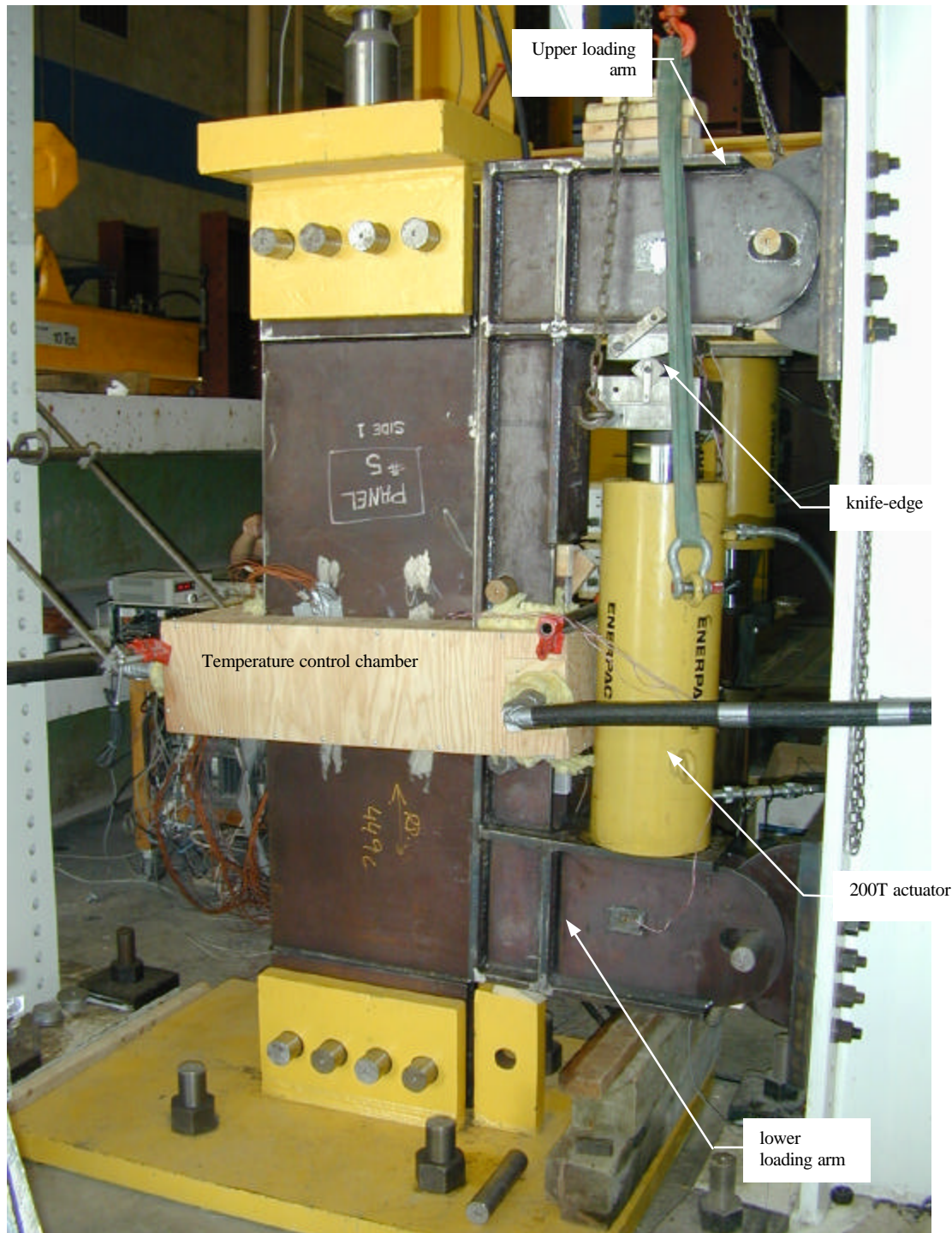


**Figure 9.19: Articulating Starter Load System**

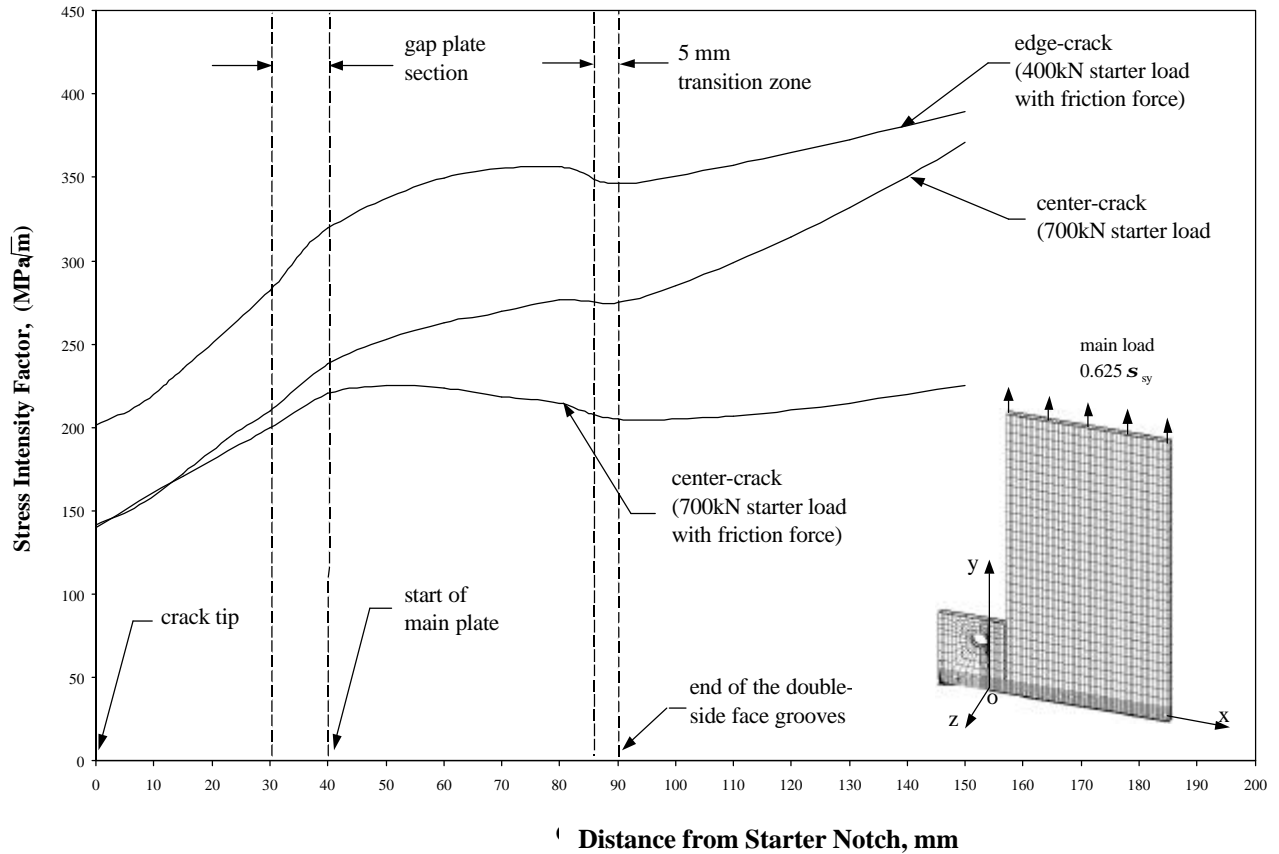


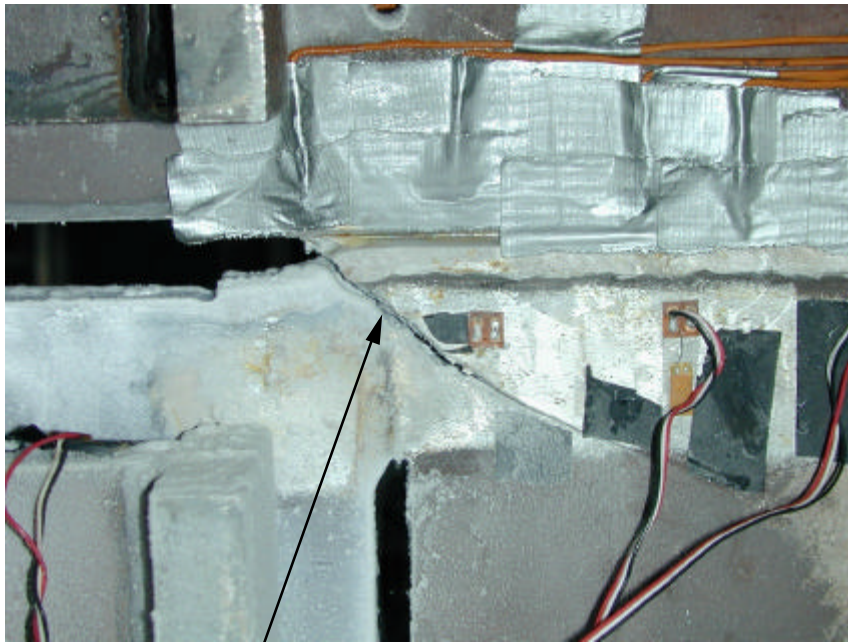
**Figure 9.20: Stress Intensity Factor Distributions for Varying Starter Load and Crack Condition**

### 9.3.11 Test LSP5 Discussion

Based on the experimental evidence, measurements of load and temperature, it was decided to conduct LSP5 under the same test conditions as LSP4 to determine whether the crack deviation was random event associated with weld defects. As before the crack propagation event occurred in two stages with an initial short run brittle crack of 10 mm along the weldment in the starter plate at a load of 177kN, which was then followed by a brittle crack of 130mm which deviated into the lower main plate. The cracks are illustrated in the photographs in Figure 9.23. The localized shear deformation in the lower section of the gap plate occurred after the second crack propagation event.



initial brittle crack  
along weldment



brittle crack  
deviates and  
extends into main plate

**Figure 9.21: Crack Initiation of LSP4**

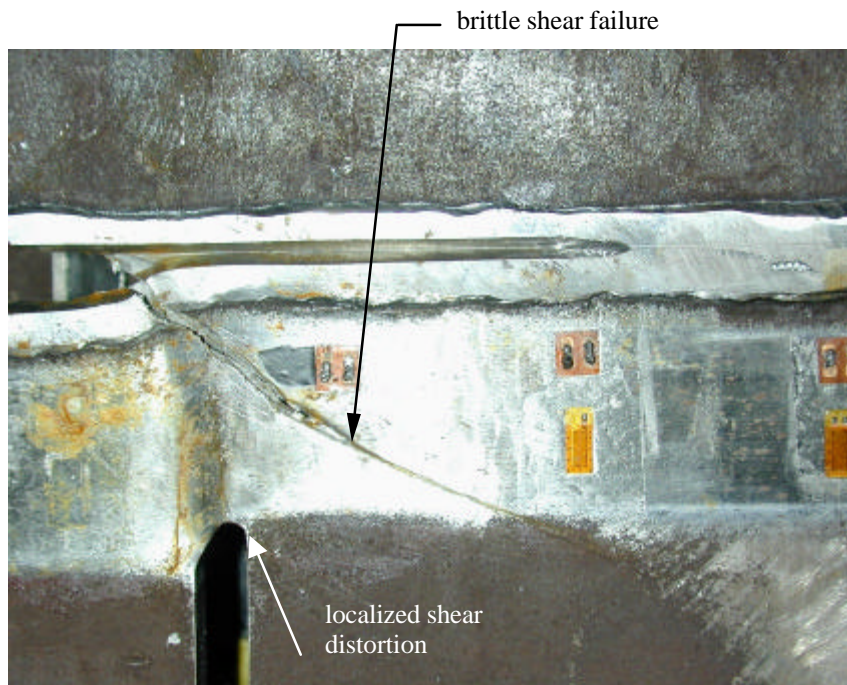


**Figure 9.22: Brittle Shear Failure for LSP4**

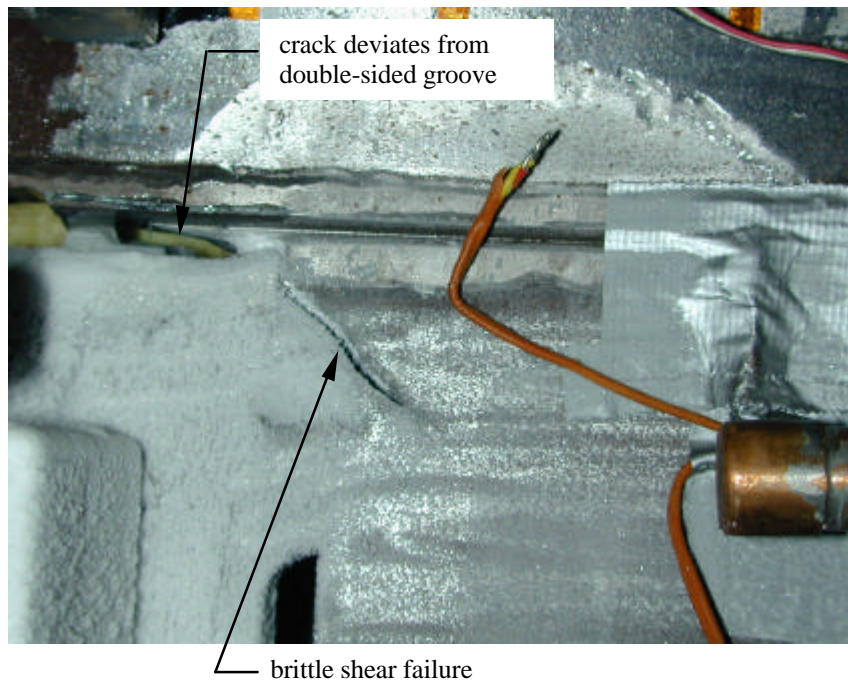
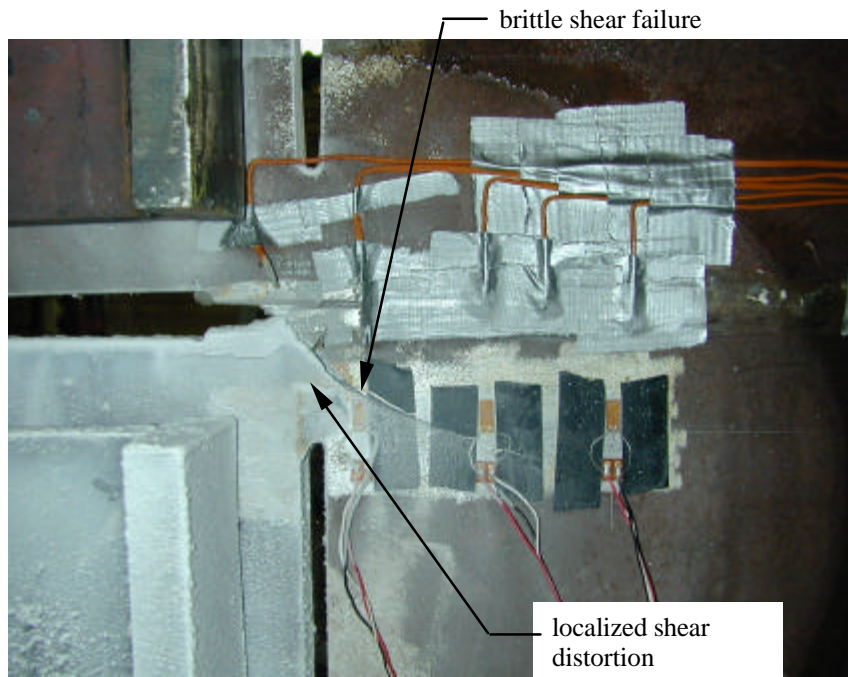


**Figure 9.23: Brittle Shear Failure for LSP5**

Subsequent to the test, additional thermocouples were placed along the length of the main plate and a series of measurements made to determine whether any significant thermal gradient existed in this direction. Over the measured length of 100mm there was a drop in temperature of approximately 20°C, varying from -25°C at 50mm above the weldment to -45°C 50mm below the weldment. The gradient was primarily due to the projection of the liquid nitrogen spray from the pinhole openings. Note this temperature cooling system was identical to that for the starter plate test series and was not necessarily suspect in affecting the crack propagation direction. Notwithstanding, the temperature control chamber was rebuilt to provide a larger volume of cooled material, 200mm deep and a double piping system as illustrated in Figure 9.24. The holes in the system were adjusted upwards to project the spray into the box (not directly at the specimen) to provide more uniform cooling of the chamber. The temperature gradient curves at 50 millimeters above and below the weldment as measured along the width of LSP6 is illustrated in Figure 9.26. The curves clearly show that the gradient along the length is virtually negligible. The gradient along the width is a curve fit of the available data. The increase in temperature prior to the thermal barrier is a function of the curve fit only. Based on previous tests with a significant number of thermocouples along this direction the drop occurred entirely within the barrier. The resultant curve is marked in red.

#### 9.3.12 Test LSP6 Discussion

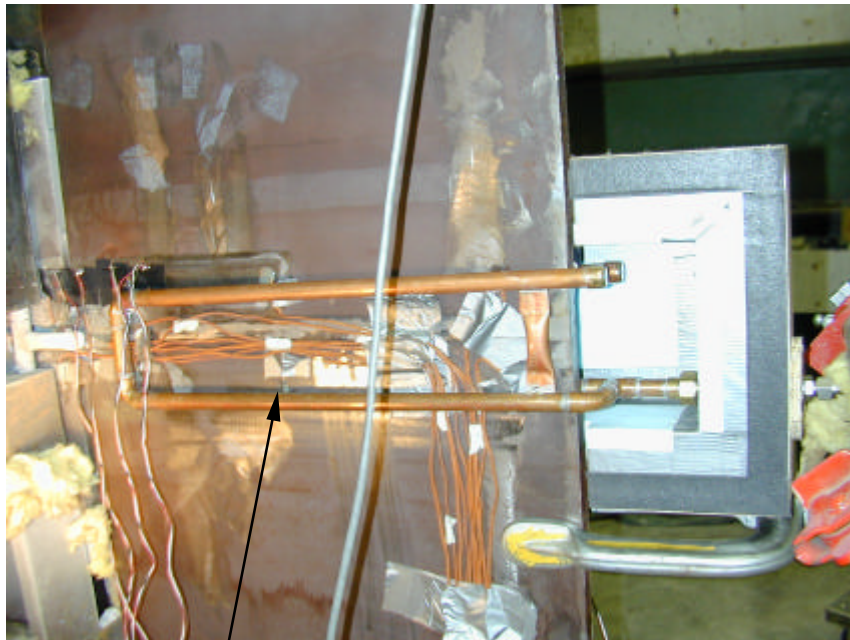
Test LSP6 was conducted with the same set of load and temperature conditions as LSP4 and LSP5. A 40mm brittle crack propagated in one stage, away from the weldment, into the lower main plate (Figure 9.25). All known possible conditions that could cause crack deviation were systematically eliminated as outlined in Table 9.2. Although the measured load in both the upper and lower load arms was similar, it was concluded that some small restraint or undetected variance in the load system must be responsible for the systematic crack deviation away from the weldment into the lower main plate. This system was abandoned for the edge crack open displacement system illustrated in Figure 9.28.

#### 9.3.13 Test LSP7 Discussion

The temperature conditions were the same as LSP6. The corresponding temperature gradient curves are given in Figure 9.27. As before, the red curve is more indicative of the true temperature gradient since the other is a manifestation of the curve fit. Load was applied through the 200T actuator and knife-edge assembly to the two loading beams welded to the starter plate. Shims were placed between the loading beams and the main plate to restrict inward rigid body displacements resulting from the opening of the sharp edge crack. A 10mm brittle crack propagated along the weldment and arrested in the starter plate as illustrated in Figure 9.28. Continued loading produced ductile tearing and could not be propagated further. With this configuration, the starter plate had insufficient internal strain energy to propagate the crack into the main plate due to the lowest starter load. A modified version of this load system with a center notch/crack as per STP4, described in the recommendations, should produce the desired results via higher strain energy before initiation.



cooling system:  
starter plate



cooling system:  
main plate

**Figure 9.24: Modification of Cooling System for Main and Starter Plate of LSP6**

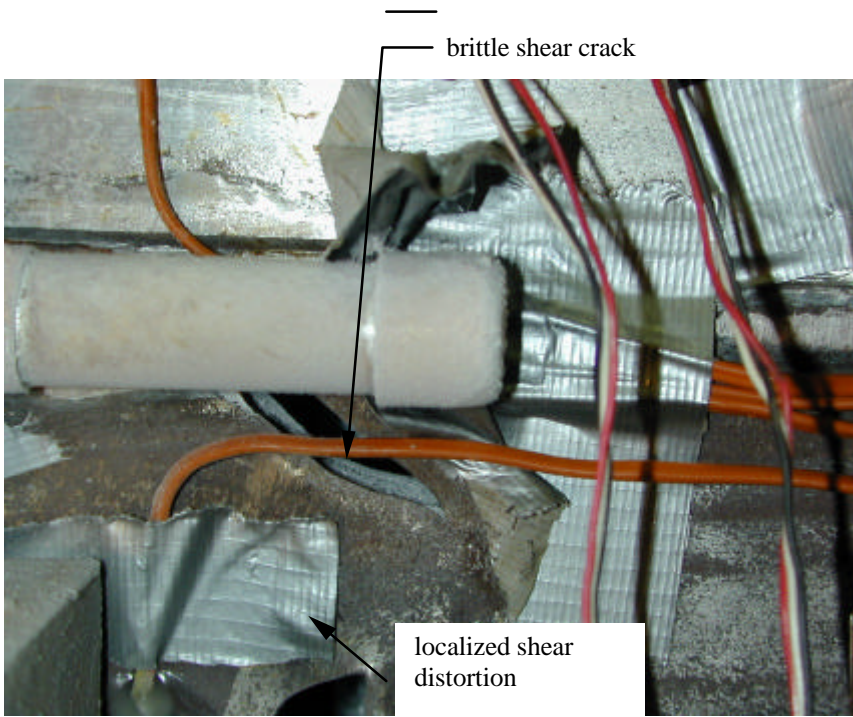
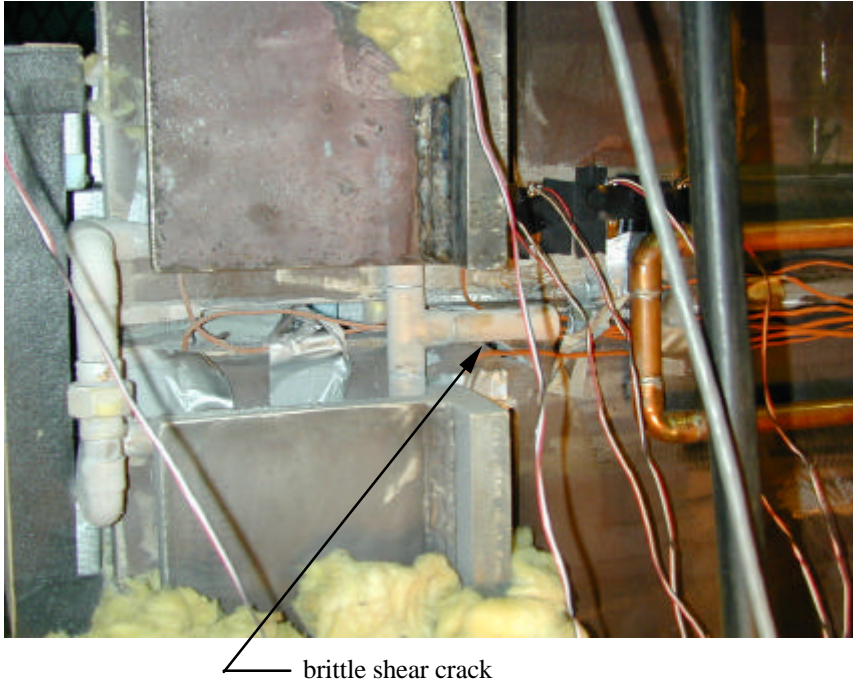


**Figure 9.25: Brittle Shear Failure of LSP6**

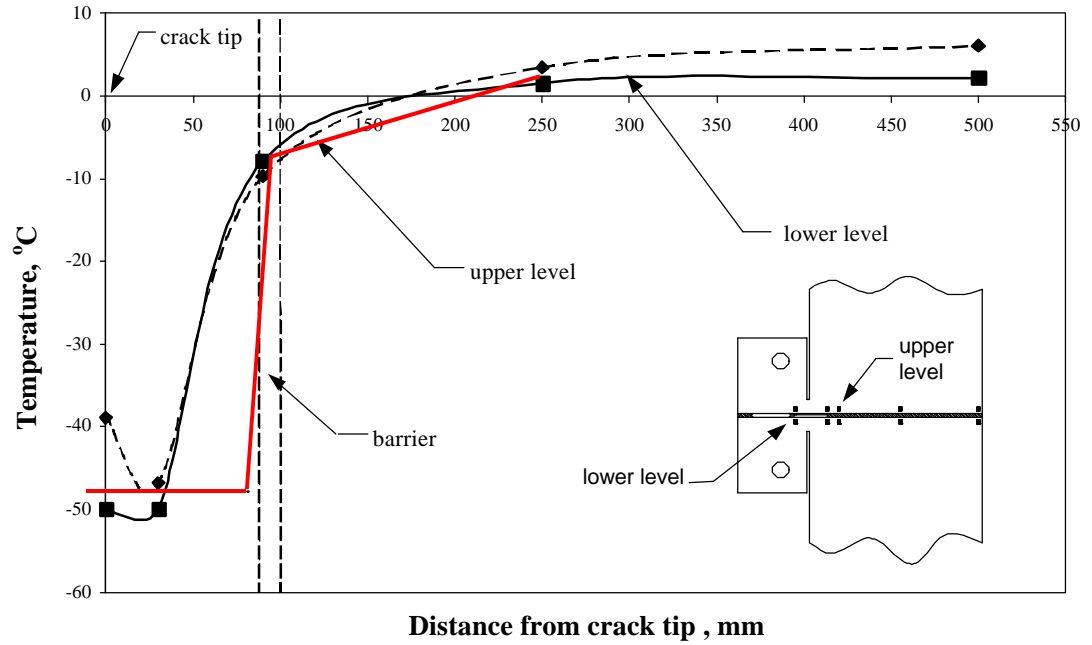


**Figure 9.26: Temperature Gradient Curves for Large-scale Test 6**

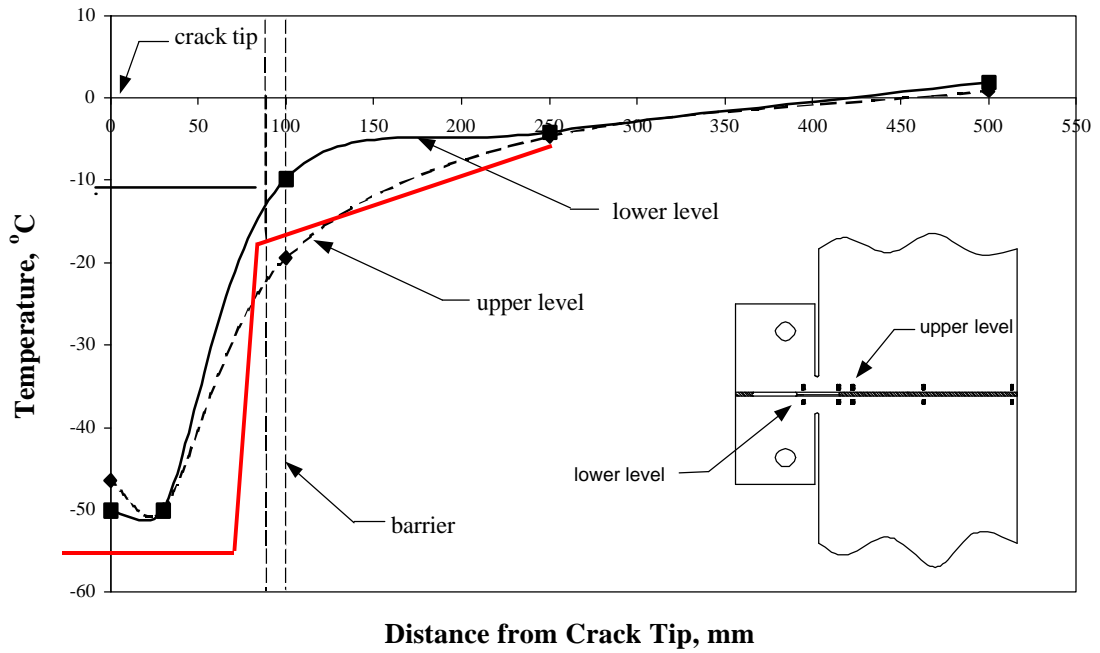


**Figure 9.27: Temperature Gradient Curves for Large-scale Test 7**

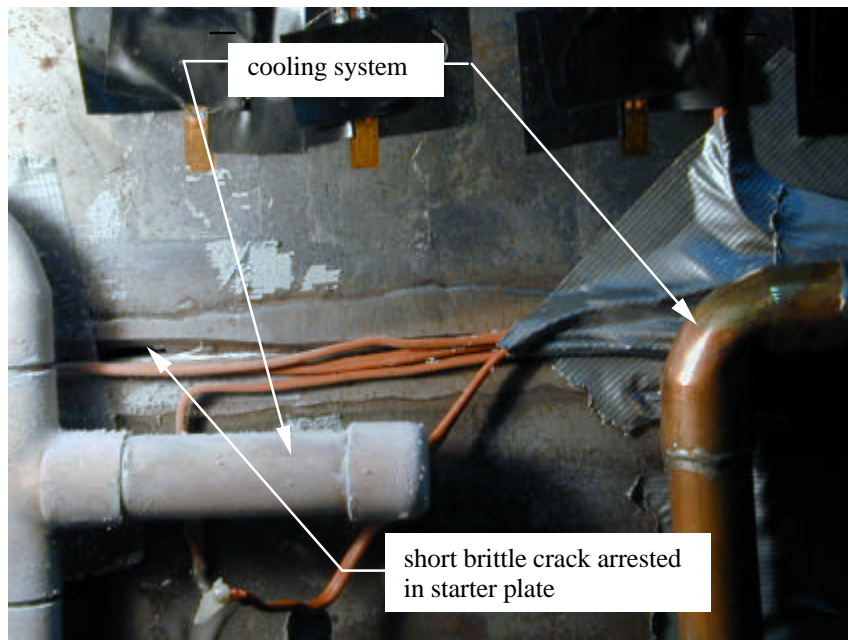
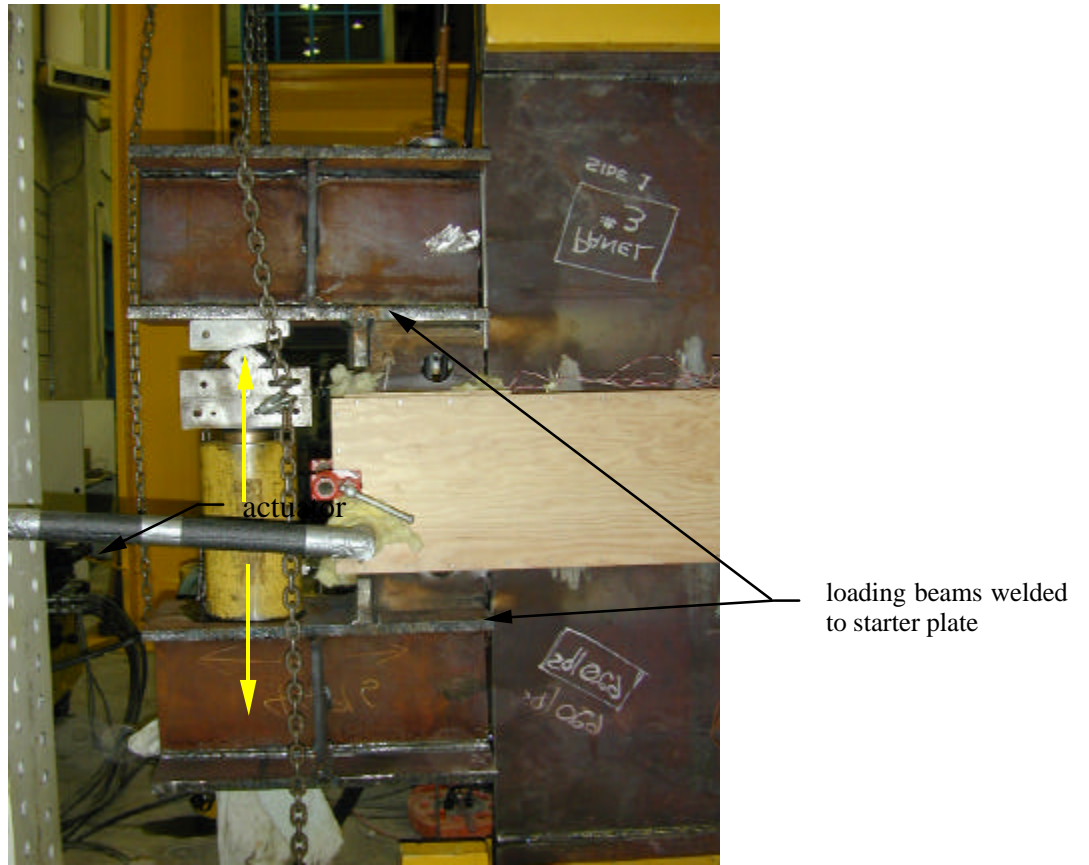


**Figure 9.28: Loading Apparatus for LSP7**

## 10. SUMMARY, CONCLUSIONS, AND FUTURE WORK

### 10.1 Summary

Since flaws are always likely to exist, then brittle fractures will continue to occur in welded structures under temperatures and loading conditions that produce unstable crack growth. Consequently, it is important for engineers to be able to characterize the toughness accurately and then to provide steel and weldments with sufficient toughness to prevent crack propagation. The toughness values determined from large-scale tests are most representative of real details and structures. These tests are not always possible or economical, hence it is important to determine the relationship between toughness values determined from small-scale tests and those obtained from large-scale tests. This then will allow engineers to conduct relatively inexpensive small-scale tests to obtain toughness data that can be used for the design and crack arrest toughness assessment of real structures.

A description of all known small-scale and large-scale tests that have been developed to determine crack arrest toughness values is given in Chapter 7. From the small-scale test series, the CCA is considered to be the most reliable and has been standardized as ASTM E1221-96 to determine plane strain crack arrest toughness ( $K_{Ia}$ ). To measure full thickness crack arrest toughness ( $K_a$ ), a procedure encompassing many of the features of the standardized ASTM procedure was employed (Part I). Twenty-two small-scale full thickness CCA tests were conducted by FTL to characterize the crack arrest toughness of a typical weldment for ship structures. These tests were conducted with different sizes for a series of temperatures as defined by expected crack arrest toughness values from other small-scale tests and with different crack starters following the guidelines of ASTM E1221-96. Six were considered to be valid and gave average crack arrest toughness values of  $90.6 \text{ MPa}\sqrt{m}$  and  $107.7 \text{ MPa}\sqrt{m}$  at  $-10^\circ\text{C}$  and  $0^\circ\text{C}$ , respectively.

Four starter plate tests of the same geometry, steel and welds that were used for the large-scale double tension tests were conducted to obtain the conditions and notch geometry required to propagate a crack across the full width. Two of these were tested with crack starter details that involved lateral pre-compression to embrittle the material locally. This method proved to be unsuccessful since the pre-compression placed the material across the potential crack path into residual compression. This was verified by the corresponding finite element analysis. The starter plate test with double-side grooves proved successful and bounded the starter load and temperature ranges required to successfully initiate a crack propagation event.

Chapter 9 describes the test apparatus, test specimen, instrumentation, test procedure and the method for evaluating test data for the large-scale double tension test that was developed to obtain crack arrest toughness values for weldments subject to varying temperature and tensile stresses. Based on the prototype test, LSP1, in which the gap plate failed in shear, a new load sequence was determined analytically.

The load sequence describes the application of starter and main plate loads such that the target loads are achieved while minimizing the shear across the gap plate and promoting crack growth along the desired crack path (through the net section between the double-side grooves). Tests LSP2 and LSP3 were tested with the modified load sequence and under varying conditions to enhance crack propagation along the weldment. Consistent brittle shear failures through the gap plate for led to decision to modify the load system to an articulating system that was designed to decouple the loading systems of the main and starter plates.

Tests LSP4, LSP5 and LSP6 were tested with a severed ligament in the starter plate (edge crack configuration) and target temperatures of  $-40^{\circ}\text{C}$  and  $0^{\circ}\text{C}$  in the starter and main plates, respectively. Tests LSP4 and LSP5 experienced a two stage brittle crack propagation event with the first crack propagating between 5mm and 10mm along the weldment and the continuing crack deviating into the lower main plate a distance between 130mm and 200mm. The temperature control chamber was enlarged and modified to include a double piping system to provide a uniform temperature across the potential crack region for test LSP6 in an attempt to provide a uniform crack arrest toughness field. Deviation of the brittle crack into the lower main plate for the test led to the decision to modify the loading system once again as undetected restraint or peculiarities with the system (not yet identified) were generating a consistent but incorrect failure mode.

Test LSP7 was tested with an edge crack configuration and a load system that was directly attached to the starter plate. The load required to propagate the brittle crack was relatively small. The corresponding strain energy was insufficient to propagate the crack into the main plate. Attempts to propagate the crack further only led to ductile tearing at the root of the crack. As a result, an alternative load system has been devised to replicate the load conditions of the small-scale starter plate test series were successful.

## 10.2 Conclusions

Based on the information presented in the literature, the test data and the results of the numerical investigations presented, it can be concluded that:

- The ratios of the stress intensity factor calculated using the displacement extrapolation method (FEA) to that determined by classic methods for a single-edge-crack and a center-crack with semi-infinitely wide plates and uniform tensile stress field are 0.991 and 1.062, respectively. The displacement extrapolation method gives the best estimate of stress intensity factor of the three methods investigated.
- The ratios of the average crack arrest toughness determined by displacement extrapolation method to that determined using expressions from ASTM E1221-96, are 1.387 and 1.291 for  $-10^{\circ}\text{C}$  and  $0^{\circ}\text{C}$ , respectively.
- Lateral compression of the weld to “embrittle” the region around the crack as a crack starter method was ineffective, as there was residual compression across the potential crack path.
- Double-side face grooves in starter plate test proved to be an effective crack starter method. These grooves enhance the embrittlement by creating a state of plane strain or triaxial tensile stress along the potential crack path. The groove also directs the crack along the desired crack path.
- The initiation toughness for the weld in the starter plate with double-side grooves for temperature of  $-40^{\circ}\text{C}$  and  $-10^{\circ}\text{C}$  were determined to be  $77 \text{ MPa}\sqrt{m}$  and  $159 \text{ MPa}\sqrt{m}$ , respectively.
- Based on the measured crack length and stress intensity factor-crack length curve for a given starter and main load, both the initiation toughness and crack arrest toughness can be determined for the large-scale double tension test subjected to either isothermal or temperature gradient conditions.
- Based on the results of FEA on the large-scale double tension test specimen, it was determined that the normal strain distribution across the welds of the main plate gives a good measure of crack length. This will need to be verified experimentally.
- The large-scale double tension test failed by either brittle shear failure through the gap plate section, or by brittle cracks that propagated into the main plate but deviated away from preferred path of the weldment, or with a brittle crack that fell short of propagating into the main plate.
- The redesign temperature control chamber provide uniform temperature field across the potential crack path and a rapid gradient through the barrier (along the weldment). The chamber provided an adequate temperature environment to accurately access the temperature profile.

### **10.3 Recommendations and Future Work**

Future work would involve a series of large-scale double tension tests with varying magnitudes of main plate load (given a function of the yield stress for the main plate) and temperatures. It is recommended that the load system and the notch/crack geometry for the starter plate emulate the small-scale starter plate test series. The appropriate load system is shown schematically in Figure 10.1. The system is independent of the main plate, assures the correct application of load, and provides sufficient space for the temperature control chamber. The proposed system is reusable.

The crack arrest toughness can be evaluated using measured crack lengths and the appropriate stress intensity value determined from the stress intensity factor curve for each given test condition. The stress intensity curve can be calculated using the displacement extrapolation method and the results of an appropriate finite element analysis such as those describe in this report.

Subsequent to completing this series of tests, a comparison can be made with the crack arrest values derived by the same analytical means for the CCA tests. This entire series, including both small-scale and large-scale tests, needs to be conducted for other materials, to broaden the database and to confirm the correlation between crack arrest toughness values obtained from the either method.

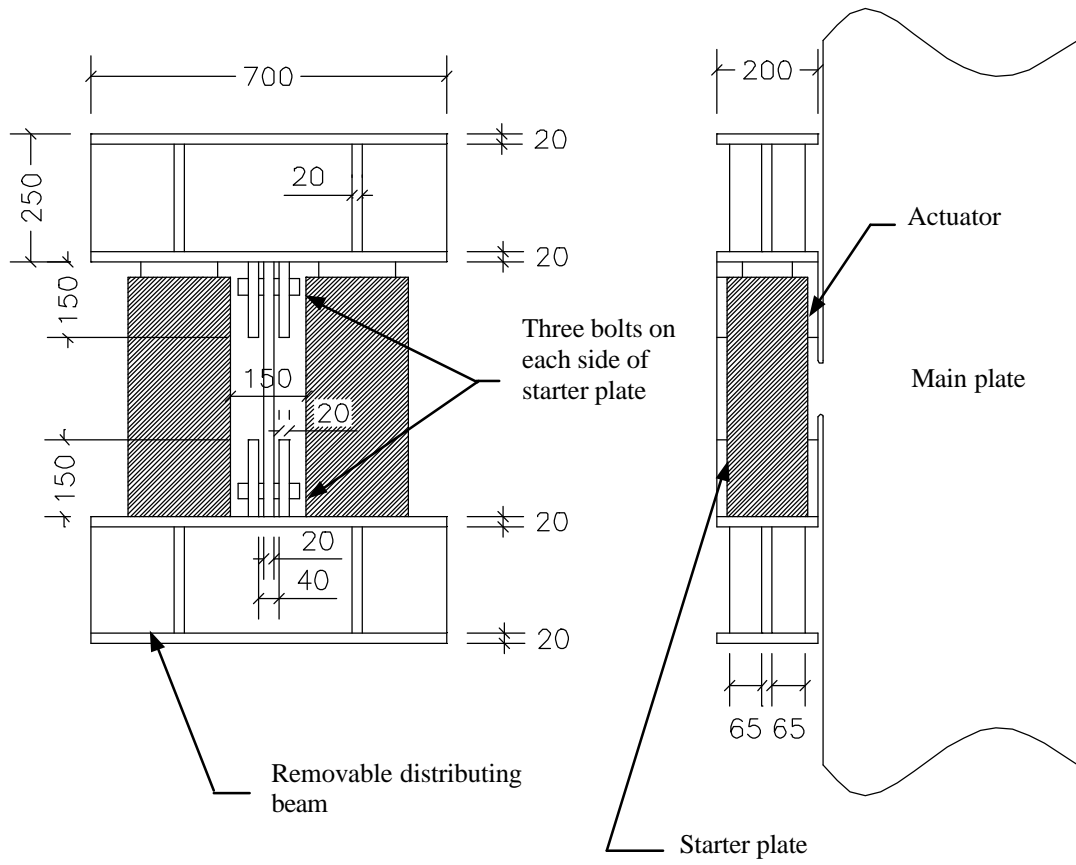


**Figure 10.1: Starter Plate Load System**

## 11. REFERENCES

- Anderson, T.L. 1995. Fracture Mechanics – Fundamentals and Applications, Second Edition. CRC Press Inc.
- ANSYS. 1998. *Release 5.4, ANSYS Analysis Guides*. ANSYS. Inc., Houston, Pennsylvania, USA
- ANSYS. 1998. *Release 5.4, ANSYS Elements Manual*. ANSYS. Inc., Houston, Pennsylvania, USA
- ANSYS. 1998. *Release 5.4, ANSYS Theory Manual*. ANSYS. Inc., Houston, Pennsylvania, USA
- ASTM E1221-96. 1996. Standard Test Method for Determining Plane-Strain Crack-Arrest Fracture Toughness,  $K_{Ia}$ , of Ferritic Steels. American Society of Testing and Materials.
- ASTM E208-95a. 1996. Standard Test Method for Conducting Drop-Weight Test to Determine Nil-Ductility Transition Temperature of Ferritic Steels. American Society of Testing and Materials. pp. 293.
- ASTM E23-96. 1996. Standard Test Methods for Notch Bar Impact Testing of Metallic Materials. American Society of Testing and Materials. pp. 136.
- ASTM E604-83. 1996. Standard Test Method for Dynamic Tear Testing of Metallic Materials. American Society of Testing and Materials. pp. 512.
- Barsom, John M. & T.Rolfe, Stanley 1987. Fracture and Fatigue Control in structures. Second Edition. Prentice-Hall, Inc.
- Bonenberger, R. J. 1994. Development of a Chevron-Notch Crack-Arrest Specimen. A Bell & Howell Company
- Broek, David 1987. Elementary Engineering Fracture Mechanics. Fourth Edition. Kluwer Academic Publishers.
- Chan, S.K., Tuba, I.S. and Wilson, W.K., 1970. On the finite element method in linear fracture mechanics, Eng. Fract. Mech., 2 pp.61-79.
- Crosley, P.B. and Ripling, E.J. 1990. A Quality Control Test for Selecting Materials to Arrest Fast-Running, Full-Thickness Cracks. Journal of Testing and Evaluation, Vol. 18, No. 6, Nov. pp. 396-400.

- Crosley, P.B. and Ripling, E.J. 1969. Dynamic Fracture Toughness of A533 Steel. *Journal of Basic Engineering*, September, pp. 525.
- Crosley, P.B. and Ripling, E.J. 1975. Plane Strain Crack Arrest Characterization of Steels. *Journal of Pressure Vessel Technology*, November. pp. 291.
- Crosley, P.B. and Ripling, E.J. 1980. A Compact Specimen for Plane Strain Crack Arrest Toughness Testing. *Journal of Testing and Evaluation*. Vol. 8, Jan. pp. 25-31.
- Granville, B.A. 1994. Short Crack Arrest Tests – Analysis and Discussion. Contract 003SQ.23440-1-9202, March, pp.26
- Granville, B.A. 1989. Evaluation of Short Crack Arrest Test Techniques. Contract 003SQ.23440-1-9202, June, pp.23
- Granville, B.A. 1993. Development of Crack Arrest Approaches to Material Specification. Contract 003SQ.23440-1-9202, March, pp.34
- Hahn, G.T., Hoagland, R.G., Kanninen, M.F. and Rosenfield, A.R. 1975. Crack Arrest in Steels. *Engineering Fracture Mechanics*, Vol. 7 pp. 583-591.
- Kanninen, M.F. 1974. Adynamic Analysis of Unstable Crack Propagation and Arrest in the DCB Test Specimen. *International Journal of Fracture*. Vol. 10, No.3, September, pp. 415.
- Lay M.G., 1982. *Structural Steel Fundamentals*. Australian Research Board.
- Malik, L. et. al. 1996. Crack Arrest Toughness of a Heat-affected Zone Containing Local Brittle Zones. *Transactions of American Society of Mechanical Engineering*. Vol. 118, pp. 242-299.
- Murakami, Y., 1987. *Stress Intensity Factor Handbook*, Pergamon Press.
- Pusegoda, L.N., Malik, L., Morrison, J. 1998. Measurement of Crack Arrest Toughness of Ship Plate Steels. *Journal of Testing and Evaluation*. Vol. 26, pp. 187-197.
- Ship Structure Committee, 1976. *A Study of Ship Hull Crack Arrest System.*, U.S. Coast Guard Headquarters, Washington D.C. Report No. SSC-265.
- Wiesner, C.S. and Hayes, B. 1984 *A Review of Crack Arrest Tests, Models and Applications*. TWI, UK.